POLYMER FOAMING WITH SUPERCRITICAL CARBON DIOXIDE

A THESIS SUBMITTED TO
THE GRADUATE SCHOOL OF NATURAL AND APPLIED SCIENCES
OF
MIDDLE EAST TECHNICAL UNIVERSITY

BY

NOVENDRA NOVENDRA

IN PARTIAL FULFILLMENT OF THE REQUIREMENTS
FOR
THE DEGREE OF MASTER OF SCIENCE
IN
CHEMICAL ENGINEERING

AUGUST 2015

Approval of the thesis:

POLYMER FOAMING WITH SUPERCRITICAL CARBON DIOXIDE

submitted by **NOVENDRA NOVENDRA** in partial fulfillment of the requirements for the degree of **Master of Science in Chemical Engineering Department, Middle East Technical University** by,

Prof. Dr. Gülbin Dural Ünver _____

Dean, Graduate School of **Natural and Applied Sciences**

Prof. Dr. Halil Kalıpçılar _____

Head of Department, **Chemical Engineering**

Assoc. Prof. Dr. Çerağ Dilek Hacıhabiboğlu _____

Supervisor, **Chemical Engineering Dept., METU**

Prof. Dr. Nesrin Hasırcı _____

Co-Supervisor, **Chemistry Dept., METU**

Examining Committee Members:

Prof. Dr. Levent Yılmaz _____

Chemical Engineering Dept., METU

Assoc. Prof. Dr. Çerağ Dilek Hacıhabiboğlu _____

Chemical Engineering Dept., METU

Prof. Dr. Nesrin Hasırcı _____

Chemistry Dept., METU

Prof. Dr. Halil Kalıpçılar _____

Chemical Engineering Dept., METU

Assoc. Prof. Dr. Eda Ayşe Aksoy _____

Basic Pharmaceutical Sciences Dept., Hacettepe University

Date: 19.08.2015

I hereby declare that all the information in this document has been obtained and presented in accordance with academic rules and ethical conduct. I also declare that, as required by these rules and conduct, I have fully cited and referenced all material and results that are not original to this work.

Name, Last Name: Novendra Novendra

Signature:

ABSTRACT

POLYMER FOAMING WITH SUPERCRITICAL CARBON DIOXIDE

Novendra, Novendra

M.Sc., Department of Chemical Engineering

Supervisor: Assoc. Prof. Dr. Çerağ Dilek Hacıhabiboğlu

Co-advisor: Prof. Dr. Nesrin Hasırcı

August 2015, 108 pages

High molecular weight semi crystalline poly(L-lactic acid) (P_LLA) was processed with environmentally benign and non-toxic supercritical carbon dioxide with and without the addition of two different additives to form porous polymeric thin films for biomedical applications such as drug delivery. One of the additives was a CO_2-philic additive, trifluoropropyl polyhedral oligomeric silsesquioxane (TFPOSS), and the other was a non CO_2-philic additive, octamethyl polyhedral oligomeric silsesquioxane (OMPOSS). Even though P_LLA has good mechanical properties, there are only a few studies in literature on porous P_LLA preparation with supercritical CO_2 since the processability of this polymer with the supercritical fluid at moderate temperatures and pressures is quite poor. In this study, the chosen processing parameters were temperature, saturation pressure, venting rate, saturation time and additive concentration in the ranges of 313-393 K, 10.3-20.7 MPa, 0.2-10.3 $MPa.min^{-1}$, 2-24 h, 10-30 wt%, respectively.

The results showed that while P_LLA did not form a porous structure when it was processed with supercritical CO_2 at a temperature as low as 313 K and a moderate pressure of 20.7 MPa, addition of 10 wt% TFPOSS to P_LLA improved its foamability

when it was processed with supercritical carbon dioxide ($scCO_2$) at the same conditions. About 27% porosity was obtained in the P_LLA film with the addition of 10% TFPOSS at these conditions in 2 h processing with $scCO_2$. At the same processing conditions, with an increase of TFPOSS to 30 wt% in the polymer matrix, the extent of porosity was improved further to value of 40%. At the same processing conditions, when 30% non CO_2-philic additive (OMPOSS) was used, i.e. does not form a homogenous mixture with the CO_2 at any temperature and pressure, no porous structure was obtained. This shows that the porosity improvement was obtained due to the CO_2-philicity of the used additive.

Conditions of processing with $scCO_2$ can change many aspects of the polymeric films as well. In the supercritical foaming of P_LLA, it was observed that increase in pressure at constant temperature resulted in increase in the pore density and decreased the average pore size. Processing at a higher temperature at constant pressure, increase the average pore size. The average pore size decreased, by decreasing the venting rate while keeping all the other conditions constant. The indentation hardness of the processed films was also analyzed and it was observed that this property was directly proportional with the processing time and POSS concentration in the P_LLA. The maximum indentation hardness was obtained as 3541 MPa, with the use of 30% POSS, at the supercritical processing conditions of 313 K and 20.7 MPa, 24 h. Similarly, crystallinity of the films also increases after supercritical processing. This shows that CO_2 had a plasticizing effect on the solid polymer, so that polymer chains gain some mobility and reorganize themselves due to $scCO_2$ processing which is leading to higher crystallinity. However, none of the parameters and the additives had a significant effect on the crystallinity of the obtained films. Finally when the obtained films with the enhanced porosity were tested for drug delivery, which is the targeted biomedical application, the films exhibited a burst release behavior, which can be suitable for local antibiotic applications.

It was observed that at 313 K and 20.7 MPa, complete extraction of TFPOSS from the P_LLA films was obtained during the processing, while at higher temperatures,

complete extraction was not observed. In order to estimate the solubility of TFPOSS in $scCO_2$ at the processing conditions, the solubility data of TFPOSS obtained from literature was modeled. Six different semi-empirical density-based models, including Chrastil, Chrastil modified by Wang, Del Valle and Aguilera, Kumar and Johnston, Mendez-Santiago and Teja, and Bartle models were used. The best solubility predicting performance was obtained with Chrastil modified by Wang model, which also exhibited a linear self-consistency test.

Keywords: poly(L-lactic acid), porous structure, supercritical carbon dioxide, drug release, semi empirical density-based model.

ÖZ

SÜPERKRİTİK KARBONDİOKSİTLE POLİMER KÖPÜKLESMESİ

Novendra, Novendra
Yüksek Lisans, Kimya Mühendisliği Bölümü
Tez Yöneticisi: Doç. Dr. Çerağ Dilek Hacıhabiboğlu
Ortak Tez Yöneticisi: Prof. Dr. Nesrin Hasırcı

Ağustos 2015, 108 sayfa

İlaç salımı gibi medikal uygulamalarda kullanılabilmesi amacıyla gözenekli ince film elde edebilmek için yüksek moleküler ağırlıklı yarı kristal yapılı poli(L-laktik asit) (P_LLA) çevreye duyarlı ve zehirli olmayan süperkritik karbondioksit ile iki farklı katkı maddesi kullanılmadan ve kullanılarak işlenmiştir. Katkı maddelerinden biri CO_2-uyumlu olan trifloropropil polihedral oligomerik silseskuioksan (TFPOSS) ve diğeri ise CO_2-uyumsuz olan oktametil polihedral oligomerik silseskuioksan (OMPOSS)'dır. P_LLA iyi mekanik özelliklere sahip olmasına rağmen, süperkritik CO_2 ile işlenmesi makul sıcaklık ve basınçlarda düşük seviyede olmasından ötürü, literatürde süperkritik CO_2 ile gözenekli P_LLA hazırlanması ile ilgili sadece bir kaç çalışma mevcutttur. Bu çalışmada kullanılan polimer işleme parametreleri sıcaklık, doyma basıncı, boşaltım hızı, doyma süresi ve katkı maddesi çeşidi ile konsanstrasyonudur; sıcaklık 313-393 K, doyma basıncı 10.3-20.7 MPa, boşaltım hızı 0.2-10.3 $MPa.dak^{-1}$, doyma süresi 2-24 saat ve katkı maddesi konsantrasyonu 10-30 % ağırlık aralığındadır.

Sonuçlar, P_LLA'nın 313 K gibi düşük ve 20.7 MPa gibi makul bir basınçta süperkritik CO_2 ile işlendiğinde gözenekli bir yapı oluşturmadığını, ancak P_LLA'ya ağırlıkça %10 TFPOSS eklendiğinde ve yine aynı koşullarda süperkritik CO_2 ($skCO_2$) ile işlendiğinde polimerin gözeneklenebilirliğinin arttırılabildiğini göstermiştir. Bu koşullarda $skCO_2$ ile iki saatlik işlenmesi sonucu P_LLA filminde yaklaşık %27 gözeneklilik elde edilmiştir. Aynı süreç koşullarında, polimer matrisindeki TFPOSS ağırlıkça % 30'a arttırıldığında, gözeneklilik derecesi de %40 değerine artmıştır. Aynı süreç koşullarında, ağırlıkça %30 CO_2-uyumsuz olan (OMPOSS), yani CO_2 ile herhangi bir sıcaklık veya basınçta homojen bir karışım oluşturmayan katkı maddesi kullanıldığında, gözenekli bir yapı elde edilmemiştir. Bu sonuç gözeneklendirilebiliriliğin kullanılan katkı maddesinin CO_2-uyumlu olmasından ötürü elde edilebildiğini göstermektedir.

$skCO_2$ ile işleme koşulları polimerik filmlerin bir çok farklı özelliğini de değiştirebilmektedir. P_LLA'nın süperkritik köpüklendirilmesinde, basıncın sabit sıcaklıkta arttırılmasının gözenek yoğunluğunu arttırdığı ve ortalama gözenek büyüklüğünü düşürdüğü gözlenmiştir. Sabit basınçta daha yüksek bir sıcaklıkta işlemenin ise ortalama gözenek büyüklüğünü arttırdığı gözlenmiştir. Tüm koşullar sabit tutulduğunda ve boşaltım hızı düşürüldüğünde ise ortalamanu gözenek boyutunun küçüldüğü gözlenmiştir. İşlenmiş filmlerin çentik darbe dayanımı da incelenmiş ve bu özelliğin işleme süresi ve P_LLA'daki POSS yoğunluğu ile doğru orantılı olduğu gözlenmiştir. En yüksek çentik darbe dayanımı, 313 K ve 20.7 MPa süperkritik işleme koşullarında ve %30 POSS kullanıldığında, 3541 MPa olarak elde edilmiştir. Benzer şekilde filmlerin kristalinitesi de süperkritik işleme sonrasında artmıştır. Bu, CO_2'nin polimer üzerinde plastikleştirme etkisinin olduğunu, dolayısıyla $skCO_2$ işlemesi nedeniyle polimer zincirlerinin bir miktar hareketlilik kazandığını ve kendilerini yeniden organize ettiklerini, bunun da daha yüksek kristaliniteye sebep olduğunu göstermektedir. Ancak hiç bir süreç koşulu ya da katkı maddesinin kristalinite üzerinde belirgin bir etkisi olmamıştır. Son olarak hedeflenen biyomedikal uygulama olan ilaç salımı için incelendiğinde, elde edilen gözenekliliği

arttırılmış filmler lokal antibiyotik uygulamaları için uygun olabilecek hızlı salım davranışı göstermiştir.

313 K ve 20.7 MPa koşullarındaki süperkritik işleme sürecinde TFPOSS'un P_LLA filmlerinden tümüyle özütlenirken, daha yüksek sıcaklıklarda tümüyle özütleme gözlenmemiştir. TFPOSS'un bu süreç koşullarındaki $scCO_2$'deki çözünürlüğünün belirlenmesi için TFPOSS'un literatürdeki çözünürlük datası modellenmiştir. Chrastil, Wang tarafından modifiye edilmiş Chrastil, Del Valle ve Aguilera, Kumar ve Johnston, Mendez-Santiago ve Teja, ve Bartle modelleri olacak şekilde altı farklı yarı empirik yoğunluk temelli model kullanılmıştır. En iyi çözünürlük tahmin performansı aynı zamanda kendi içinde tutarlılık testi de doğrusal olan Wang tarafından modifiye edilmiş Chrastil modeli ile elde edilmiştir.

Anahtar kelimeler: poli(L-laktik asit), gözenekli yapı, süperkritik karbondioksit, ilaç salımı, yarı empiric yoğunluk temelli model

To my family…

ACKNOWLEDGEMENTS

I would like to express my deepest appreciation to my supervisor, Assoc. Prof. Dr. Çerağ Dilek Hacıhabiboğlu for her continuous support, advice, patience, criticism and encouragement throughout the study. It was a great honor for me to be one of the first students to study under her supervision.

I am deeply thankful to my co-supervisor Prof. Dr. Nesrin Hasırcı who introduced me to this brand new world of biomedical and tissue engineering, and always giving me supports and new insights about the research.

I would like to thank Aysun Güney for her tremendous help and lessons during my first semester of the study that set me up to be able to complete the research

I would also like to thank Elbay Malikmammadov and Emre Kırcı for continuously supporting and helping me during my study and research, through bad and good times.

I would like to show my thanks also to Tuğba Endoğan and Dr. Arda Büyüksungur for the help during the SEM and μ-CT analysis.

I want to express my gratitude to my family, my parents, my brothers and my sister who never stopped to encourage me and pray for me during my study.

I want to express my gratitude also to all of my Indonesian friend in Turkey for all the friendship and the memories.

Finally I also would like to acknowledge the support that I receive during my study provided by Scientific and Technological Research Council of Turkey (TÜBITAK) Career Grant 110M465 and 2215 Graduate Scholarship Programme for International Students.

TABLE OF CONTENTS

ABSTRACT v
ÖZ viii
ACKNOWLEDGEMENTS xii
LIST OF TABLES xvi
LIST OF FIGURES xvii
NOMENCLATURE xxii
CHAPTERS
1 INTRODUCTION 1
1.1 Basic Principles of Supercritical Fluid 1
1.2 Porous Poly(L-lactic Acid) (P_LLA) Preparation with Supercritical Carbon Dioxide ($scCO_2$) Processing 2
1.2.1 Poly(lactic acid) (PLA) 2
1.2.2 PLA processing with $scCO_2$ for Biomedical Application 3
1.2.3 Literature Study on PLA and $scCO_2$ System 5
1.2.3.1 Solubility of P_LLA and $P_{DL}LA$ in $scCO_2$ 5
1.2.3.2 Foaming of P_LLA and $P_{DL}LA$ without the Addition of Additive 6
1.2.3.3 Foaming of P_LLA with the Addition of Additive 9
1.3 Solubility Modeling of TrifluoropropylPOSS in Supercritical Carbon Dioxide 10
1.3.1 Importance of Solubility Data 10
1.3.2 Solubility Modeling Methods 10
1.3.3 Semi-empirical Density-based Models 11
1.3.3.1 Chrastil Model 11
1.3.3.2 Chrastil Modified by Wang Model 12
1.3.3.3 Del Valle and Aguilera Model 13
1.3.3.4 Kumar and Johnston Model 13
1.3.3.5 Mendez-Santiago and Teja Model 14
1.3.3.6 Bartle Model 14

1.3.4 Solubility Data Correlation with Semi-Empirical Density-based Models 15
1.4 Aim of This Study 15
2 EXPERIMENTAL 17
2.1 Porous Film Preparation with $ScCO_2$ Processing 17
2.1.1 Materials 17
2.1.2 Polymer Film Preparation 18
2.1.3 Foaming Process of Polymers with $scCO_2$ 19
2.1.4 Surface Modification with Plasma Etching 21
2.1.5 Characterization of the Films 21
2.1.5.1 Differential Scanning Calorimetry 21
2.1.5.2 Scanning Electron Microscopy and Energy-dispersive X-ray Spectroscopy 21
2.1.5.3 Micro Computed Tomography 22
2.1.5.4 Mechanical Test (Hardness) 22
2.1.6 Drug Release Studies 23
2.1.6.1 Preparation of Phosphate Buffered Saline (PBS) solution 23
2.1.6.2 Drug Loading 23
2.1.6.3 Drug Release Studies 23
3 RESULTS and DISCUSSION 25
3.1 Porous Film Preparation with $scCO_2$ Processing 25
3.1.1 Pore Morphology 25
3.1.1.1 Effect of Saturation Temperature 25
3.1.1.2 Effect of Saturation Pressure 33
3.1.1.3 Effect of Venting Rate 37
3.1.1.4 Effect of Saturation Time 39
3.1.1.5 Effect of Type and Concentration of Additive 44
3.1.2 3D Reconstruction of the Samples and Porosity Calculation 49
3.1.3 Extraction of the TFPOSS 53
3.1.4 Hardness of the Films 56
3.1.5 Differential Scanning Calorimetry (DSC) Results 59
3.1.6 Drug Releases Studies 63

3.1.6.1 Drug Loading 63
3.1.6.2 Release Studies 65
3.2 Solubility Modelling Result 67
4 CONCLUSIONS 75
REFERENCES 79
APPENDICES
A. PARTICLE SIZE DISTRIBUTION OF THE ADDITIVES 87
B. CALIBRATION CURVE 89
C. EDX MAPPING RESULT 91
D. DSC THERMOGRAM 93
E. CORRELATED TFPOSS SOLUBILITY WITH DIFFERENT MODELS 97
F. SELF-CONSISTENCY TESTS OF TRIFLUOROPROPYLPOSS WITH DIFFERENT MODELS 101
F.1 Chrastil Model 101
F.2 Del Valle and Aguilera Model 102
F.3 Kumar and Johnston Model 103
F.4 Mendez-Santiago and Teja Model 104
F.5 Bartle Model 105
G. CALCULATION OF TFPOSS SOLUBILITY 107

LIST OF TABLES

TABLES

Table 1.1 Critical properties of some SCF 2
Table 2.1. Polymer film compositions 19
Table 3.1 Summary of processing conditions and resulting pore size for all sample. 48
Table 3.2 Quantification of EDX analysis result for samples processed at 373 K .56
Table 3.3 Indentation Hardness of the Films 57
Table 3.4 DSC results of the samples.....60
Table 3.5 Solubility data for TrifluoropropylPOSS at 308 K and 323 K.....68
Table 3.6 *AARD* and parameters of all the models for trifluoropropylPOSS.....69
Table 3.7 *AARD* and parameters for C-W model fitted separately for each temperature for trifluoropropylPOSS 72
Table G.1 Parameters for C-W model.....107
Table G.2 Parameters for TFPOSS mol fraction calculation 108

LIST OF FIGURES

FIGURES

Figure 1.1 P-T phase diagram 1

Figure 1.2 Summary of foaming process of $P_{DL}LA$ with M_w = 52000 $g.mol^{-1}$ with supercritical carbon dioxide. (a) Starting granular polymers, (b) Plasticized polymer, (c) Supercritical phase transition, (d) Liquefied polymer melt, (e) Foaming of the polymer, (f) Final structure. 4

Figure 2.1 Chemical structure of P_LLA 18

Figure 2.2 Chemical structure of (a) TFPOSS, (b) OMPOSS 18

Figure 2.3 Experimental setup for the foaming process 20

Figure 3.1 SEM micrographs of the cross-section of the processed thin P_LLA film samples processed at *SP* = 20.7 MPa, *Stime* = 2 h, *VR* = 10.3 $MPa.min^{-1}$ and *ST* = (1) 313 K, (2) 333 K; (a) 1000x magnification, (b) 10000x magnification, (3) 373 K; (a) 500x magnification, (b) 10000x magnification and (4) 393 K; (a) 250x magnification, (b) 10000x magnification, (c) 100x magnification (surface) 26

Figure 3.2 SEM micrographs of the cross-section of the processed thin P_LLA-10T film samples processed at *SP* = 20.7 MPa, *Stime* = 2 h, *VR* = 10.3 $MPa.min^{-1}$ and *ST* = (1) 313 K, (2) 333 K, (3) 373 K; (a) 1000x magnification, (b) 10000x magnification, and (4) 393 K; (a) 250x magnification, (b) 10000x magnification, (c) 100x magnification (surface) 29

Figure 3.3 (a) SEM micrographs of TFPOSS particles' agglomeration on the cross-section of the P_LLA-10T film processed at *SP* = 20.7 MPa, *Stime* = 2 h, *VR* =10.3 $MPa.min^{-1}$ and *ST* = 313 K, 5000x magnification (b) EDX analysis of the highlighted part 31

Figure 3.4 SEM micrographs of the cross-section of the processed thin PLLA film samples processed at *Stime* = 2 h, *VR* = 10.3 MPa.min^{-1}, (1.a.) *ST* = 313 K, *SP* = 20.7 MPa; 1000x magnification, (1.b.) *ST* = 313 K, *SP* = 10.3 MPa; 1000x magnification, (2.a.) *ST* = 373 K, *SP* = 20.7 MPa; 500x magnification, (2.b.) *ST* = 373 K, *SP* = 10.3 MPa; 1000x magnification. 34

Figure 3.5 SEM micrographs of the cross-section of the processed thin PLLA-10T film samples processed at *Stime* = 2 h, *VR* = 10.3 MPa.min^{-1} (1) *ST* = 313 K, *SP* = 20.7 MPa, (2) ST = 313 K, SP = 10.3 MPa, (3) ST = 373 K, *SP* = 20.7 MPa, (4) ST = 373 K, SP = 10.3 MPa; (a) 1000x magnification, (b) 10000x magnification 35

Figure 3.6 SEM micrographs of the cross-section of the processed thin PLLA film samples processed at *Stime* = 2 h, *SP* = 20.7 MPa, *ST* = 373 K, and *VR* = (a) 10.3 MPa.min^{-1}; 500x magnification (b) 0.2 MPa.min^{-1}; 20000x magnification 38

Figure 3.7 SEM micrographs of the cross-section of the processed thin PLLA-10T film samples processed at *Stime* = 2 h, *SP* = 20.7 MPa, *ST* = 373 K, and *VR* = (a) 10.3 MPa.min^{-1} (b) 0.2 MPa.min^{-1}; 10000x magnification 39

Figure 3.8 SEM micrographs of the cross-section of the processed thin PLLA film samples processed at *SP* = 20.7 MPa, *ST* = 313 K, *VR* = 10.3 MPa.min^{-1} and *Stime* = (1) 2 h, (2) 24 h; (a) 1000x magnification (b) 10000x magnification 41

Figure 3.9 SEM micrographs of the cross-section of the processed thin PLLA film samples processed at *SP* = 20.7 MPa, *ST* = 373 K, *VR* = 10.3 MPa.min^{-1} and *Stime* = (1) 2 h, (2) 24 h; 500x magnification 42

Figure 3.10 SEM micrographs of the cross-section of the processed thin PLLA-10T film samples processed at *SP* = 20.7 MPa, *VR* = 10.3 MPa.min^{-1} and (1) *ST* = 313 K, *Stime* = 2 h, (2) *ST* = 313 K, *Stime* = 24 h, (3)

ST = 373 K, *Stime* = 2 h, (4) *ST* = 373 K, *Stime* = 2 h; (a) 1000x magnification (b) 10000x magnification.....42
Figure 3.11 SEM micrographs of the cross-section of the processed thin P_LLA-30T film samples processed at *SP* = 20.7 MPa, *ST* = 313 K, *VR* = 10.3 MPa.min^{-1} and *Stime* = (1) 2 h, (2) 24 h; (a) 1000x magnification (b) 10000x magnification.....44
Figure 3.12 SEM micrographs of the cross-section of the processed thin P_LLA and P_LLA with additive film samples processed at *SP* = 20.7 MPa, *ST* = 313 K, *VR* = 10.3 MPa.min$^{-1,}$ *Stime* = 2 h and (1) 10% TFPOSS addition, (2) 30% TFPOSS addition (3) 30% OMPOSS addition; (a) 1000x magnification (b) 10000x magnification.....45
Figure 3.13 EDX mapping results of unprocessed films; (1) Fluorine map, (2) Silicon map; (a) P_LLA-10T, (b) P_LLA-30T. 47
Figure 3.14 µCT analysis of the film processed at *SP* = 20.7 MPa, *Stime* = 2 h, and *VR* = 10.3 MPa.min^{-1}; µCT images of the sample (first column); three-dimensional µCT reconstruction (second column); photograph of the samples (third column) 50
Figure 3.15 EDX analysis result of P_LLA-30T films (a) unprocessed, (b) after processing with *SP* = 20.7 MPa, *ST* = 313 K, *VR* = 10.3 MPa.min$^{-1,}$ *Stime* = 2 h (c) after processing with *SP* = 20.7 MPa, *ST* = 313 K, *VR* = 10.3 MPa.min^{-1}, *Stime* = 24 h 54
Figure 3.16 EDX analysis result of P_LLA-10T films (a)unprocessed, (b)after processing with *SP* = 20.7 MPa, *ST* = 373 K, *VR* = 10.3 MPa.min$^{-1,}$ *Stime* = 2 h (c) after processing with *SP* = 20.7 MPa, *ST* = 373 K, *VR* = 10.3 MPa.min$^{-1,}$ *Stime* = 24 h.....55
Figure 3.17 Indentation hardness of the samples.....58
Figure 3.18 Crystallinity of P_LLA samples before and after $scCO_2$ processing.....61
Figure 3.19 Crystallinity of P_LLA-10T samples before and after $scCO_2$ processing.....62

Figure 3.20 Crystallinity of P_LLA-30T samples before and after $scCO_2$ processing 62
Figure 3.21 SEM micrographs of the surface of the processed thin P_LLA-30T film samples processed at *SP* = 20.7 MPa, *ST* = 313 K, *VR* = 10.3 $MPa.min^{-1}$ and *Stime* = 2 h; (1) before plasma application (2) after plasma application (a) 1000x magnification (b) 10000x magnification 64
Figure 3.22 Picture of drop of drug solution on top of the P_LLA-30T films (1) before plasma application, (2) after plasma application 64
Figure 3.23 Drug release result of Ceftriaxone Sodium with using different processed films. 66
Figure 3.24 Experimental solubility data for trifluoropropylPOSS and the correlations with semi-empirical models at 308 K. 67
Figure 3.25 Experimental solubility data for trifluoropropylPOSS and the correlations with semi-empirical models at 323 K. 69
Figure 3.26 Linear plot of the experimental solubility data of TFPOSS and the C-W model 70
Figure 3.27 Linear plot of the experimental solubility data of TFPOSS and the C-W model fitted separately for each temperature 71
Figure 3.28 Self-consistency plot of trifluoropropylPOSS, by using the C-W model. 73
Figure A.1 Particle size distribution of TFPOSS with average size of 648.5nm 87
Figure A.2 Particle size distribution of OMPOSS with average size of 455.1nm .. 88
Figure B.1 Calibration curve of ceftriaxone sodium 89
Figure C.1 EDX mapping results of P_LLA-10T film samples processed at *ST* = 313 K, *SP* = 20.7 MPa, *VR* = 10.3 $MPa.min^{-1}$ and *Stime* = (1) 2 h, (2) 24 h; (a) Fluorine map, (b) Silicon map 91
Figure D.1 First heating DSC thermogram of the neat P_LLA films processed at different conditions 93

Figure D.2 First heating DSC thermogram of the PLLA-10T films processed at different conditions. 94
Figure D.3 First heating DSC thermogram of the PLLA-30T films processed at different conditions. 95
Figure E.1 The correlated solubility data of trifluoropropylPOSS with different models, (a) Chrastil, (b) d-A, (c) K-J, (d) MST, (e) Bartle models 97
Figure F.1 Self-consistency tests of trifluoropropylPOSS with Chrastil model ... 101
Figure F.2 Self-consistency tests of trifluoropropylPOSS with del Valle and Aguilera model 102
Figure F.3 Self-consistency tests of trifluoropropylPOSS with Kumar and Johnston model 103
Figure F.4 Self-consistency tests of trifluoropropylPOSS with Mendez-Santiago and Teja model 104
Figure F.5 Self-consistency tests of trifluoropropylPOSS with Bartle model 105

NOMENCLATURE

SCF	: Supercritical fluid
T	: Temperature
P	: Pressure
T_c	: Critical temperature
P_c	: Critical pressure
CO_2	: Carbon dioxide
$scCO_2$	: Supercritical carbon dioxide
PLA	: Poly(lactic acid)
P_LLA	: Poly(L-lactic acid)
P_{DL}LA	: Poly(D,L-lactic acid)
TFPOSS	: Trifluoropropyl polyhedral oligomeric silsesquioxane
OMPOSS	: Octamethyl polyhedral oligomeric silsesquioxane
PB	: Phosphate buffer
PBS	: Phosphate buffered saline
T_g	: Glass transition temperature
T_m	: Melting temperature
ST	: Saturation temperature
SP	: Saturation pressure

Stime : Saturation time

VR : Venting rate

M_w : Molecular weight

ρ_1 : Density of $scCO_2$

y_2 : Solubility of solute in the $scCO_2$ in mol fraction

AARD : Absolute average relative deviation

CHAPTER 1

INTRODUCTION

1.1 Basic Principles of Supercritical Fluid

Supercritical fluid (SCF) can be defined as substance that exist above its critical temperature (T_c) and critical pressure (P_c). In nature substance exists in one of the three phases; solid, liquid, or gas and are separated by phase boundaries. Unlike these three phases, in supercritical fluid there is no existence of distinct liquid or gas phase (Figure 1.1). The properties of supercritical fluid is unique, having density and solvent power similar to liquid phase but diffusivity and mass transfer similar to gas phase. Additionally those properties can be fine-tuned by changing the temperature and/or pressure of the SCF [1].

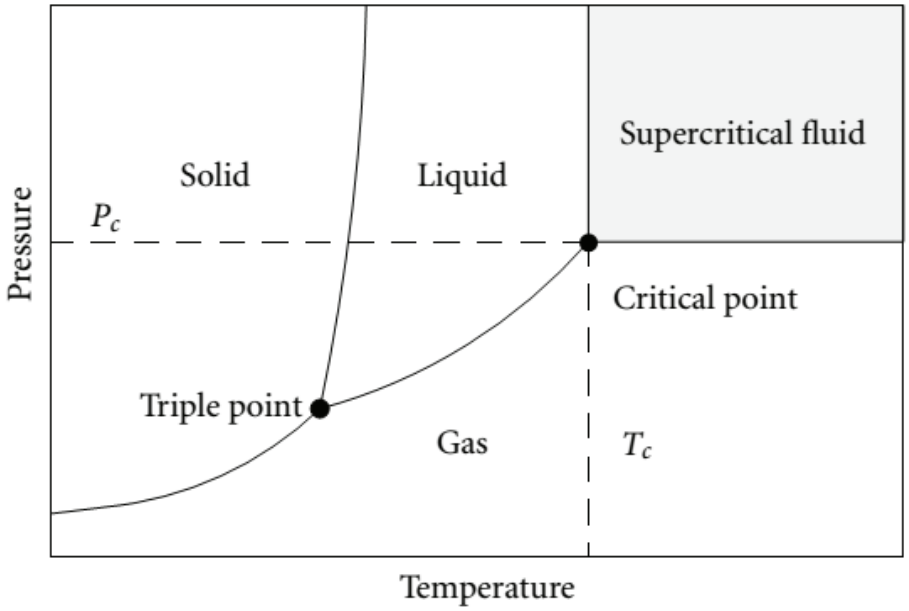

Figure 1.1 P-T phase diagram

Critical properties of some SCF is given in Table 1.1. The choice of supercritical fluid to be used greatly depends on the targeted application. Among those available SCF, carbon dioxide is the most desirable and most commonly used because it is inert, non-flammable, non-toxic, and widely available. Its application is not harmful to the environment and human health. Relatively low critical temperature and pressure of CO_2 (T_c = 304.2 K, P_c = 7.4 MPa) also make it suitable to process thermally labile materials. Additionally carbon dioxide also received the generally recognized as safe (GRAS) solvent status. These advantages allow supercritical carbon dioxide ($scCO_2$) to be used as an alternative solvent for greener material processing including extraction, chromatography, cleaning, and polymer processing [2–5].

Table 1.1 Critical properties of some SCF

Name	Critical Temperature (T_c) (K)	Critical Pressure (P_c) (MPa)
Carbon dioxide	304	7.4
Water	647	22.1
Ethane	305	4.9
Propane	370	4.3
Xenon	290	5.8
Ammonia	406	11.4
Fluoroform	299	4.9

1.2 Porous Poly(L-lactic Acid) (P_LLA) Preparation with Supercritical Carbon Dioxide ($scCO_2$) Processing

1.2.1 Poly(lactic acid) (PLA)

The interest to replace conventional petroleum-based polymers, for both industrial and biomedical applications, has increased significantly in the recent years due to their non-degradable properties which cause environmental concerns [6,7]. Poly(lactic acid) (PLA), a biobased polymer, has shown a great potential as a replacement for the petroleum-based polymers for both application areas. PLA foam

is a notable substitute for polystyrene (PS) foam in various commodity applications including thermal insulation, packaging and plastic utensils due to their similar mechanical properties [8–12]. Additionally, PLA is also a widely used polymer in biomedical applications, such as scaffolds for bone tissue engineering, artificial vasculature and matrix for controlled release drug delivery system due to its biocompatible and biodegradable nature, thermal plasticity and suitable mechanical properties [13–20].

1.2.2 PLA processing with $scCO_2$ for Biomedical Application

$scCO_2$ is known as a plasticizer for many polymers, which allows its uses as a foaming agent for polymers, including PLA to produce porous structure. Conventional processes to produce porous structure include solvent casting-particle leaching, freeze-drying-particle leaching, electrospinning, thermally induced phased separation and many others which requires the use of organic solvent. These fabrication processes consequently require further purification process for the removal of the organic solvent. Sometimes complete removal might not be possible, and this is not preferable for biomedical applications. Additionally some of these processes are performed at low or high temperatures, which may not be suitable for thermally labile material. $scCO_2$ processing overcome both of these disadvantages of conventional processes and thus is a good candidate as an alternative process [3,21].

Figure 1.2 shows the summary of foaming process of poly(D,L-lactic acid) ($P_{DL}LA$) with M_w = 52000 $g.mol^{-1}$ with supercritical carbon dioxide, taken with CCD camera [22]. In general, in the foaming process of a polymer with $scCO_2$, the polymer is loaded with $scCO_2$ at high pressure (Figure 1.2.a). Due to the plasticizing property of $scCO_2$, the glass transition temperature (T_g) of the polymer decreases, which allows the polymer to be processed at temperatures lower than its T_g (Figure 1.2.b,c.d). When $scCO_2$ is released, the pressure drop reduces the solubility of $scCO_2$ in the polymer which causes supersaturation and induces nucleation of bubbles. These nuclei then grow to form the pores (Figure 1.2.e,f) [3,22–26].

In supercritical carbon dioxide processing of polymer, there are several important processing parameters, which are saturation temperature (*ST*), saturation pressure (*SP*), saturation time (S*time*), and venting rate of $scCO_2$ (*VR*). *ST*, *SP* and *Stime* are the temperature, pressure and time in which the polymer is allowed to be in contact with the $scCO_2$ inside the high pressure vessel. The "saturation" word is the common term used in the field because during the process at this temperature, pressure and time, the $scCO_2$ is allowed to be in contact and diffuse to the polymer, thus it is allowed to saturate the polymer.

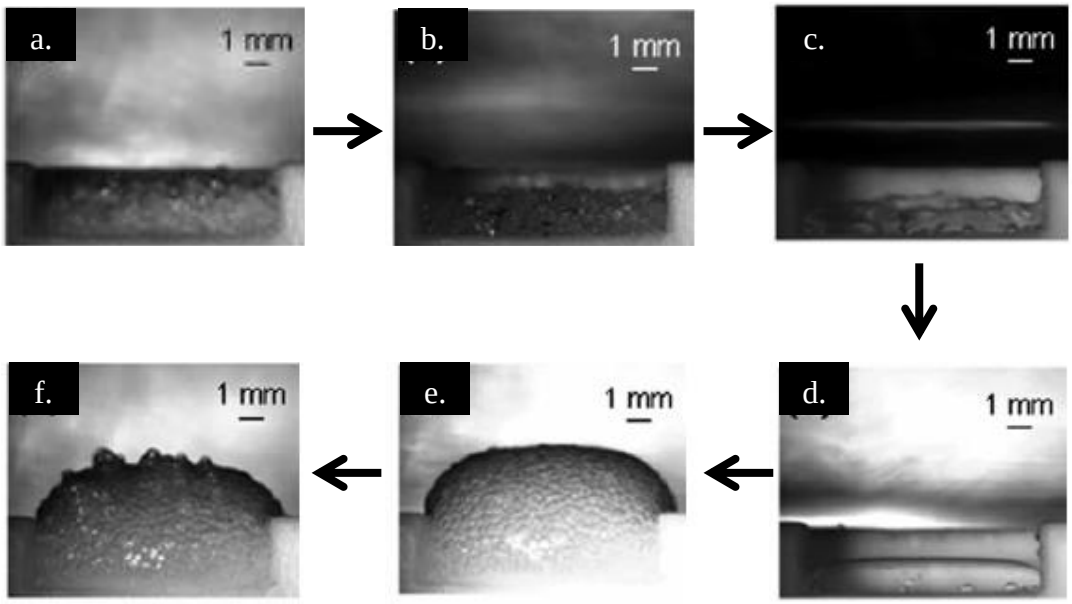

Figure 1.2 Summary of foaming process of $P_{DL}LA$ with M_w = 52000 $g.mol^{-1}$ with supercritical carbon dioxide. (a) Starting granular polymers, (b) Plasticized polymer, (c) Supercritical phase transition, (d) Liquefied polymer melt, (e) Foaming of the polymer, (f) Final structure.

1.2.3 Literature Study on PLA and $scCO_2$ System

1.2.3.1 Solubility of P_LLA and $P_{DL}LA$ in $scCO_2$

The critical parameters in the foaming process are concentration of CO_2 in the polymer and the venting rate of CO_2 [27]. Venting rate is one of the process parameters that can be modified, while solubility of $scCO_2$ in a polymer is dependent on both the molecular structure and morphology (crystallinity) of the polymer [28]. The properties of the PLA depend on the ratio of the L- and D-isomers. Isotactic PLA homopolymer, poly(L-lactic acid) (P_LLA), is a semicrystalline polymer with the highest T_m (melting point), T_g and crystallinity among all PLA types. Poly(D,L-lactic acid) ($P_{DL}LA$), which contain both L- and D-isomers has lower T_m, T_g and crystallinity compared to P_LLA. As the D-content increases, all of these properties decrease. $P_{DL}LA$ becomes completely amorphous when the D-content is higher than 12-15% [29,30]. Based on these facts, $scCO_2$ would have different solubility in P_LLA and $P_{DL}LA$.

Several study has been conducted to measure the solubility of CO_2 in both P_LLA and $P_{DL}LA$. It has been found that the main intermolecular interaction between the polymer chain and CO_2 is the Lewis acid-base interaction between the carbonyl groups of the PLA and the CO_2 molecules. [31]. Oliveira et al. [32] conducted a study on measuring the solubility of CO_2 in $P_{DL}LA$ by using quartz crystal microbalance (QCM). The measurement was done between temperature of 303 and 323 K and pressures up to 5 MPa. They obtained that CO_2 has higher solubility in $P_{DL}LA$ with 20% D-content (fully amorphous) than $P_{DL}LA$ with 2% D-content (semi crystalline). In a more recent works, Pini et al. [33] also worked on the measurement of solubility of CO_2 in $P_{DL}LA$ by using a magnetic suspension balance. The experiment was done at 308 K, with pressure ranging from 3 to 20 MPa, which means the measurement was done both in the gaseous and supercritical state of the CO_2. They reported that the solubility of $scCO_2$ in $P_{DL}LA$ with M_w = 52000 $g.mol^{-1}$ is more than 50 wt% at 308 K and 20 MPa, and they mentioned that the molecular weight of the polymers has small effect on the resulting solubility.

Measurement of solubility of $scCO_2$ in P_LLA was studied by Aionicesei et al. [34]. The polymer used had M_w = 42000 $g.mol^{-1}$, and the measurement method was done with magnetic suspension balance, similar to what was done by Pini et al. The measurement was done at temperature ranging from 308 to 323 K and pressure from 10 to 32 MPa. This measurement range lies only in the supercritical region of the CO_2. They obtained that the solubility of supercritical carbon dioxide in the P_LLA increases as temperature decreases and as pressure increases. Additionally they obtained that diffusivity of supercritical carbon dioxide in the P_LLA increases as temperature of the system increases. Finally, comparing with the finding of Pini et al at 313 K and 20 MPa, Aionicesei et al obtained the solubility of $scCO_2$ in P_LLA to be 39 wt% by which is lower than solubility of $scCO_2$ in $P_{DL}LA$ (50 wt%) at the same condition. Due to the lower solubility of $scCO_2$ in P_LLA with respect to $P_{DL}LA$, foaming of pure P_LLA with $scCO_2$ is not preferable compared to $P_{DL}LA$. The reason for this is because much higher pressures are required to achieve the same concentration of CO_2 dissolved in the P_LLA matrix, compared with $P_{DL}LA$.

1.2.3.2 Foaming of P_LLA and $P_{DL}LA$ without the Addition of Additive

Several works about foaming of PLA, both P_LLA and $P_{DL}LA$ are available in the literature. In this part both P_LLA and $P_{DL}LA$ studies available will be described to compare the foamability of both polymers.

White et al. [24] worked on foaming of $P_{DL}LA$ with supercritical carbon dioxide. The studied parameters were the effect of M_w of $P_{DL}LA$ and the $scCO_2$ venting rate (*VR*), in the range of 15000-57000 $g.mol^{-1}$ and 0.39-2.32 $MPa.min^{-1}$, respectively. The scaffold fabrication was done using the raw material directly without any sample preparation. The polymer was placed in a Teflon mold with height and diameter of 10 mm, and then put inside the high pressure vessel. The processing temperature was 308 K. They observed that $P_{DL}LA$ with M_w = 57000 $g.mol^{-1}$, the one with highest molecular weight had the smallest pores and most homogeneous pore distribution.

On the other hand, the slower *VR* resulted in wider pore distributions with larger and more interconnected pores.

The effects of saturation temperature (*ST*), saturation pressure (*SP*), saturation time (*Stime*), and venting rate (*VR)* on $P_{DL}LA$ foaming were studied by various groups. Tai et al. [35] studied these parameters in the range of 278-328 K, 6-15 MPa, 1-4 h and 0.19-2.3 $MPa.min^{-1}$, respectively. The foaming process was done directly with the raw polymer without any sample preparation, and was done by using Teflon mold, similar with the work done by White et al. [24]. The targeted application is for scaffold preparation for tissue engineering applications. They observed that the pore size of the scaffold can be changed by changing the processing conditions. The effect of each processing conditions were obtained as follows; high *ST*, low *SP*, short *Stime*, and slow *VR* lead to larger pores. At all conditions the pores are in hundreds of micrometer size. A more recent work was done by Rouholamin et al. [36] with similar objective with the work done by Tai et al. [35]. The polymer used was $P_{DL}LA$ with M_w = 406000 $g.mol^{-1}$. The main difference with the work done by Tai et al. is that Rouholamin et al. processed the raw material first to form cylindrical polymer disk before processing with $scCO_2$, while Tai et al directly use the raw material as it is, in granular form. The studied processing parameters are *ST*, *SP*, *Stime*, and *VR* in the range of 305-323 K, 10-18 MPa, 0.5-2 h, and 1.4-14 $MPa.min^{-1}$, respectively. Rouholamin et al also observed that higher *SP* leads to smaller pores higher *ST* lead to larger pores, and slower *VR* lead to larger pores. However, they observed different effect of *Stime* on the pore size. Tai et al. observed that longer *Stime* lead to smaller pores, while Rouholamin et al. found the longer *Stime* lead to formation of larger pores. Tai et al. believed that longer *Stime* lead to more homogeneous distribution of CO_2 in the polymer matrix and this lead to formation of more uniform and smaller pores. However Rouholamin et al. explained that longer *Stime* lead to more amount of CO_2 in the polymer matrix, which leads to higher expansion of pores in the structure. In addition to the fabrication of the porous scaffold, Rouholamin et al. also did cell culture study where bone cells were introduced to the scaffolds that has pore

size in the range of 200-500 µm. They observed that the scaffold is indeed biocompatible, cell number increase over time and no toxicity effect was observed.

In the recent works of P_LLA foaming with $scCO_2$, Yu et al. [37] worked on the processing of P_LLA films with supercritical carbon dioxide at *ST* = 313 K, *SP* = 20 MPa, *Stime* = 1 h and a venting time (*Vtime*) of 40 s. The P_LLA used has M_w = 11300 $g.mol^{-1}$. Yu et al also first processed the raw material to produce P_LLA films before processing with $scCO_2$. The film preparation was done by solvent casting method. After processing at *ST* = 313 K, *SP* = 20 MPa, and *Stime* = 1 h they observed that there was no formation of pores occurred on the cross-section of the P_LLA films processed. Additionally, they also observed decrease in crystallinity degree of the film after $scCO_2$ processing.

Another work was also done by Lopez-Periago et al. [38] to process P_LLA with M_w = 350000 $g.mol^{-1}$ with $scCO_2$. The raw polymer was processed directly as it is in pellet form without any sample preparation. The parameters of the $scCO_2$ processing were *SP* = 12 MPa, *ST* = 323-393 K and *Stime* = 24 h. Similar with what was obtained by Yu et al, Lopez-Periago et al also observed that there were no pore formation on the P_LLA films after processing at *SP* = 12 MPa, *ST* = 323-393 K and *Stime* = 24 h. Despite no formation of pores, they observed change in the thermal properties of the film. The crystallinity of the film increased by 4% after processing at 323 K, and further increase by 15% was obtained when the film was processed at 393 K.

An extensive study was also done by Kiran [29] on the foaming of P_LLA with M_w = 127000 $g.mol^{-1}$ with $scCO_2$. He performed the supercritical processing directly by using the raw material, which was in powder form, with the help of a metal molds. The most important observation that he obtained was that the lowest *SP* that can be reached to induce foaming was 20 MPa with *ST* at least 392 K. He also observed that it is possible to produce pores at lower temperature, however the pressure has to be increased. He found the value to be 353 K as the lowest *ST* needed for foaming with *SP* at least 41 MPa. In both cases, the *Vtime* was less than 10 s, which means very

fast venting rate. At lower *ST* and *SP* than this limit, he observed no formation of pores.

1.2.3.3 Foaming of P_LLA with the Addition of Additive

As can be seen from the previous section, P_LLA is more difficult to process in order to produce porous structure compared to the $P_{DL}LA$ counterpart. To process P_LLA much higher processing temperature and pressure is needed. The main reason for this is due to the lower solubility of $scCO_2$ in P_LLA compared to $P_{DL}LA$, and also due to the high crystallinity of P_LLA. During the $scCO_2$ processing, the $scCO_2$ is only able to diffuse and initiate the pore nucleation in the amorphous part of the polymer, thus presence of crystalline region will hinder the foaming process. To overcome this, it is possible to improve the foamibility of P_LLA either by increasing temperature and pressure or by using micro- and nano-sized additives [10]. Several works has been done by using additives to improve the foamibility of P_LLA. Mathieu et al. [39] tried to improve the foamibility and strength of the P_LLA foams by adding ceramic powders, hydroxyapatite and β-tricalcium phosphate to the polymer. The polymer blend was prepared by melt extrusion to ensure homogeneous dispersion of the ceramic powders. The studied processing parameters were *SP* = 10-25 MPa, *ST* = 468 K, *Stime* = 10 mins, *VR* = 0.37-1.19 $MPa.sec^{-1}$ and filler concentration between 0-30 wt%. After processing they observed that the neat P_LLA foams without the addition of additive produces interconnected pores with size of 200-400 μm and porosity between 78-92%. With the addition of the filler more heterogeneous pore structure with more closed pores compared to neat P_LLA was produced. However the modulus and compressive strength of the foam were improved up to 250 MPa and 6 MPa with the addition of filler up to 10 wt%, respectively. Additionally biocompatibility study also showed that both neat and composite P_LLA scaffolds were biocompatible, thus can be used for tissue engineering application.

In the recent work by Delabarde et al. [40], hydroxyapatite was also used to improve the porosity and mechanical structure of the P_LLA scaffold. The P_LLA used has M_w = 150000 $g.mol^{-1}$ and prior to the foaming process the composite of P_LLA and

hydroxyapatite was prepared by melt-extrusion to ensure homogeneity of the additive distribution. The studied processing parameters were *SP* = 10-25 MPa, *ST* = 438-448 K, *VR* = 0.25-2.11 MPa.sec^{-1} and filler concentration between 0 - 4.17 wt%. They observed that with the addition of the additive, smaller pore size with more homogeneous structure were obtained, which was in contrast with the study of Mathieu et al. [39]. Additionally, with the addition of up to 4.17 vol% hydroxyapatite, they did not observe any significant change on the mechanical properties of the polymer. For the effect of processing parameters, they observed that higher *SP* leads to smaller pores, higher *ST* lead to larger pores but less uniform structure, and slower *VR* lead to smaller pores size.

1.3 Solubility Modeling of TrifluoropropylPOSS in Supercritical Carbon Dioxide

1.3.1 Importance of Solubility Data

To design the optimum condition and parameters for SCF processes, solubility data of the materials in SCF and knowledge of phase behavior of the systems are needed. However, experimental studies to obtain the accurate solute solubility data in SCF and phase behavior of the systems is a time consuming and tedious process. Therefore there is limited availability of solute solubility data in SCF in the literature. To overcome this problem, mathematical modeling of the solubility data has gained a lot of interest to predict the solute solubility at a wider range of conditions [41–43].

1.3.2 Solubility Modeling Methods

There are two main approaches that are mainly used to correlate the solubility data. One is equation of state models (EOS) which are based on theoretical models, and the other is semi-empirical density-based models. The correlation of solubility data with EOS require the information of pure component parameters of the solutes such as critical pressure, critical temperature, vapor pressure and accentric factor [44,45]. These parameters are usually not readily available for many compounds with

complex structures, and thus have to be predicted by other methods such as group contribution techniques. The parameter estimation methods for complex molecules, such as one with irregular molecules are usually unreliable [46]. Because of the inaccuracies introduced by these parameter predictions, errors are also produced by the EOS correlation [47,48]. Additionally, due to the availability of several mixing rules for calculation of the mixture parameters, the selection of the appropriate mixing rule would also affect the accuracy of the mixture phase calculations with EOS [49]. Unlike EOS correlation, the information of solute properties is not required by semi-empirical density-based models. Semi empirical density-based models relate the solvent density or the logarithm of the solvent density with the logarithm of the solubility data in a linear fashion. Only available parameters such as temperature, pressure and density of the SCF is required in this approach. Because of this, semi-empirical models are widely used for the correlation of solute solubility in SCF. The only disadvantage is that these models generally work only in certain range of temperature and pressure, generally in the pressure range of 10 to 30 MPa. The model is not suitable for extreme regions, where the density of the solvent approaches those of liquids [50].

1.3.3 Semi-empirical Density-based Models

There are several semi-empirical density-based models that consider the effect of both temperature and pressure to correlate the experimental solubility data.

1.3.3.1 Chrastil Model

One of the most commonly used model is proposed by Chrastil [51]. This model is based on the existence of solvato complex molecule $AB_{k,}$ consisted of one molecule of solute A with k molecules of solvent B, which is in equilibrium with the gas.

The Chrastil equation takes the temperature (T) and density (ρ) as individual terms and is expressed in the following form:

$$\ln(S_2) = a\, ln(\rho_1) + \frac{b}{T} + c$$

where a is an association number, b is a parameter that depends on the heat of solvation and the heat of vaporization of the solute, and c is a parameter that depends on the molecular weights of the solute and $scCO_2$. 1 denotes the $scCO_2$ phase and 2 denotes the solute phase. The b and c parameters are expressed as:

$$b = \frac{\Delta H}{R}$$

$$c = \ln(MW_2 + kMW_1) + q - kln(MW_1)$$

where ΔH is the total of solvation and vaporization enthalpy, R denotes ideal gas constant, and MW_2 and MW_1 are the molecular weight of solute, 2, and solvent, 1, respectively.

S_2 is correlated with mole fraction (y_2) with the following equation:

$$S_2 = \frac{\rho_1 MW_2 y_2}{MW_1(1 - y_2)}$$

1.3.3.2 Chrastil Modified by Wang Model

Due to the limitations of Chrastil's model, such as inapplicability to high solubility region (more than 100-200 $kg.m^{-3}$) and low applicable temperature range [52], some modifications were proposed. One of these modified models is the one proposed by Wang, which was derived from the solvation theory, phase equilibrium rules and high-pressure reaction equilibrium constant [44]. The proposed equation contains four parameters and is given as:

$$\ln(y_2) = a + \frac{b}{T} + c\,\rho_1 + d\,\ln(P)$$

Where y_2 represents the mol fraction of the solute. Despite being modification of Chrastil model, the definition of each parameter on the Chrastil modified by Wang model is not similar with the Chrastil model. Here the parameter a depends of the

vapor pressure and solvation entropy. The value of b depends on the vapor pressure of the solute, solvation enthalpy and the molar volume, the constant c is related to the association number (k), solute second virial coefficient (B_{22}) and mixed second virial coefficient (B_{12}), and lastly the parameter d is related to the association number only.

1.3.3.3 Del Valle and Aguilera Model

Another modification was proposed by Del Valle and Aguilera to the Chrastil's equation, and this modification was especially targeted for the correlation of solubility of vegetable oils in supercritical carbon dioxide [53]. The modification was proposed to compensate the variation of enthalpy of vaporization ΔH_{vap} with temperature. The equation is:

$$\ln(S_2) = a\, ln(\rho_1) + \frac{b}{T} + \frac{c}{T^2} + d$$

Where S_2 has the same definition as the Chrastil model, and the value of ΔH_{vap} is given as:

$$\Delta H_{vap} = R\left(b + \frac{2c}{T}\right)$$

The model proposed by Del Valle and Aguilera can be applied to a wide range of temperature, between 293-353 K and pressure from 15 MPa up to 88 MPa.

1.3.3.4 Kumar and Johnston Model

Another density-based model was proposed by Kumar and Johnston [54] and was based on the linear relationship between ln y_2 and ρ_1 similar to the Chrastil model and is expressed as:

$$\ln(y_2) = a + \frac{b}{T} + c\rho_1$$

The parameter b has similar definition with the parameter in Chrastil model, which is related to the solvation and evaporation enthalpy, and is given as:

$$b = \frac{\Delta H}{R}$$

1.3.3.5 Mendez-Santiago and Teja Model

The density-based model proposed by Mendez-Santiago and Teja [55] for solid solubility is based on the theory of dilute solutions. This model is good to determine the consistency of solubility data at different temperatures. However the model requires the solute sublimation pressure data, which is in many times not available. To overcome this problem, Antoine equation was used for the solute sublimation pressure and the model was expressed as:

$$Tln(y_2 P) = a + b\rho_1 + cT$$

1.3.3.6 Bartle Model

The semi-empirical model proposed by Bartle et al. [56] is intended for solids and liquids with low volatility in supercritical carbon dioxide, and is given as:

$$\ln\left(\frac{y_2 P}{P_{ref}}\right) = a + \frac{b}{T} + c\left(\rho_1 - \rho_{ref}\right)$$

Here P_{ref} is standard pressure (P_{ref} = 0.1 MPa) and ρ_{ref} is reference density (ρ_{ref} = 700 kg.m^{-3}). ρ_{ref} is used to reduce the sensitivity of a and b due to the possible experimental error in the solubility data and to avoid the error due to extrapolation to zero density [57]. Parameter b is related to the enthalpy of vaporization of the solute, ΔH_{vap} and can be expressed by the following expression

$$\Delta H_{vap} = -Rb$$

where R is the gas constant.

1.3.4 Solubility Data Correlation with Semi-Empirical Density-based Models

The solubility data of trifluoropropylPOSS was correlated by using six different density-based semi-empirical models; Chrastil, Chrastil modified by Wang (C-W), del Valle and Aguilerra (d-A), Kumar and Johnston (K-J), Mendez-Santiago and Teja (MST), and Bartle. The parameters of each model were obtained with MATLAB by minimizing the *AARD* (absolute average relative deviation) as the objective function.

$$AARD\ (\%) = \frac{100}{N}\sum_{i}^{N}\left|\frac{y_2^p - y_2^e}{y_2^e}\right|$$

Where N is the number of data points, y_2^p is the predicted solubility data from the semi-empirical model and y_2^e is the experimentally obtained solubility data. The performance of each model is evaluated by comparing the respective *AARD*.

1.4 Aim of This Study

The aim of this study is to try to improve the processability of the high molecular weight semi crystalline P_LLA films with environmentally benign and non-toxic scCO_2 at lower *SP* and *ST* for biomedical applications such as drug delivery devices. The improvement was done by using a CO_2-philic additive, trifluoropropyl polyhedral oligomeric silsesquioxane (TFPOSS). Additionally, the effect of a non CO_2-philic additive, octamethyl polyhedral oligomeric silsesquioxane (OMPOSS) was also studied and the obtained data were compared. Lastly, the resulting porous films were also used for drug release study. The drug used in the study was Ceftriaxone Sodium (CS), an antibiotic. The drug solution was prepared by using phosphate buffered saline (PBS) solution and was loaded to the films with vacuum pressure cycle. The release study was then performed by immersing the loaded film in PBS solution and the release rate was obtained by measuring the drug concentration in the solution.

The additive particles can act as heterogeneous nucleating agents, or nucleators, which stimulate higher rate of cell nucleation by decreasing the free energy barrier

for nucleation and provide new sites where the formation of pores can take place [10,58,59]. The novelty of the study is that there has been no work on using a CO_2-philic additive during PLLA processing with $scCO_2$. Dilek [60] has recently shown that TFPOSS has significant solubility in $scCO_2$, up to 4.4 wt% at 10.7 MPa and 308 K due to the presence of CO_2-philic fluorinated hydrocarbons, in its structure. With high solubility of TFPOSS in $scCO_2$, it is hypothesized that the presence of the TFPOSS in the polymer matrix can improve the affinity of $scCO_2$ in the polymer composite. Thus, the amount of $scCO_2$ dissolved in the matrix can be increased compared to the neat PLLA at the same processing conditions. This, in turn, can improve the foaming performance.

In addition to this, the available experimentally obtained solubility data of TFPOSS was also modeled with six different semi-empirical density-based models, including Chrastil, Chrastil modified by Wang, Del Valle and Aguilera, Kumar and Johnston, Mendez-Santiago and Teja, and Bartle models. The model with the best prediction was then used to estimate the solubility of TFPOSS at the $scCO_2$ processing conditions which were in the vicinity of the experimental solubility data of TFPOSS in the literature.

CHAPTER 2

EXPERIMENTAL

2.1 Porous Film Preparation with $ScCO_2$ Processing

2.1.1 Materials

Poly(L-lactic acid) (P_LLA), a biodegradable and biocompatible polymer (M_w = 100000 $g.mol^{-1}$) was obtained from Polysciences, Inc (USA) in granular form and stored at room temperature (Figure 2.1). The additives for the polymer used in this study were trifluoropropylPOSS (TFPOSS) ($(C_3H_4F_3)_8(SiO_{1.5})_8$, M_w = 1193.15 $g.mol^{-1}$, Hybridplastics, USA) and octamethylPOSS (OMPOSS) ($C_8H_{24}O_{12}Si_8$, Mw = 536.96 $g.mol^{-1}$, Hybridplastics, USA) both in powder form and stored at room temperature (Figure 2.2). Particle size analysis (Malvern Zetasizer Nano ZS90, Malvern Instruments Ltd, England) was used to measure the size distribution of the additive by dispersing them in ethanol. The average size of TFPOSS was obtained to be 648.5 nm and the average size of OMPOSS was 455.1 nm and the particle size distribution is given in APPENDIX A. Chloroform (99-99.4 % purity, Sigma-Aldrich, Germany) was used as the solvent for the preparation of the polymeric films by solvent casting. Carbon dioxide (99.9 %) was obtained from Linde Gas (Turkey).

For the drug release test the drug used was an antibiotic, Ceftriaxone Sodium ($C_{18}H_{16}N_8Na_2O_7S_3$, $3^1/_2$ H_2O, M_w = 662 $g.mol^{-1}$, Nobel Kimya, Turkey) in powder form and stored at room temperature. The loading of the drug and release studies were done by dissolving the drug in with phosphate buffered saline (PBS) solution, prepared with deionized water (DI water) that was obtained by a deionizer water equipment (TKA-Pacific, Germany). Sodium chloride (NaCl) (≥99.5% purity), disodium hydrogen phosphate (Na_2HPO_4) (≥98% purity), sodium dihydrogen

phosphate (NaH_2PO_4) (≥98% purity) (Merck, Germany), sodium hydroxide (≥98% purity) (J.T. Baker, Holland) were used in the preparation of PBS solution.

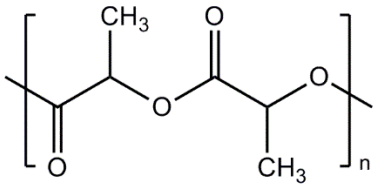

Figure 2.1 Chemical structure of PLLA

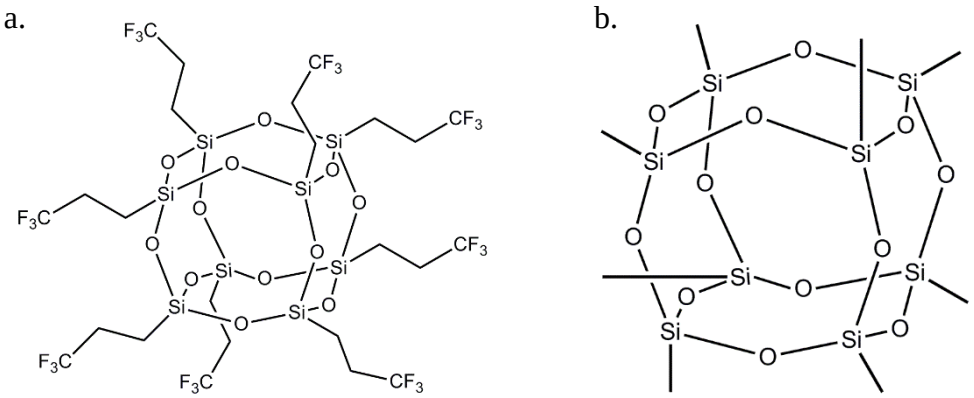

Figure 2.2 Chemical structure of (a) TFPOSS, (b) OMPOSS

2.1.2 Polymer Film Preparation

Solvent casting method was used to produce the starting thin polymer films. The polymer solution was prepared by dissolving PLLA in chloroform with concentration of 150 g/L in a sealed glass bottle to avoid solvent evaporation. The additive was added to the solution at a specific weight percent with respect to the polymer. The ratio of the PLLA and additive for different samples is given in Table 2.1.

Table 2.1. Polymer film compositions

Sample Name	TFPOSS wt%	OMPOSS wt%
PLLA	0	0
PLLA-10T	10	0
PLLA-30T	30	0
PLLA-30O	0	30

The solution was agitated with a magnetic stirrer to obtain a homogeneous solution. It was then poured onto a glass plate (2.5 cm x 7.6 cm), 4 mL of solution on each plate. The solution was let to evaporate at ambient pressure and temperature for 70 min and then covered with another glass plate to prevent excessive bending of the film. After covering with glass plate, the system is left overnight at ambient temperature and pressure to allow the rest of the solvent to evaporate. The resulting film was then removed from the glass and cut into small pieces (~0.7 cm x 0.7 cm, 11 ± 1 mg) and stored in desiccator.

2.1.3 Foaming Process of Polymers with $scCO_2$

The foaming process was conducted in a sealed stainless-steel high-pressure vessel (Micro Reactor model 4592, Parr Instruments, USA), equipped with a thermocouple and a pressure transducer that is connected to a reactor controller (model 4848, Parr Instruments, USA) to monitor the pressure and to control and monitor the temperature inside the vessel. A jacket electrical heater was used to heat the vessel to achieve the desired operating temperature. A syringe pump (model 260D, Teledyne ISCO, USA) was used to supply the required amount of CO_2 into the vessel. The experimental setup is shown in Figure 2.3.

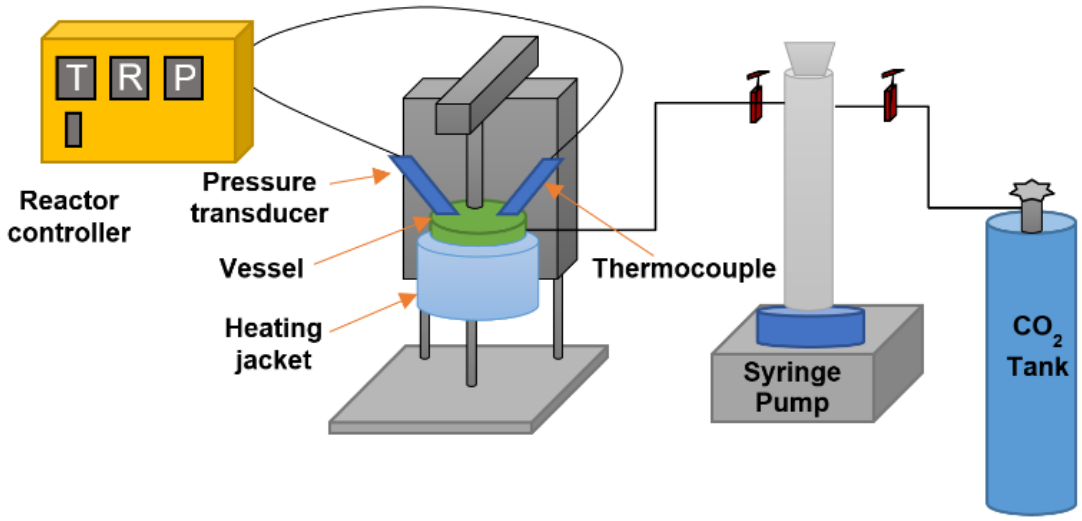

Figure 2.3 Experimental setup for the foaming process

To fabricate the porous matrices, the films were placed into the high pressure vessel, followed by the sealing of the vessel. For each run 4 pieces of the sample were placed into the vessel and processed at the same time. Teflon sheets were used to cover the wall of the vessel to prevent the contact between the films and the vessel wall, and also to split the inside of the vessel to four sections. Each section was filled with one film sample. The vessel was first heated to *ST* (313-393 K), and then pressurized to *SP* (10.3-20.7 MPa) at a specific pressurization rate of 0.5 MPa.min^{-1}. The system was kept at *ST* and *SP* over a period of *Stime*, which was 2 or 24 h. The vessel was then depressurized to ambient pressure with a specific *VR* between 0.2 and 10.3 MPa.min^{-1}, and let cool down to ambient temperature before obtaining the processed matrices. The processing parameters were chosen based on the commonly used parameters available in the literature. Moreover, low temperature such as 313 K was also chosen to see the performance of the additives on the foamability of the polymer at low temperature.

2.1.4 Surface Modification with Plasma Etching

Surface of some of the films were modified with plasma etching to remove the skin layer. The plasma applied was low temperature oxygen plasma (Advanced Plasma Systems Inc., USA). The power used was 50 W RF power generated by SerenR300 13.56 MHz power generator. The plasma treatment was done for 5 minutes.

2.1.5 Characterization of the Films

2.1.5.1 Differential Scanning Calorimetry

Differential Scanning Calorimetry (DSC) analysis (Diamond DSC, Perkin Elmer, United States) was used to determine the thermal properties of the P_LLA, P_LLA-10T, and P_LLA-30T, films before and after processing with $scCO_2$. The measurements were performed at a heating rate of 10 $K.min^{-1}$ in the test range of 273-473 K. For all films the data is taken form the first heating thermogram. In addition to the T_g and T_m, the crystallinity values of the film were also calculated from the specific enthalpy of melting of the samples obtained from the DSC analysis and the melting enthalpy of 100% crystalline PLA obtained from literature ($\Delta H_m^0 = 93.1 J.g^{-1}$)[61]

2.1.5.2 Scanning Electron Microscopy and Energy-dispersive X-ray Spectroscopy

Scanning Electron Microscopy (SEM) (Quanta 400 FEG, FEI, USA) was used to determine the pore morphology of the films at the cross-section. To obtain the cross-section SEM micrographs, the samples were freeze fractured under liquid nitrogen and coated with Au-Pd before the SEM analysis. The measurements were performed at a voltage of 5 kV and spot size 3.0. The average pore diameter of the samples was approximated by;

$$D = \frac{\sum d_i n_i}{\sum n_i}$$

Where D is the average diameter, d_i denotes the diameter of a single pore and n_i is the number of the pores measured. For each sample at least 50 pores were measured.

For the films that contain additive, trifluoropropylPOSS or octamethylPOSS, additionally Energy-dispersive X-ray spectroscopy (EDX) analysis was done after taking the images to quantify the amount of the additive on the cross-section of the samples. In addition to local EDX analysis, EDX mapping of the cross-section was also done to see the distribution.

2.1.5.3 Micro Computed Tomography

Micro Computed Tomography (Micro-CT) system (µCT; Skyscan 1172, Skyscan, Belgium) was used to obtain high resolution micro-CT images. The samples were placed on the rotary stage inside the apparatus and scanned. The measurements were performed at a voltage of 100 kV, a current of 100 µA, image pixel size of 1.85 µm, exposure time of 670 ms, 0.250 degree rotation step and without using filter. The resulting 2-D images were used to reconstruct the 3-D images.

2.1.5.4 Mechanical Test (Hardness)

Mechanical data (hardness) of the films were obtained by nanoindentation module (Nano-micro combi tester, CSM Instrument, Switzerland) on submicron scale. The analysis was done by using pyramidal Berkovich tips at room temperature. For each sample the measurement was done at least for 9 different points. The load was applied at a loading rate of 80 mN/min to a maximum load of 40 mN and with pause time of 20 seconds before releasing the load.

2.1.6 Drug Release Studies

2.1.6.1 Preparation of Phosphate Buffered Saline (PBS) solution

PBS solution was used as the media to dissolve the drug for loading process and also as the media for the release study. The solution was prepared by first preparing a phosphate buffer (PB) stock solution by dissolving 2.96 g of NaH_2PO_4 and 8.31 g of Na_2HPO_4 in 100 mL of distilled water. 9.7 g of NaCl was dissolved in 20 mL of PB solution, and then the volume was completed to 1 L with addition of 980 mL of distilled water. The pH of the solution was adjusted to 7.4 by using NaOH solutions.

2.1.6.2 Drug Loading

The films that had been processed with $scCO_2$ were then loaded with drug for the drug release study. The films had an average size of approximately 0.7 cm x 0.7 cm. To load the drug to the films, first drug solution was prepared by dissolving Ceftriaxone Sodium (CS) in the PBS solution with 1 g/L concentration. The drug was loaded by vacuum-pressure cycle to force the drug to diffuse into the pores of the films. 10 µL of drug solution was dropped on top of the film and then vacuum was applied for 5 minutes. After 5 minutes the vacuum was released and then repeated again for a total of 3 times vacuum-pressure cycle. This process is repeated until 100 µL of drug solution was added into the film.

2.1.6.3 Drug Release Studies

The drug release analysis was performed by immersing the films loaded with drug to 3 or 5 mL of PBS solutions at room temperature. For each films that were processed at the same condition with $scCO_2$, three replicates were used in the drug release analysis to ensure reproducibility of the results. After immersing the film, drug was let to diffuse out from the film and dissolve in the PBS solution for a specific time span, which was 30 minutes, 1, 2, 3, 6, 24 h, 2, 4 and 7 days. After the specific time was reached, the PBS solution was replaced with a fresh one and the concentration of the drug dissolved in the previous PBS solution was measured by UV-visible

spectrophotometer (8453 UV-Vis, Agilent Technologies, USA). The absorbance for the drug was obtained at 300 nm and the concentration was correlated with the absorbance by using the previously obtained calibration curve, given in APPENDIX B.

CHAPTER 3

RESULTS and DISCUSSION

3.1 Porous Film Preparation with $scCO_2$ Processing

3.1.1 Pore Morphology

The neat P_LLA films and the P_LLA films with addition of TFPOSS or OMPOSS were processed with $scCO_2$ at different processing parameters to observe the effects of the additive and the process parameters on the resulting pore structure and porosity of the films. The studied process parameters were *ST*, *SP*, *VR*, *Stime*, POSS type and POSS concentration which were examined separately while changing only one and keeping the others constant at certain values. The pore morphologies of the films after $scCO_2$ processing were analysed with SEM.

3.1.1.1 Effect of Saturation Temperature

SEM micrographs of the cross-section of the freeze fractured P_LLA films processed by keeping *SP*, *Stime* and *VR* constant (20.7 MPa, 2 h, and 10.3 $MPa.min^{-1}$, respectively), and varying the saturation temperature (313, 333, 373 and 393 K) are shown in Figure 3.1.

It can be seen from Figure 3.1.1.a,b that, there was no significant pore formation in the cross-section of the P_LLA film processed at 313 K. The diffusivity and solubility of $scCO_2$ in a polymer are known to be a function of temperature and pressure. As temperature increases, diffusivity of the $scCO_2$ increases but its solubility in the polymer matrix decreases [62,63]. At 313 K the diffusivity of $scCO_2$ is lower than that of at higher temperatures. From the Figure 3.1.1.a,b it was observed that during

the 2 h of *Stime*, the amount of $scCO_2$ that was able to diffuse into the polymer matrix might not have been sufficient enough, therefore during depressurization no nucleation of bubbles occurred, and so a porous structure was not obtained. At 333 K the diffusivity of $scCO_2$ is higher than at 313 K with polymer chains being more flexible, which results in more $scCO_2$ able to diffuse to the polymer. Because of this, less time is needed to reach the equilibrium point with the higher rate of diffusion. This resulted in higher amount of $scCO_2$ in the polymer structure [36], and allowed nucleation of nano-sized pores with average size of 300 nm during the depressurization. The pores formed were not homogeneous throughout the cross-section.

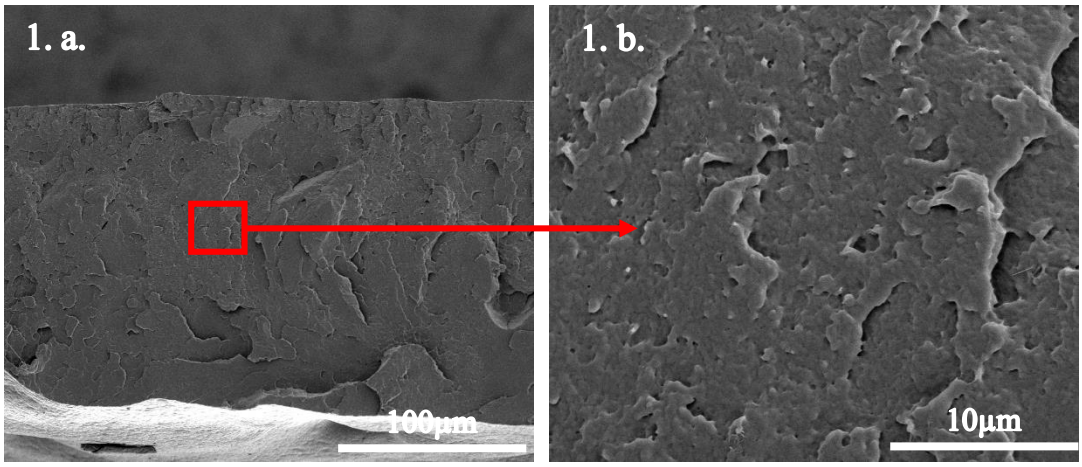

Figure 3.1 SEM micrographs of the cross-section of the processed thin P_LLA film samples processed at *SP* = 20.7 MPa, *Stime* = 2 h, *VR* = 10.3 $MPa.min^{-1}$ and *ST* = (1) 313 K, (2) 333 K; (a) 1000x magnification, (b) 10000x magnification, (3) 373 K; (a) 500x magnification, (b) 10000x magnification and (4) 393 K; (a) 250x magnification, (b) 10000x magnification, (c) 100x magnification (surface)

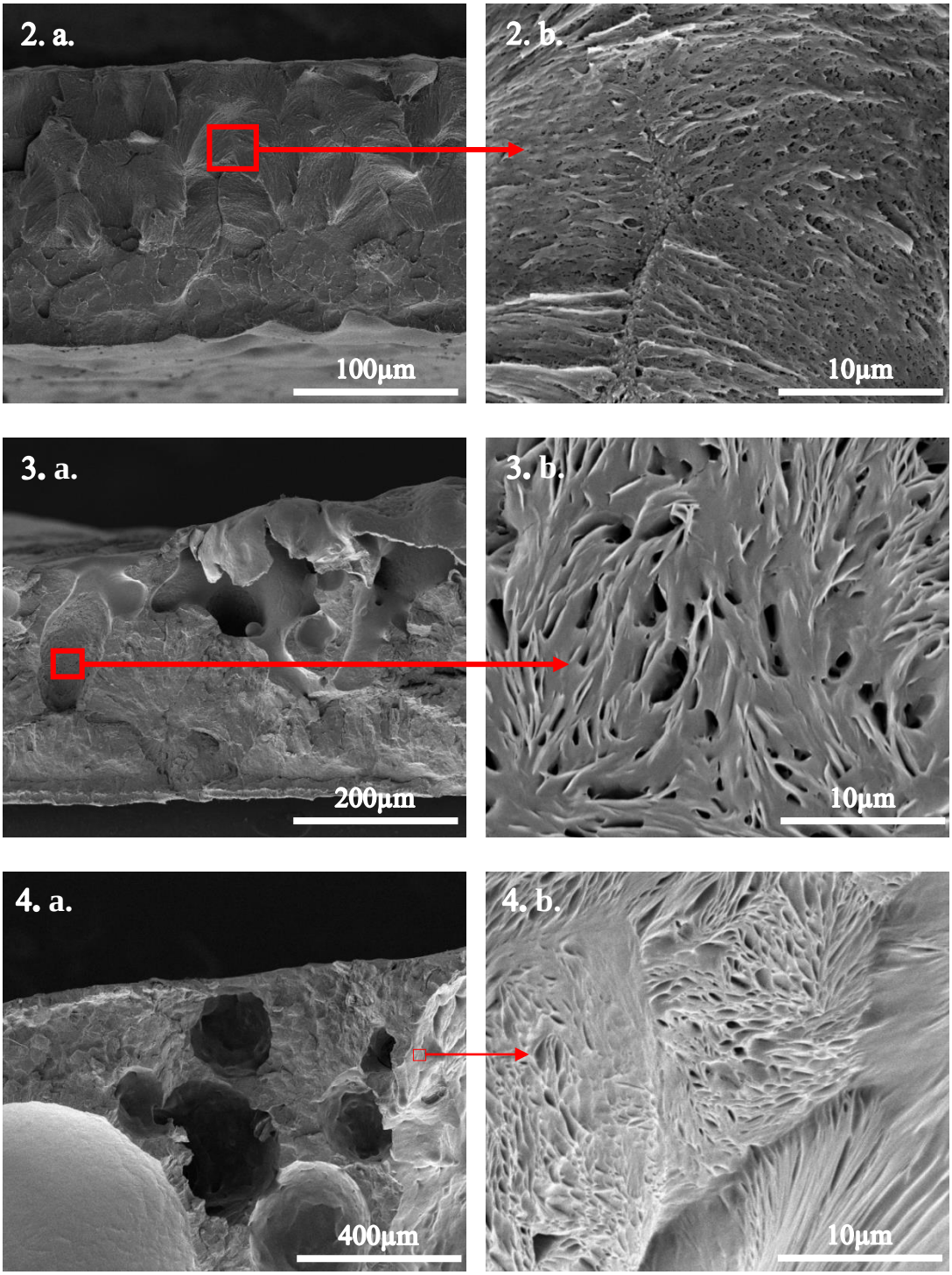

Figure 3.1 (continued)

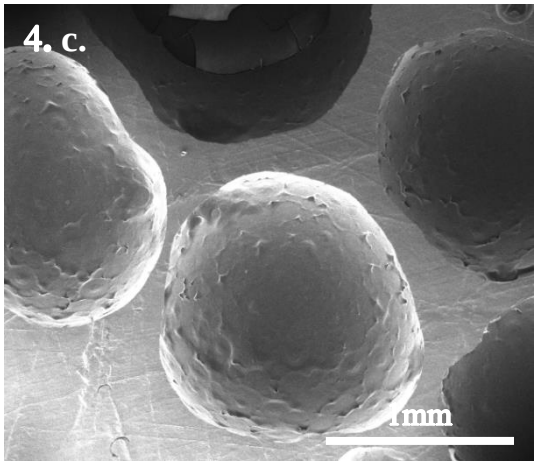

Figure 3.1 (continued)

The formation of pores can be clearly seen in the P_LLA films that were processed at 373 and 393 K (Figure 3.1.3 and Figure 3.1.4). It is possible to induce the nucleation of bubbles and formation of pores at these temperatures because of the high diffusivity of CO_2 and more flexible polymer chains. In fact it was visually observed after the foaming that the P_LLA film had a significant shape deformation at both temperatures, while the P_LLA films that were processed at 313 and 333 K had no change in their shapes. It is possible that as the CO_2 dissolved in the polymer, the T_m of the P_LLA decreased and approached the *ST* at these processing conditions. It can also be seen from Figure 3.1.4 that processing at 393 K resulted in formation of more distinct and larger micro-pores compared to 373 K, which can be due to the higher diffusivity of CO_2 and higher flexibility of the polymer chains. Moreover, at 393 K it was also observed that there were pores formed at the surface of the sample (Figure 3.1.4.c) whereas at lower temperatures non porous skin formations were observed at the sample surfaces. In both cases, the pores formed were not homogeneous, with a wide range of pore size distribution. The sizes varied from small micro-pores about 1 μm to large micro-pores with average sizes of 100 μm and 765 μm for the ones processed at 373 K and 393 K, respectively (Figure 3.1.3 and Figure 3.1.4).

The addition of 10 % TFPOSS had a significant effect on the morphology of the cross-section (Figure 3.2). At 313 K there was no pore formation observed in the cross-section of neat PLLA film (Figure 3.1.1.a,b), whereas there was a significant formation of pores in the cross-section of PLLA-10T films (Figure 3.2.1.a,b). The pores were formed regionally. TFPOSS particles are not soluble in chloroform so TFPOSS was not distributed homogenously forming agglomerations of TFPOSS throughout the film. The pores mostly occur at the regions where the TFPOSS agglomerations exist (Figure 3.3.a), as verified with EDX analysis (Figure 3.3.b) which shows high concentration of silicon (Si) and fluorine (F). Upon closer inspection, the pores appear to be locally interconnected with average size of 625 nm (Figure 3.2.1.b). These results show that the addition of TFPOSS which can act as a CO_2 enricher at the polymer/TFPOSS interface can improve the rate of cell nucleation, due to the affinity of TFPOSS in the polymer to $scCO_2$.

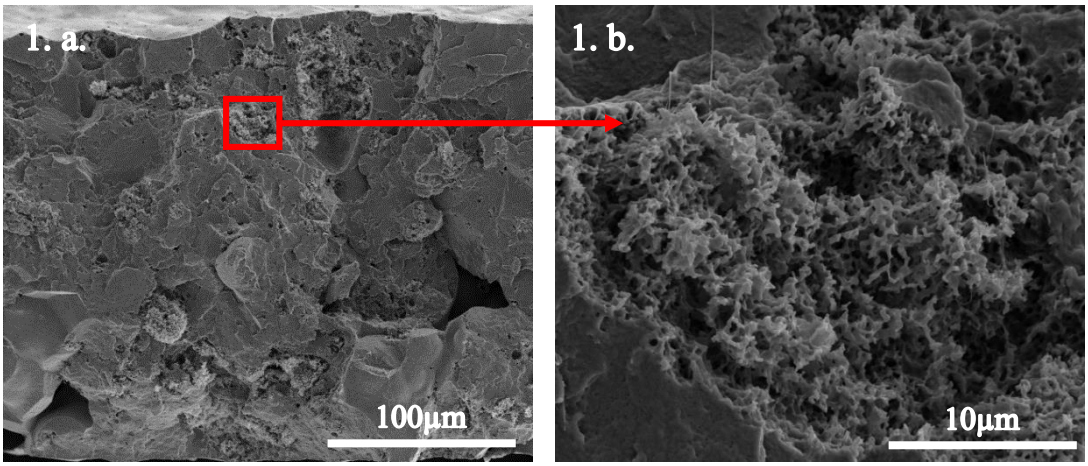

Figure 3.2 SEM micrographs of the cross-section of the processed thin PLLA-10T film samples processed at *SP* = 20.7 MPa, *Stime* = 2 h, *VR* = 10.3 MPa.min^{-1} and *ST* = (1) 313 K, (2) 333 K, (3) 373 K; (a) 1000x magnification, (b) 10000x magnification, and (4) 393 K; (a) 250x magnification, (b) 10000x magnification, (c) 100x magnification (surface)

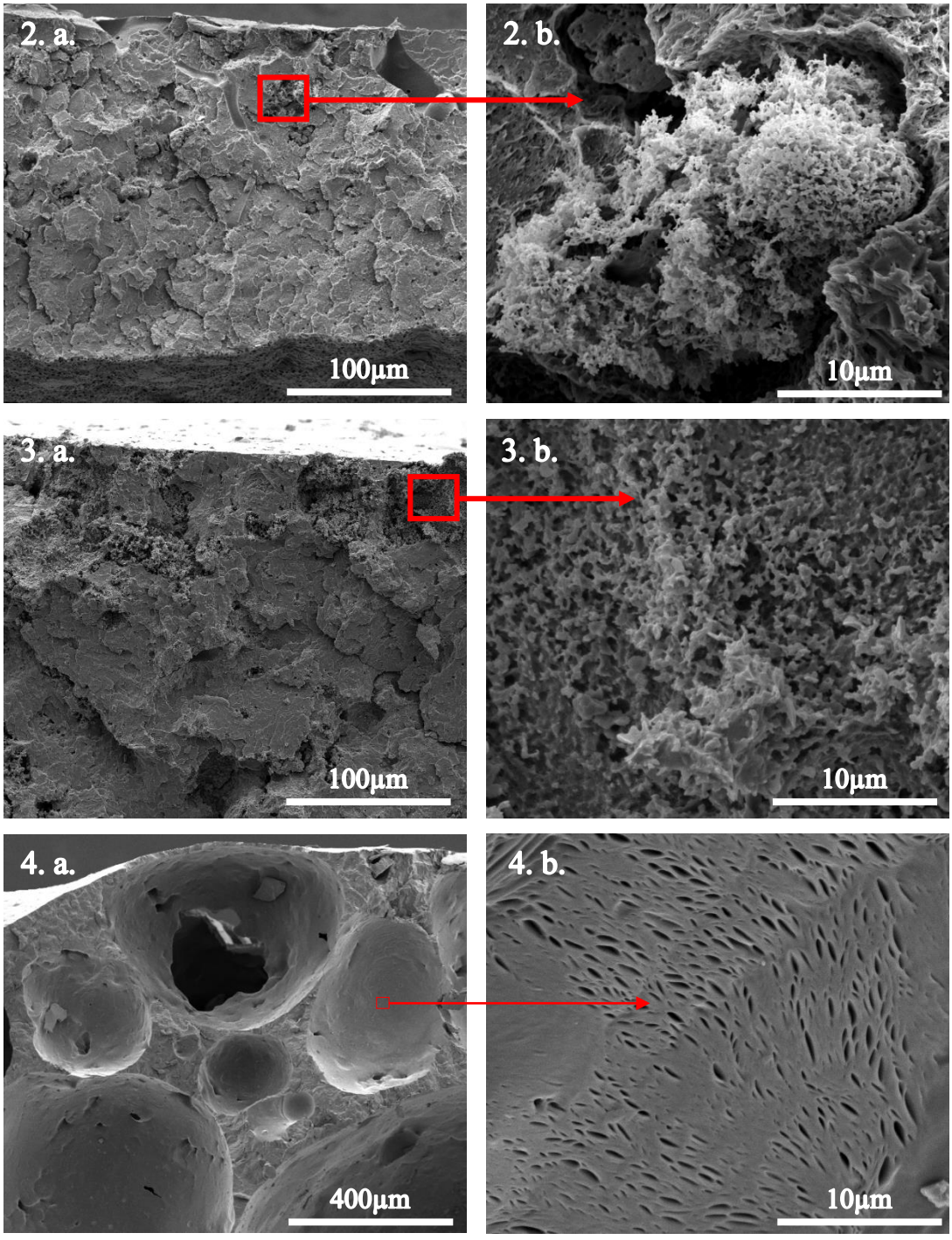

Figure 3.2 (continued)

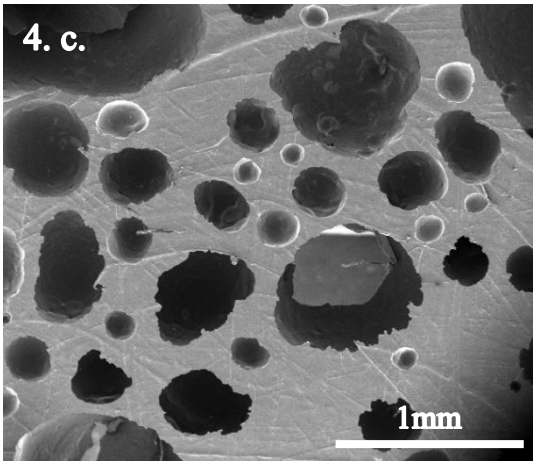

Figure 3.2 (continued)

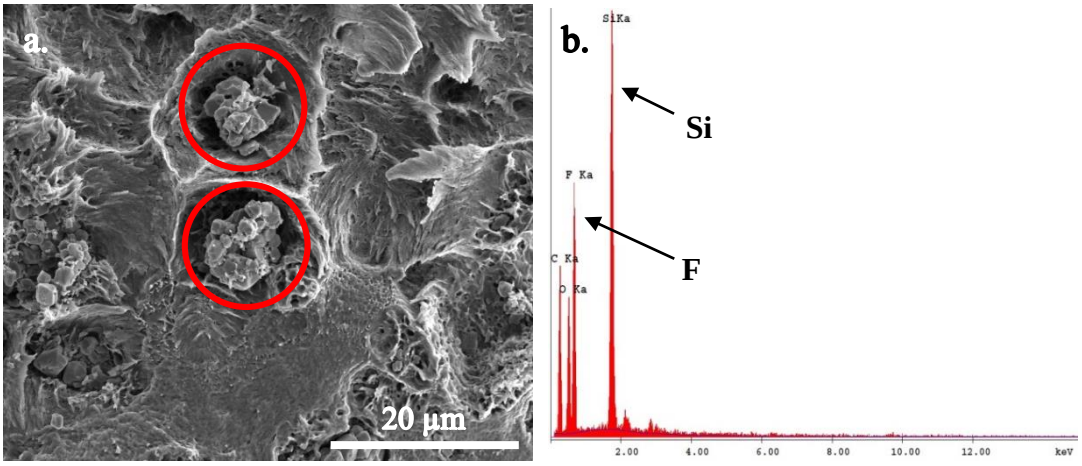

Figure 3.3 (a) SEM micrographs of TFPOSS particles' agglomeration on the cross-section of the P_LLA-10T film processed at *SP* = 20.7 MPa, *Stime* = 2 h, *VR* =10.3 MPa.min^{-1} and *ST* = 313 K, 5000x magnification (b) EDX analysis of the highlighted part

At 333 K (Figure 3.2.2.a), less pores were formed on the cross-section compared to the films with TFPOSS processed at 313 K (Figure 3.2.1.a), however the films were still more porous compared to neat P_LLA film (Figure 3.1.2.a). Although at 313 K, TFPOSS might significantly enhance the pore formation as an interfacial CO_2

enricher in the polymer, the less pore formation at 333 K is possibly due to the negative effect of temperature on the solubility of $scCO_2$ in the polymer [34]. Thus compared to the one processed at 313 K, less amount of CO_2 might have probably dissolved in the polymer at 333 K, resulting in less pore nucleation. In the region where pores were formed, upon closer inspection the structure was observed to be similar with pores on the film processed at 313 K (Figure 3.2.1.b), locally interconnected and open with average size of 625 nm (Figure 3.2.2.b).

There was a significant difference between the pore structure in the cross-section of the neat P_LLA and P_LLA-10T films processed at 373 K. Neat P_LLA film had large micro-sized pores (Figure 3.1.3) while P_LLA-10T films had much smaller pores with average size of 950 nm (Figure 3.2.3.b). The formation of smaller pores was expected to occur due to the presence of the nano-sized TFPOSS particles that can act as a pore nucleation center. This agrees with the findings of Costeux [59].

However, it can also be observed that the pores were formed regionally and were not homogeneous. This is possible due to the non-homogeneous distribution of TFPOSS particles in the matrix. In addition to this, it can be seen that the film that was processed at 373 K had more porous region than the one processed at 333 K. It is known that as temperature decreases, the solubility of $scCO_2$ increases while its diffusivity decreases. Thus it is possible that at 333 K the decrease in diffusivity outweighed the increase in solubility, which resulted in less $scCO_2$ in the polymer, while at higher temperature (373 K) the opposite occurred. At 373 K, the increase in diffusivity outweighed the decrease in solubility which resulted in more amount of $scCO_2$ diffuse into the polymer, and thus more nucleation occurred. Comparing the size of the pores formed at 373 K and lower temperatures, 313 and 333 K, it can be seen that the ones formed at higher temperature had larger size. This may be due to the higher diffusivity of $scCO_2$ and more flexible polymer chains which can allow the pores to coalesce with each other, resulting in larger pores.

At a higher temperature, 393 K (Figure 3.2.4), a similar pore structure between P_LLA-10T and neat P_LLA processed at the same condition was observed. The pores

consisted of large micro-pores with nano-pores on the wall of the micro-pores. Additionally, pore formation can also be observed at the surface of the sample (Figure 3.2.4.c), similar with the neat PLLA film processed at 393 K (Figure 3.1.4.c). In overall, the sizes of the pores are smaller than the pores formed in neat PLLA film. This pore size reduction can be attributed to the presence of TFPOSS particles, similar to the result obtained with the films processed at 373 K. The large micro-pores have an average size of 335 μm, while the small nano-pores have an average size of 650 nm. In addition to this, similar to neat PLLA films that were processed at 373 and 393 K, deformation was also observed in the PLLA-10T films that were processed at higher temperatures, 373 and 393 K. Because of this these temperatures were determined to be not preferable for processing with $scCO_2$. Lower temperatures such as 313 K were more preferable because porous structure could be obtained at this temperature with the addition of TFPOSS without deformation in the polymer.

3.1.1.2 Effect of Saturation Pressure

Porous PLLA and PLLA-10T films were produced with $scCO_2$ foaming at different *SP* while keeping other processing parameters constant to see the effect of *SP* on the foamability of the film and the resulting pores. Figure 3.4.1.a and b shows the SEM micrographs of the PLLA films processed at 20.7 MPa and 10.3 MPa respectively, both of which were processed at 313 K. It can be seen from Figure 3.4.1.b that the film that was processed at lower *SP* had no pore formation observed in the cross-section, similar to the film that was processed at higher pressure, 20.7 MPa (Figure 3.4.1.a). This result is expected because as pressure decreases, the solubility and diffusivity of $scCO_2$ in the polymer also decreases [62]. Because of this, there will be significantly less amount of $scCO_2$ diffused into the polymer which results in no foaming and no change in the morphology of the cross-section of the film processed at 10.3 MPa.

In the cross-section of the PLLA film that was processed at 373 K, foaming observed at 20.7 MPa but no pores were observed in the film that was processed at 10.3 MPa

(Figure 3.4.2.a,b). This can also be attributed to the $scCO_2$ solubility and diffusivity that decreased at lower pressure.

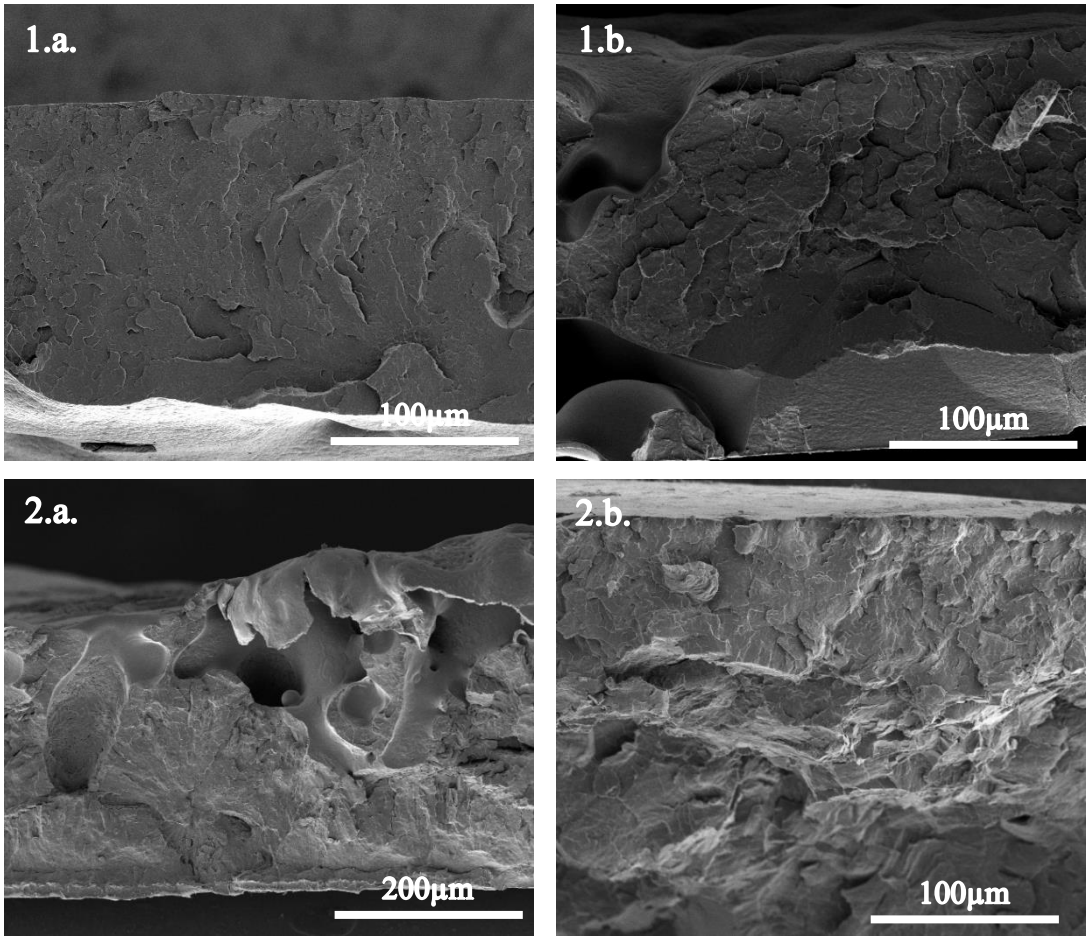

Figure 3.4 SEM micrographs of the cross-section of the processed thin PLLA film samples processed at *Stime* = 2 h, *VR* = 10.3 MPa.min^{-1}, (1.a.) *ST* = 313 K, *SP* = 20.7 MPa; 1000x magnification, (1.b.) *ST* = 313 K, *SP* = 10.3 MPa; 1000x magnification, (2.a.) *ST* = 373 K, *SP* = 20.7 MPa; 500x magnification, (2.b.) *ST* = 373 K, *SP* = 10.3 MPa; 1000x magnification.

The effect of *SP* at different *ST* on pore formation in PLLA-10T films can be observed in Figure 3.5.

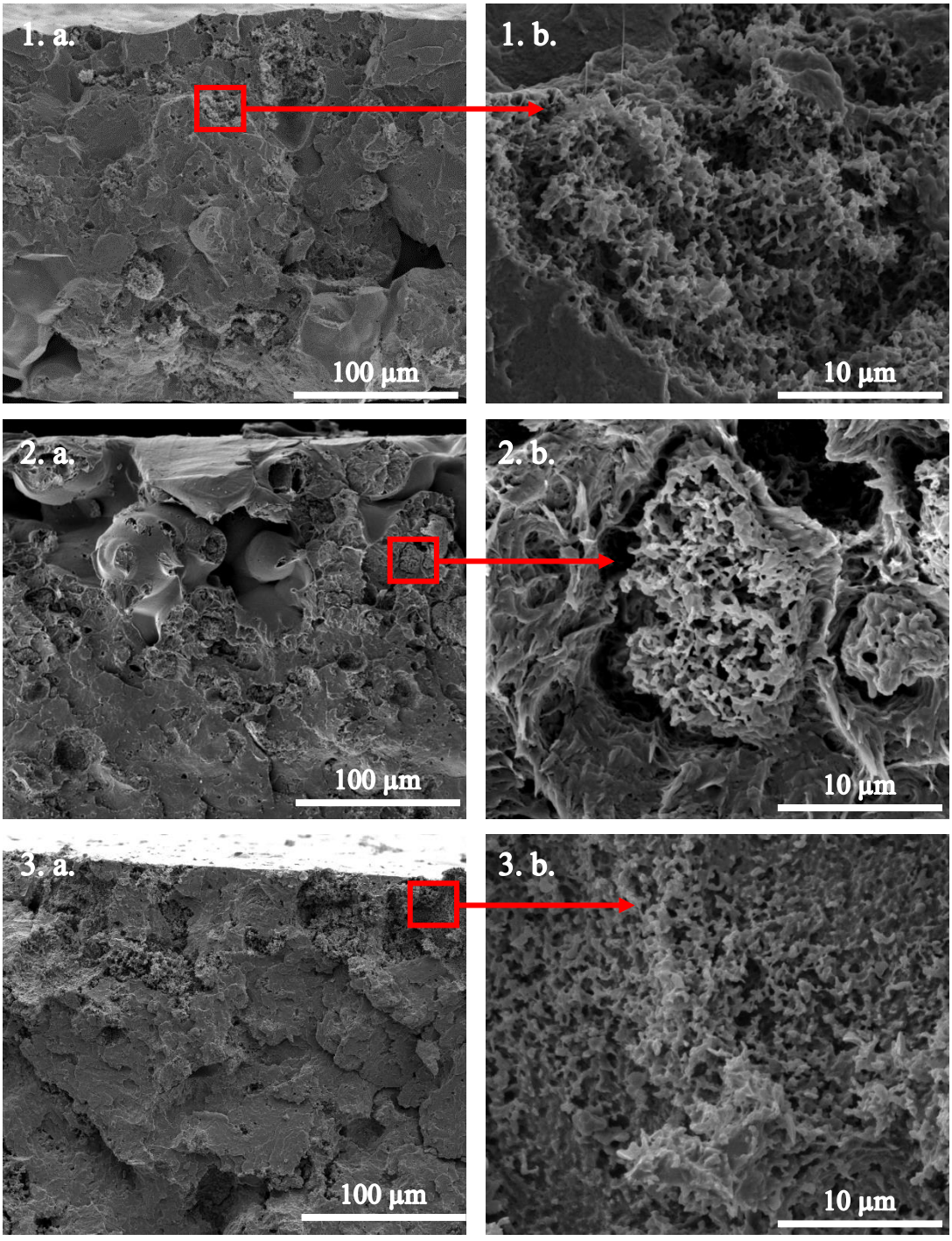

Figure 3.5 SEM micrographs of the cross-section of the processed thin P_LLA-10T film samples processed at *Stime* = 2 h, *VR* = 10.3 MPa.min^{-1} (1) *ST* = 313 K, *SP* = 20.7 MPa, (2) ST = 313 K, SP = 10.3 MPa, (3) ST = 373 K, *SP* = 20.7 MPa, (4) ST = 373 K, SP = 10.3 MPa; (a) 1000x magnification, (b) 10000x magnification

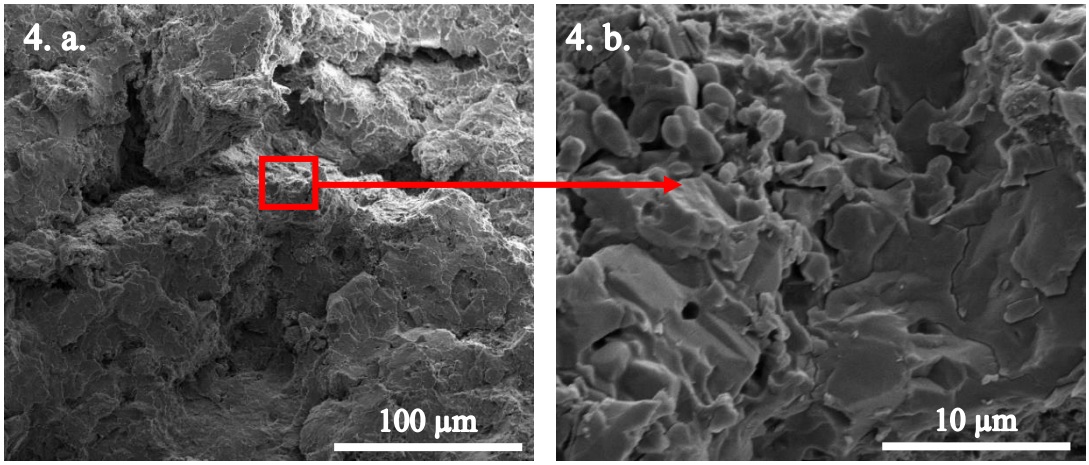

Figure 3.5 (continued)

Comparing Figure 3.5.1 and Figure 3.5.2 it can be seen that it is possible to form pores in the PLLA-10T films by processing with $scCO_2$ at a lower *SP*, 10.3 MPa, and at low *ST*, 313 K, while there was no change observed in the cross-section of the neat PLLA films at this condition. Comparing with the PLLA-10T film that was processed at *SP* = 20.7 MPa (Figure 3.5.1), it can be seen that higher *SP* resulted in formation of more pores and more homogeneous distribution of the pores on the cross-section. On closer inspection, both films that were processed at 10.3 and 20.7 MPa had similar nano-pore structure, locally interconnected to a certain extent, with average size of 715 nm and 625 nm, respectively. Higher concentration of pores with smaller average pore size obtained in the polymeric films at 20.7 MPa shows that a higher rate of nucleation was attained at the higher *SP*. This can be attributed to the increase in the amount of $scCO_2$ diffused into the polymeric film with the increase in the processing pressure [34].

At higher *ST*, 373 K, processing the film at lower *SP*, 10.3 MPa, resulted in formation of no pores in the cross-section of the film (Figure 3.5.4) similar with neat PLLA film, while at higher *SP*, 20.7 MPa, formation of pores were clearly observed (Figure 3.5.3). Since the solubility of $scCO_2$ decreases with decreasing pressure and increasing temperature, processing at high *ST* and low *SP* results in much less $scCO_2$ dissolved

in the polymeric film, which in turn produces no nucleation of pores during depressurization [34].

3.1.1.3 Effect of Venting Rate

To see the effect of *VR*, the films were processed by varying the *VR* from 0.2 to 10.3 MPa.min^{-1} and keeping the other processing parameters constant (*Stime* = 2 h, *SP* = 20.7 MPa, and *ST* = 373 K). It can be observed that for the neat P_LLA film, reducing the *VR* from 10.3 to 0.2 MPa.min^{-1} resulted in significant reduction of pore size (Figure 3.6). At 10.3 MPa.min^{-1} of venting rate, large micro-sized pores up to 100 µm were formed (Figure 3.6.a) along with smaller micro-sized pores with average size of 1µm, while the film that processed at *VR* = 0.2 MPa.min^{-1} produced much smaller pores with average size of about 1.1 µm (Figure 3.6.b). The formation of the smaller pores with more uniform size at the lower *VR* is probably due to the smaller pressure difference that occur during the venting, resulting in less supersaturation degree. This leads to the nucleation of smaller cells and consequently smaller pores. Additionally at the *VR* of 0.2 MPa.min^{-1} a specific orientation of the pores was also observed, which is possibly in the direction of $scCO_2$ leaving the film during depressurization.

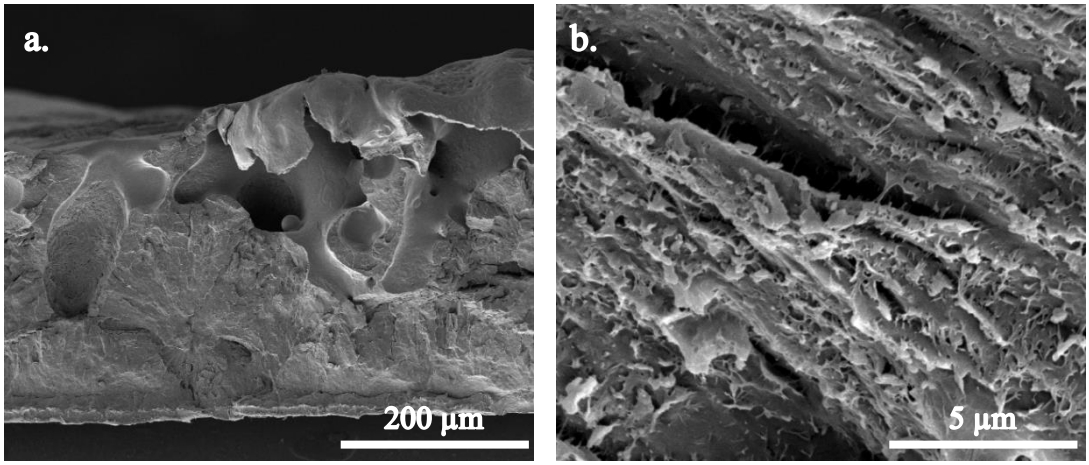

Figure 3.6 SEM micrographs of the cross-section of the processed thin PLLA film samples processed at *Stime* = 2 h, *SP* = 20.7 MPa, *ST* = 373 K, and *VR* = (a) 10.3 MPa.min^{-1}; 500x magnification (b) 0.2 MPa.min^{-1}; 20000x magnification

Slight decrease in pore size was also observed in the PLLA-10T films that were processed at lower venting rate, 0.2 MPa.min^{-1} (Figure 3.7.b) compared to the one processed at higher venting rate, 10.3 MPa.min^{-1} (Figure 3.7.a). The average pore size was measured to be 950 nm for the PLLA-10T film processed at 10.3 MPa.min^{-1} and 680 nm for the one processed at 0.2 MPa.min^{-1}. This behaviour where pore size increases as *VR* increases have been shown also before by Delabarde et.al [40], which used hydroxyapatite as the additive to the PLLA film.

For both neat PLLA and PLLA-10T films, the effect of venting rate was observed to be not significant at the low processing temperature, i.e. 313K.

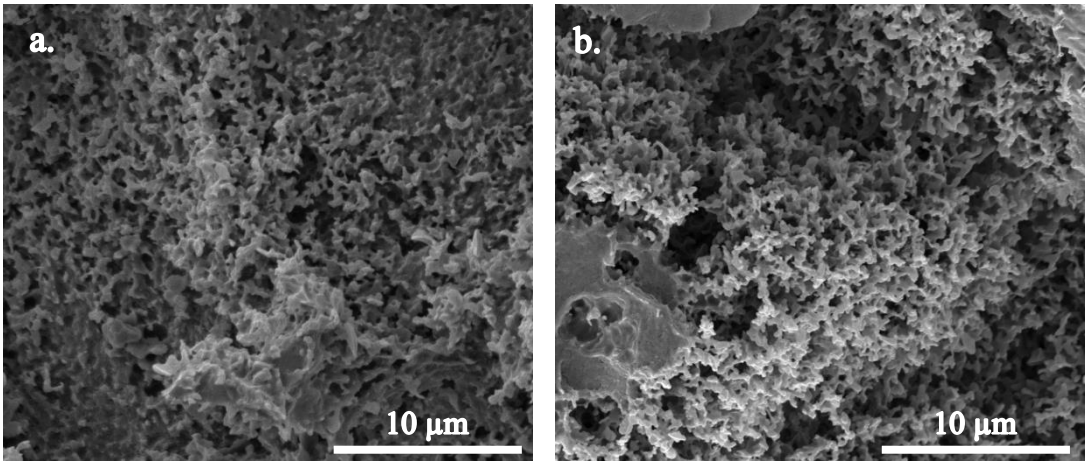

Figure 3.7 SEM micrographs of the cross-section of the processed thin PLLA-10T film samples processed at *Stime* = 2 h, *SP* = 20.7 MPa, *ST* = 373 K, and *VR* = (a) 10.3 MPa.min^{-1} (b) 0.2 MPa.min^{-1}; 10000x magnification

3.1.1.4 Effect of Saturation Time

To see the effect of *Stime*, the films were processed by varying the *Stime* from 2 to 24 h and keeping the other processing parameters constant (*VR* = 10.3 MPa.min^{-1}, *SP* = 20.7 MPa, and *ST* = 313 K and 373 K). It can be seen that for neat PLLA films (Figure 3.8), while no pores were obtained in 2 h processing at 313 K increasing the saturation time from 2 to 24 h allowed formation of pores to some extent in the polymeric matrix. The pores were formed locally and were not homogeneous. As explained earlier while 2 h did not allow sufficient diffusion of $scCO_2$ into the polymer, increasing the processing time to 24 h enhanced the diffusion of $scCO_2$ into the polymer matrix [36,64]. Therefore, after 24 h of *Stime*, formation of pores can be observed in neat PLLA films, with average pore size of 720 nm.

At a higher temperature, 373 K, increasing the saturation time had a different effect on the resulting film. At short *Stime*, 2 h, formation of micro-sized pores were observed (Figure 3.9.1). After increasing the *Stime* to a longer period, 24 h, no formation of pores were observed (Figure 3.9.2). Supercritical carbon dioxide has a plasticization effect on the polymer, which allows it to decrease the glass transition

temperature and melting temperature of the polymer during the supercritical fluid processing. This plasticization effect has also been shown to induce and accelerate PLA crystallization, and the crystallinity increases as processing time increases [65]. Therefore, it was possible that due to the long processing time of 24 h, significant increase of crystallinity of the film occurred, which could hinder the nucleation process of the foam, and thus no pores were formed in the polymer. This increase in crystallinity was later confirmed with the DSC analysis, where significant increase of crystallinity by 18.82% was observed when the processing time was increased from 2 to 24 h at 373 K.

For PLLA-10T films (Figure 3.10), both at 313 K and 373 K similar pore structure and similar non homogeneous distribution of pores were observed after processing for both 2 h and 24 h *Stime*. In all cases the pores were formed regionally in the polymer matrix, and upon closer inspection similar pore structure can be observed between the film that was processed at 2 h and 24 h at 313 K or 373 K. This is possibly due to the presence of TFPOSS which increased the affinity to $scCO_2$ and allowed 2 h of processing time to be sufficient for the effective diffusion of $scCO_2$ to saturate the polymer. Thus increasing the saturation time caused no significant change in the resulting pore structure. The average pore size after processing at 24 h at 313 K and 373 K were 570 nm and 1200 nm, slight difference compared to the films that were processed for 2 h with average pore size of 625 nm and 950 nm at 313 K and 373 K, respectively.

Similar behavior where no significant change in the resulting pore structure when the processing time was increased from 2 h to 24 h can be seen also for PLLA-30T (Figure 3.11). The average pore size of PLLA-30T films processed at 313 K were 860 nm and 805 nm at *Stime* 2 and 24 h respectively, but the porosity increased parallel to the amount of added TFPOSS.

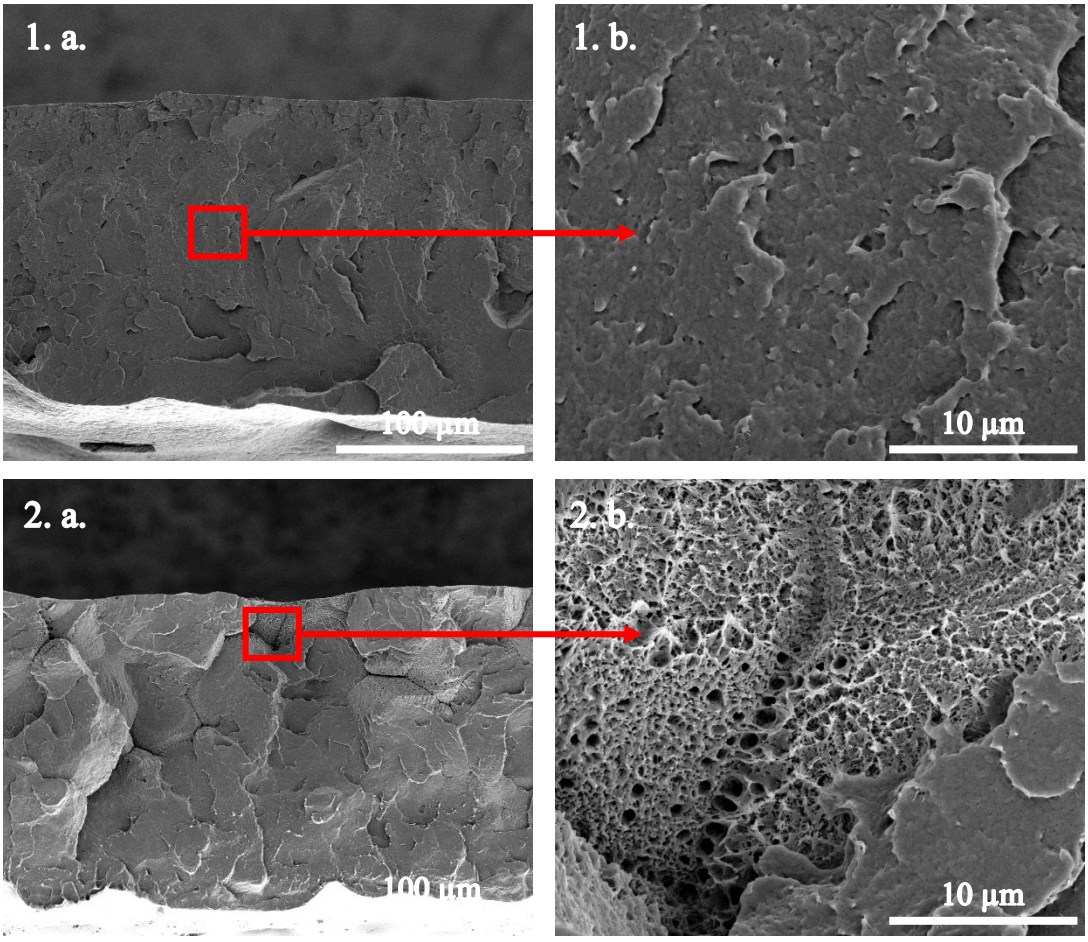

Figure 3.8 SEM micrographs of the cross-section of the processed thin PLLA film samples processed at *SP* = 20.7 MPa, *ST* = 313 K, *VR* = 10.3 MPa.min^{-1} and *Stime* = (1) 2 h, (2) 24 h; (a) 1000x magnification (b) 10000x magnification

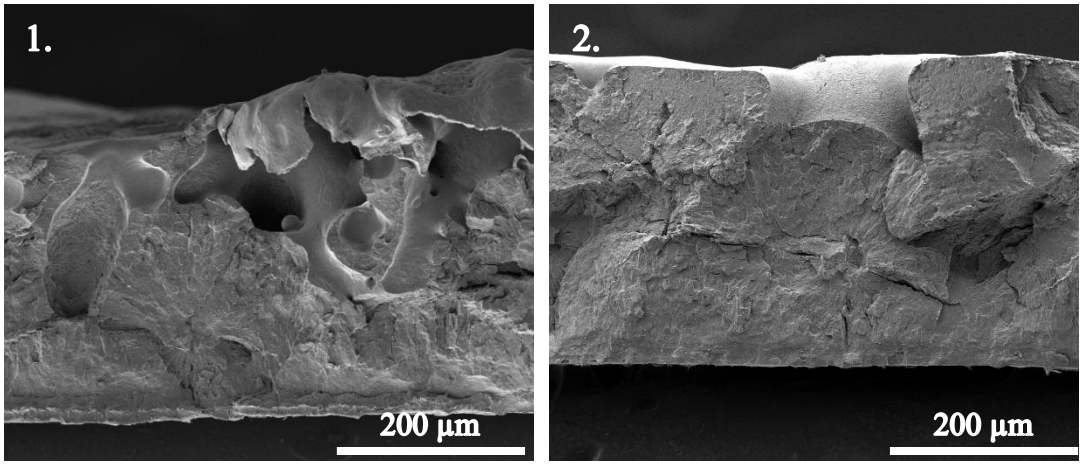

Figure 3.9 SEM micrographs of the cross-section of the processed thin PLLA film samples processed at *SP* = 20.7 MPa, *ST* = 373 K, *VR* = 10.3 MPa.min^{-1} and *Stime* = (1) 2 h, (2) 24 h; 500x magnification

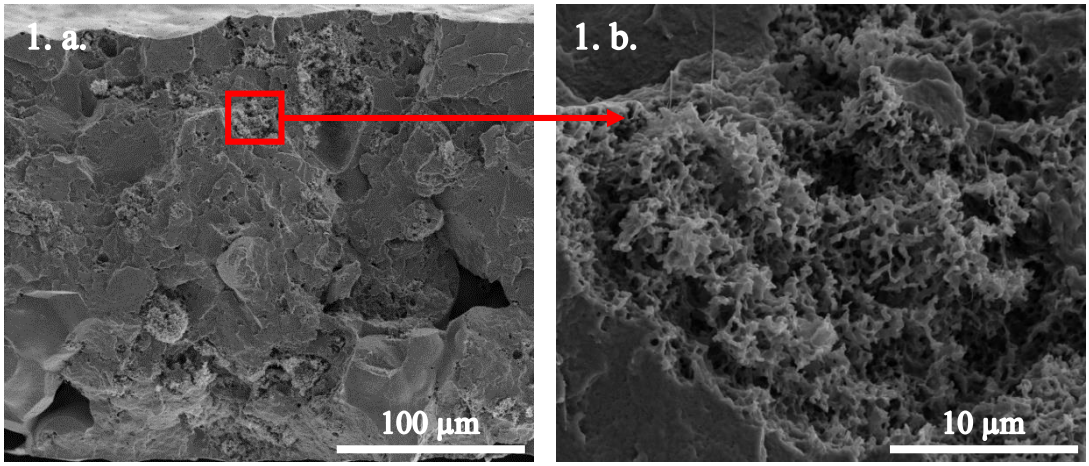

Figure 3.10 SEM micrographs of the cross-section of the processed thin PLLA-10T film samples processed at *SP* = 20.7 MPa, *VR* = 10.3 MPa.min^{-1} and (1) *ST* = 313 K, *Stime* = 2 h, (2) *ST* = 313 K, *Stime* = 24 h, (3) *ST* = 373 K, *Stime* = 2 h, (4) *ST* = 373 K, *Stime* = 2 h; (a) 1000x magnification (b) 10000x magnification

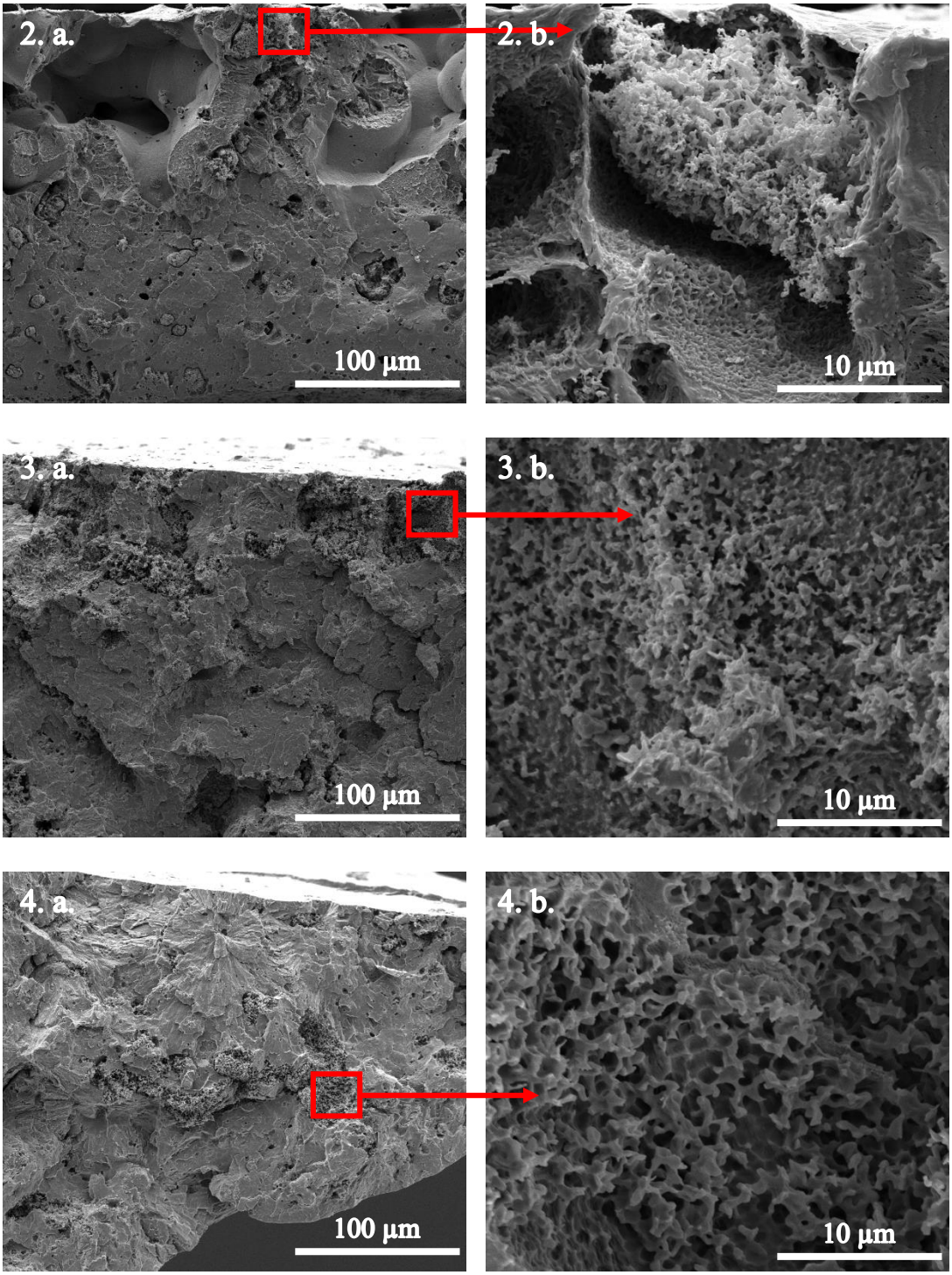

Figure 3.10 (continued)

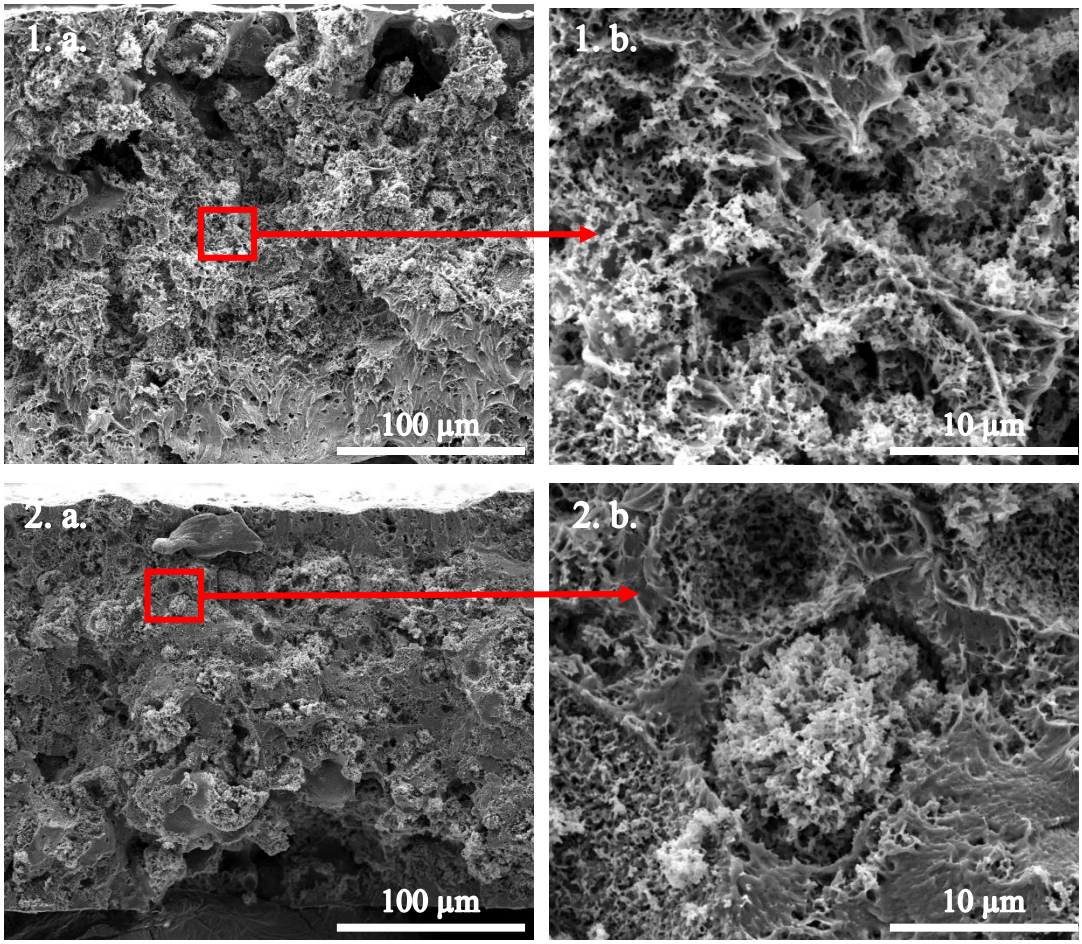

Figure 3.11 SEM micrographs of the cross-section of the processed thin P_LLA-30T film samples processed at *SP* = 20.7 MPa, *ST* = 313 K, *VR* = 10.3 MPa.min^{-1} and *Stime* = (1) 2 h, (2) 24 h; (a) 1000x magnification (b) 10000x magnification

3.1.1.5 Effect of Type and Concentration of Additive

To see the effect of type and concentration of additive, the films were processed using two different types of additives to see the effect of the CO_2-philic groups. The effect of higher concentration, i.e. 30% additive was also studied keeping the other processing parameters constant (*Stime* = 2 h, *VR* = 10.3 MPa.min^{-1}, *SP* = 20.7 MPa, and *ST* = 313 K). The effect of different additive concentrations and types can be seen from Figure 3.12.

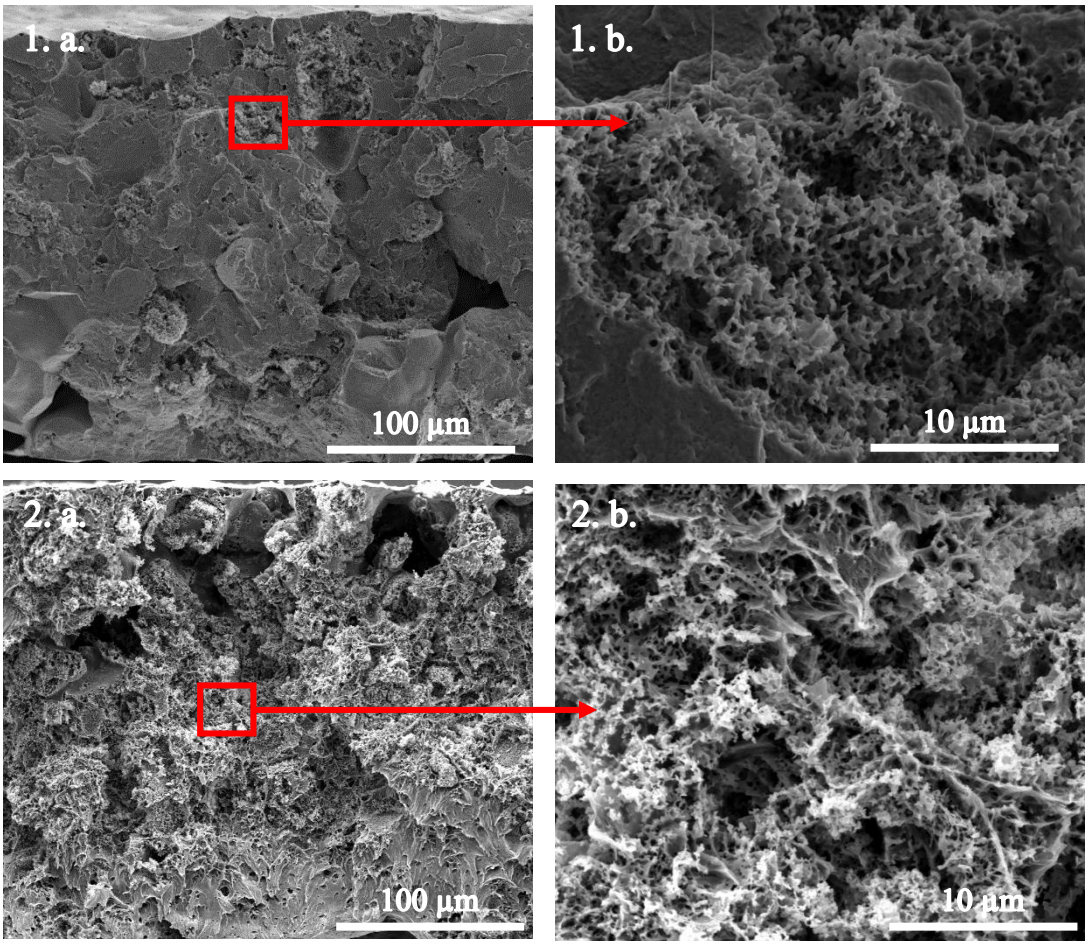

Figure 3.12 SEM micrographs of the cross-section of the processed thin PLLA and PLLA with additive film samples processed at *SP* = 20.7 MPa, *ST* = 313 K, *VR* = 10.3 MPa.min$^{-1,}$ *Stime* = 2 h and (1) 10% TFPOSS addition, (2) 30% TFPOSS addition (3) 30% OMPOSS addition; (a) 1000x magnification (b) 10000x magnification

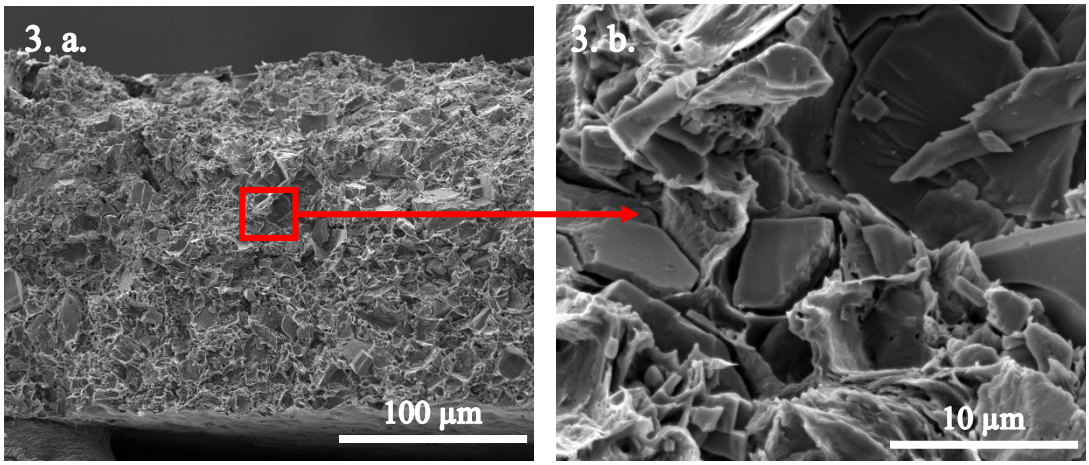

Figure 3.12 (continued)

Figure 3.12.1 and Figure 3.12.2 show that increasing the TFPOSS concentration to 30% (PLLA-30T) from 10% (PLLA-10T) gave a much more homogeneously distributed pores in the cross-section after $scCO_2$ processing. This can be attributed to the higher concentration of TFPOSS increasing the film affinity to $scCO_2$ due to its CO_2-philicity. More TFPOSS existing in the film can also allow higher number of nucleation sites. This effect of higher TFPOSS concentration was also observed by the EDX mapping on the unprocessed films, PLLA-10T and PLLA-30T films (Figure 3.13). The EDX mapping image shows the distribution of the F and Si elements, which is present in TFPOSS only, in the cross-section of the film. As can be seen from Figure 3.13.a and b, after the addition of 10% TFPOSS the distribution of the particle was not homogeneous in the cross-section. There were some regions where TFPOSS was not detected. This can be directly correlated to the resulting pore structure where the pores were formed locally where the TFPOSS was concentrated. When the TFPOSS concentration was increased to 30% (Figure 3.13.2), the distribution was more homogeneous, resulting in more homogeneous distribution of pores in the cross-section. However, no change was observed in the resulting pore structure upon the change in the additive concentration.

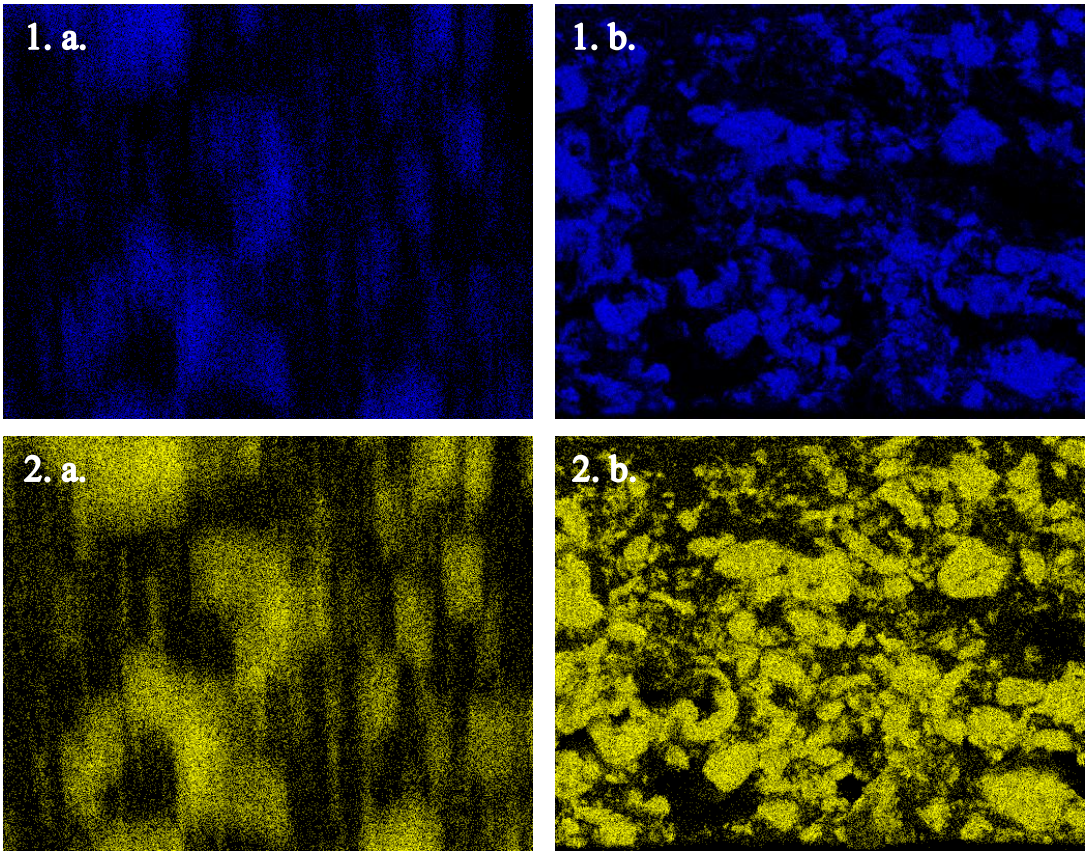

Figure 3.13 EDX mapping results of unprocessed films; (1) Fluorine map, (2) Silicon map; (a) PLLA-10T, (b) PLLA-30T.

When the additive is changed to a non-CO_2-philic POSS, OMPOSS, it can be seen that there is no formation of pores at all in the cross-section even with 30 % OMPOSS addition (PLLA-30O) (Figure 3.12.3). This can be attributed to the non CO_2-philic nature of the additive, rendering no increase in the affinity of the film with $scCO_2$, thus no enhancement in the $scCO_2$ diffusion into the film. As a result non CO_2-philic additive did not contribute to the pore formation in the film.

The effect of all processing parameters (*ST*, *SP*, *VR*, *Stime*, type and concentration of additive) on the resulting average size of the pores in the films are summarized in Table 3.1

Table 3.1 Summary of processing conditions and resulting pore size for all sample.

Film Type	Processing Condition				Pore Size	
	ST **(K)**	***SP*** **(MPa)**	***VR*** **(MPa.min^{-1})**	***Stime*** **(h)**	**Mean**	**SD (Standard Deviation)**
P_LLA	313	10.3	10.3	2	non-porous	
	313	20.7	10.3	2	non-porous	
	313	20.7	10.3	24	720nm	260nm
	333	20.7	10.3	2	300nm	140nm
	373	10.3	10.3	2	non-porous	
	373	20.7	0.2	2	1.1µm	0.76µm
	373	20.7	10.3	2	1 µm – 100µm	0.36 µm – 45 µm
	373	20.7	10.3	24	non-porous	
	393	20.7	10.3	2	1 µm – 765µm	0.31 µm – 377 µm
P_LLA-10T	313	10.3	10.3	2	715nm	295nm
	313	20.7	10.3	2	625nm	205nm
	313	20.7	10.3	24	570nm	220nm
	333	20.7	10.3	2	625nm	250nm
	373	10.3	10.3	2	non-porous	
	373	20.7	0.2	2	680nm	240nm
	373	20.7	10.3	2	950nm	340nm
	373	20.7	10.3	24	1200nm	450nm
	393	20.7	10.3	2	650 nm – 335µm	200nm – 170µm
P_LLA-30T	313	20.7	10.3	2	860nm	360nm
	313	20.7	10.3	24	805nm	260nm
P_LLA-30O	313	20.7	10.3	2	non-porous	

3.1.2 3D Reconstruction of the Samples and Porosity Calculation

The microstructures of the porous films processed at 313, 373 and 393 K, were further investigated with μCT analysis (Figure 3.14). μCT images and 3D reconstruction of the P_LLA-10T film processed at 313 K (Figure 3.14.a) show the distribution of the pores on the surface and cross-section of the film. The porosity of the film was calculated to be 27.3%, which was a significant increase from the non-porous P_LLA film. Increasing the TFPOSS concentration to 30 wt% further improved the porosity of the processed film to 40.2% (Figure 3.14.b) with more uniformly distributed pores throughout the film. The μCT images and 3D reconstruction of the P_LLA-30T film also shows denser pores compared to the P_LLA-10T film. This result agrees with the SEM analysis result (Figure 3.12.1 and 2, Page 45), where it was seen that PLLA-30T film after processing shows formation of more homogeneous pores in the cross-section of the film.

At 373 K, non-uniform formation of micro-sized pores can be observed in the cross-section of P_LLA film (Figure 3.14.c). This result agrees with the SEM image (Figure 3.1.3, Page 26), and the porosity was obtained to be 23.2%. Adding 10 wt% TFPOSS and processing at 373 K resulted in formation of less porous film, with smaller pore size (Figure 3.14.d). Additionally the porosity was obtained to be 7.6%, which is lower than the P_LLA film counterpart. This lower porosity percent can be attributed to profound increase in the crystallinity of the film, which was determined with the DSC analysis (these results will be explained in section 3.1.5, Page 59). Higher crystallinity hinder the pore formation because the nucleation can only occur in the amorphous part of the polymer where the CO_2 are dissolved [66,67]. Because of this less region is available for pore formation in the P_LLA-10T. This resulted in lower porosity. Additionally, compared to the films processed at 313 K, by observing the μCT images and photographs of the films, small deformation in the shape of the film can be observed after processing at 373 K. This can be attributed to the increased difference between the processing temperature and the decreased T_g of the polymer during the $scCO_2$ processing.

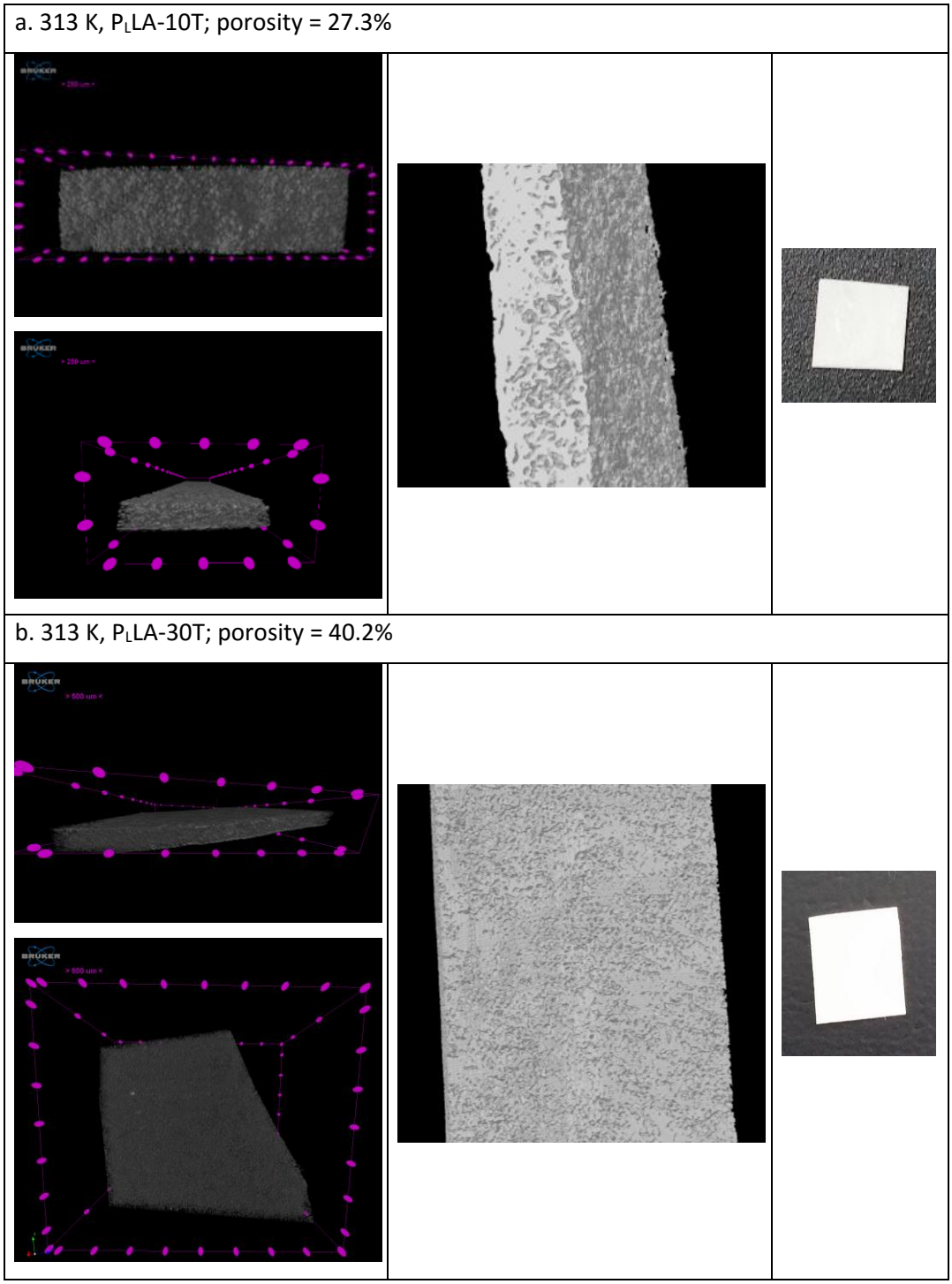

Figure 3.14 µCT analysis of the film processed at *SP* = 20.7 MPa, *Stime* = 2 h, and *VR* = 10.3 MPa.min^{-1}; µCT images of the sample (first column); three-dimensional µCT reconstruction (second column); photograph of the samples (third column)

c. 373 K, P_LLA; porosity = 23.2%		
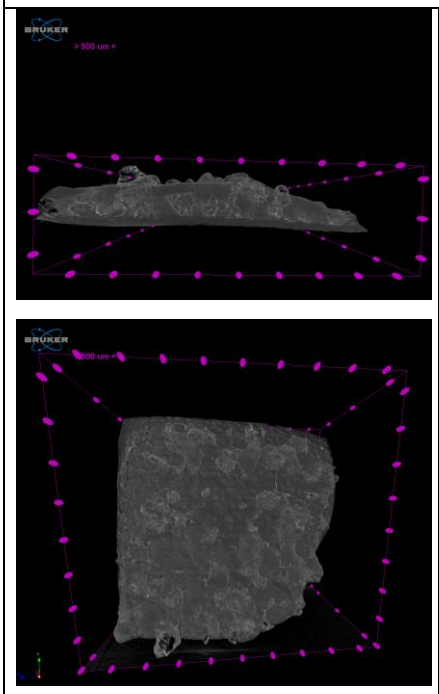	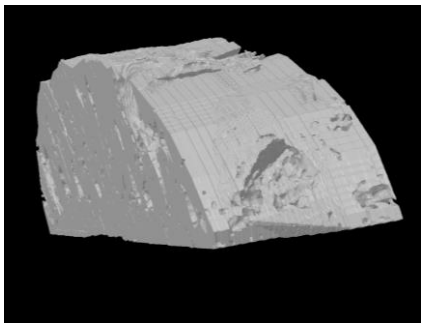	
d. 373 K, P_LLA-10T; porosity = 7.6%		
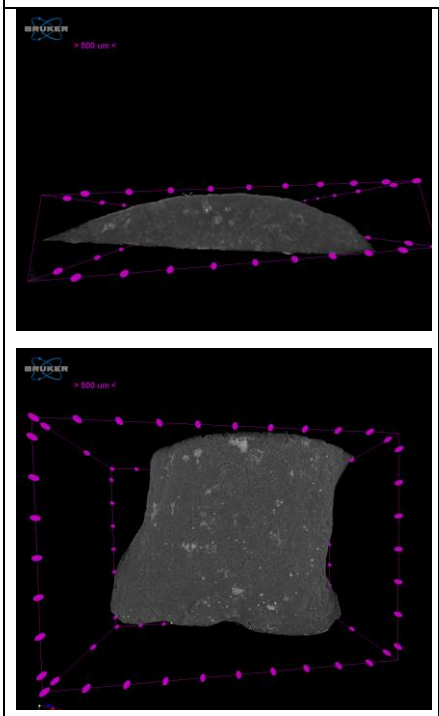	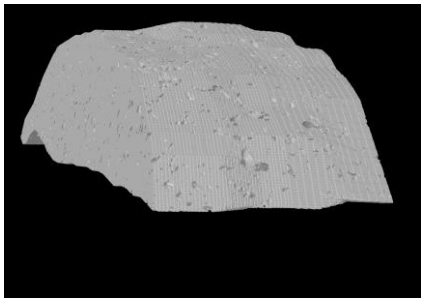	

Figure 3.14 (continued)

e. 393 K, P_LLA; porosity = 79.7%		
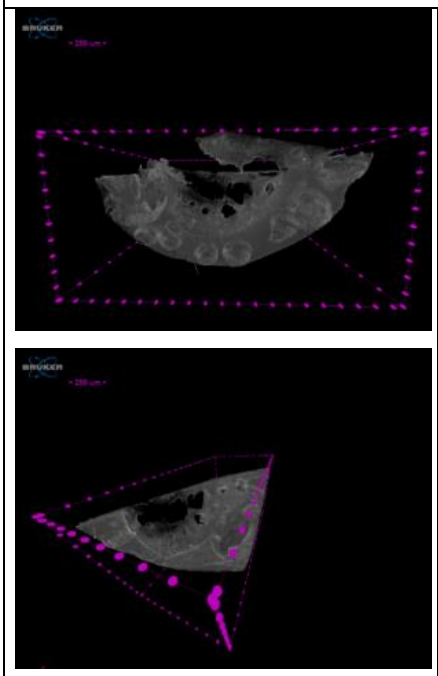	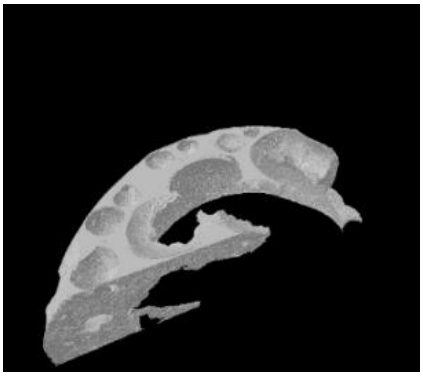	
f. 393 K, P_LLA-10T; porosity = 71.1%		
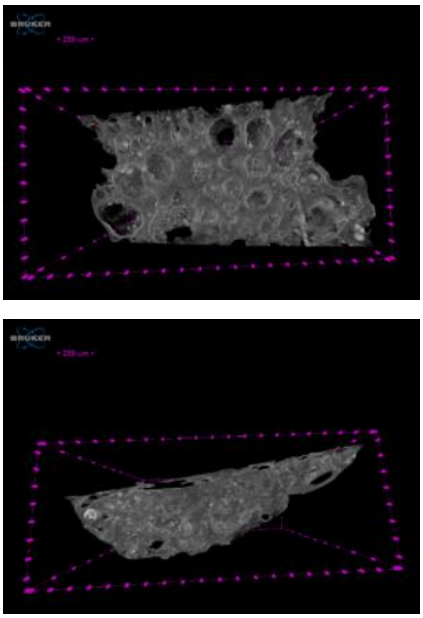	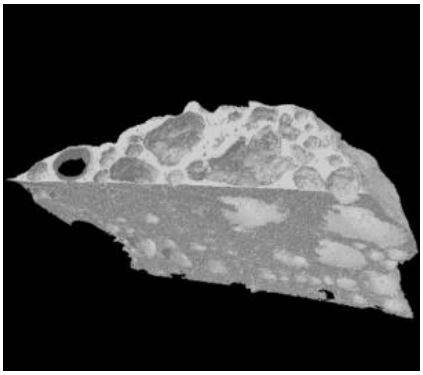	

Figure 3.14 (continued)

At 393 K, in both PLLA and PLLA-10T films (Figure 3.14.e. and f.) formation of pores in micron sizes can be observed, similar to what was observed in SEM analysis (Figure 3.1.4, Page 26 and Figure 3.2.4, Page 29). The pores formed at PLLA-10T films were observed to be smaller and more homogeneously distributed compared to the PLLA film. From the μCT images and photographs of the films, deformation of the films processed at 393 K can also be seen, with a greater level of deformation along with the color change showing that thermal degradation occurred at this processing temperature. Because of this film processing at 393 K is not preferable. PLLA-10T film exhibited less color change compared to the PLLA film, which could indicate that the addition of POSS improved the thermal stability of the film, and decreased its degradation at high processing temperature. This is expected since POSS are commonly used to improve the thermal properties of the polymer nanocomposites [68–70]. For both PLLA and PLLA-10T films processed at 393 K, the porosity values were obtained to be 79.7% and 71.1% respectively. Among all of the processing parameters studied in this work, 313 K saturation temperature, 20.7 MPa saturation pressure, 10.3 $MPa.min^{-1}$ venting rate and 2 h processing time was determined to be promising conditions for PLLA-10T and PLLA-30T film processing because of the formation of the most homogeneous pores, low processing temperature, short processing time and absence of deformation and color change.

3.1.3 Extraction of the TFPOSS

Figure 3.15 shows the EDX analysis of the cross-section of the PLLA-30T films before and after processing at the conditions of *SP* = 20.7 MPa, *ST* = 313 K, *VR* = 10.3 $MPa.min^{-1,}$ *Stime* = 2 h and 24 h. From Figure 3.15.a it can be seen that before processing peak of Si and F exist in the EDX spectrum, presenting the TFPOSS in the film, while after processing at 2 and 24 h (Figure 3.15.b and c), no Si or F signal exist in the spectrum. This shows that all of the TFPOSS was extracted by the $scCO_2$ processing. The extraction of the additives with $scCO_2$ can be beneficial for

applications that require very high purity such as biomedical applications, where presence of impurities in the polymer is undesirable.

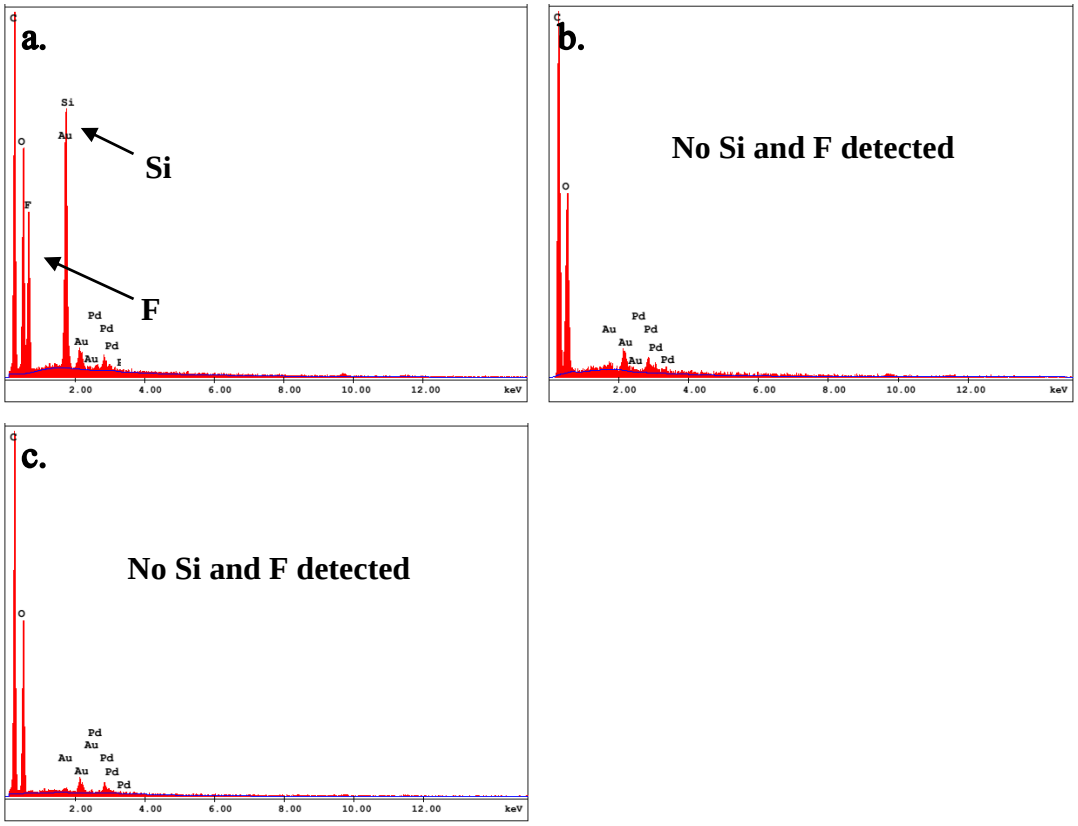

Figure 3.15 EDX analysis result of PLLA-30T films (a) unprocessed, (b) after processing with *SP* = 20.7 MPa, *ST* = 313 K, *VR* = 10.3 MPa.min$^{-1,}$ *Stime* = 2 h (c) after processing with *SP* = 20.7 MPa, *ST* = 313 K, *VR* = 10.3 MPa.min^{-1}, *Stime* = 24 h

Comparing with the EDX results of the film processed at *SP* = 20.7 MPa, *ST* = 373 K, *VR* = 10.3 MPa.min$^{-1,}$ *Stime* = 2 h and 24 h (Figure 3.16) it can be seen that even after 24 h there were still some Si and F atoms detected in the film, showing that there was still some TFPOSS left in the film. Table 3.2 shows the quantification of the EDX result for the samples that was processed with $scCO_2$ at *SP* = 20.7 MPa, *ST* = 373 K, and *VR* = 10.3 MPa.min^{-1}, and the EDX mapping of the sample is also given in APPENDIX C. From Table 3.2 it can be seen that the TFPOSS wt% in the film

decreased after 2 h processing and decreased more after 24 h processing. In the previous case it was shown that at 313 K saturation temperature, even at 30 wt% initial TFPOSS concentration, it was possible to extract all the TFPOSS after only 2 h processing. However this time with only 10 wt% initial TFPOSS concentration, it was not possible to extract all the TFPOSS, even after very long processing time, 24 h. This can be attributed to the solubility of TFPOSS decreases as temperature increase. Because of the lower solubility at higher temperature, the driving force for the extraction will be weaker, thus longer processing time will be needed to completely extract the TFPOSS. In addition to this, it was also possible that the solubility of TFPOSS at 373 K is lower than the concentration of TFPOSS in the vessel if all of the TFPOSS is extracted from the film. In this case $scCO_2$ would only be able to dissolve part of the TFPOSS, and thus complete extraction would not be possible.

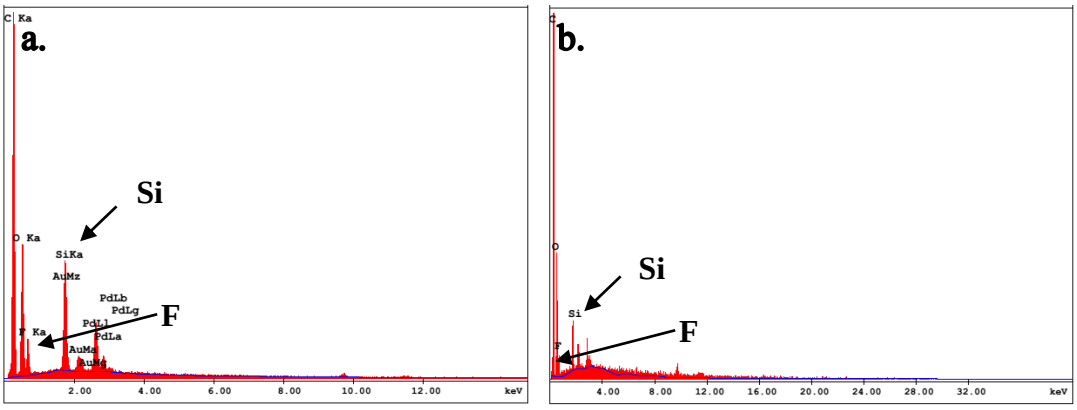

Figure 3.16 EDX analysis result of PLLA-10T films (a)unprocessed, (b)after processing with *SP* = 20.7 MPa, *ST* = 373 K, *VR* = 10.3 MPa.min$^{-1,}$ *Stime* = 2 h (c) after processing with *SP* = 20.7 MPa, *ST* = 373 K, *VR* = 10.3 MPa.min$^{-1,}$ *Stime* = 24 h

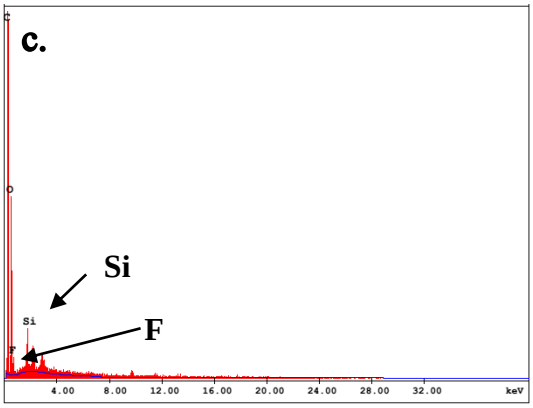

Figure 3.16. (continued)

Table 3.2 Quantification of EDX analysis result for samples processed at 373 K

Sample Type	Processing Temperature (K)	Processing Time (h)	Si wt%	F wt%
PLLA-10T	373	0	2.9	5.1
PLLA-10T	373	2	1.4	3.7
PLLA-10T	373	24	1.2	2.8

3.1.4 Hardness of the Films

Indentation hardness of the film was obtained by nanoindentation by using pyramidal Berkovich tip. Nanoindentation analysis requires the sample to have a flat smooth surface and thus not all of the samples were possible to be analyzed because some of the samples had a very large deformation after $scCO_2$ processing, especially the ones that were processed at 373 and 393 K. The indentation hardness data is given in Table 3.3 and Figure 3.17. From the table and figure it can be seen that some of the samples have quite large standard deviation. The reason for this is because of the presence of pores and the surface of the samples that were not very smooth.

Table 3.3 Indentation Hardness of the Films

Sample Type	*ST* (K)	*Stime* (h)	Indentation Hardness (MPa)	Standard Deviation (%)
P_LLA	313	2	529	35
		24	2070	6
P_LLA-10T	313	2	64	16
		24	430	37
P_LLA-10T	373	2	114	9
		24	1675	9
P_LLA-30T	313	2	2472	10
		24	3541	3

In Figure 3.17 the number after the sample type refers to the *ST,* for example P_LLA-313 refer to P_LLA sample processed at 313K. From Table 3.3 and Figure 3.17 it can be seen that at all processing temperature, increasing processing time results in increase in indentation hardness. This can be due to the plasticization effect of $scCO_2$ on the polymer. During the processing, $scCO_2$ allows the chains to move more easily and thus rearrange themselves. With the longer processing time, larger amount of CO2 would diffuse into the polymer and more uniform distribution of CO2 would be achieved in the polymer matrix. This would allow more profound plasticization effect of CO2, allowing easier movement and rearrangement of the polymer chains. Also with the longer processing time, chains would also have more time to rearrange themselves. These would in turn strengthen the intermolecular interactions between the chains, which would result in increase in the mechanical properties such as hardness of the polymer.

It also can be seen that for P_LLA-10T sample, increasing the saturation temperature from 313 to 373 also increases the indentation hardness. The reason for this effect is also the increase in the enhancement in the mobility of the polymer chains which did not only increase due to the higher processing temperature, which was above the T_g

of the unprocessed polymer but also due to the higher diffusion coefficient of the polymer, allowing more amount of CO_2 diffuse into the polymer matrix with more uniform distribution. Therefore, at higher temperature the chains would be able to rearrange better than they do at lower temperature, enhancing the intermolecular interactions between the chains, and thus enhancing the mechanical properties of the polymer.

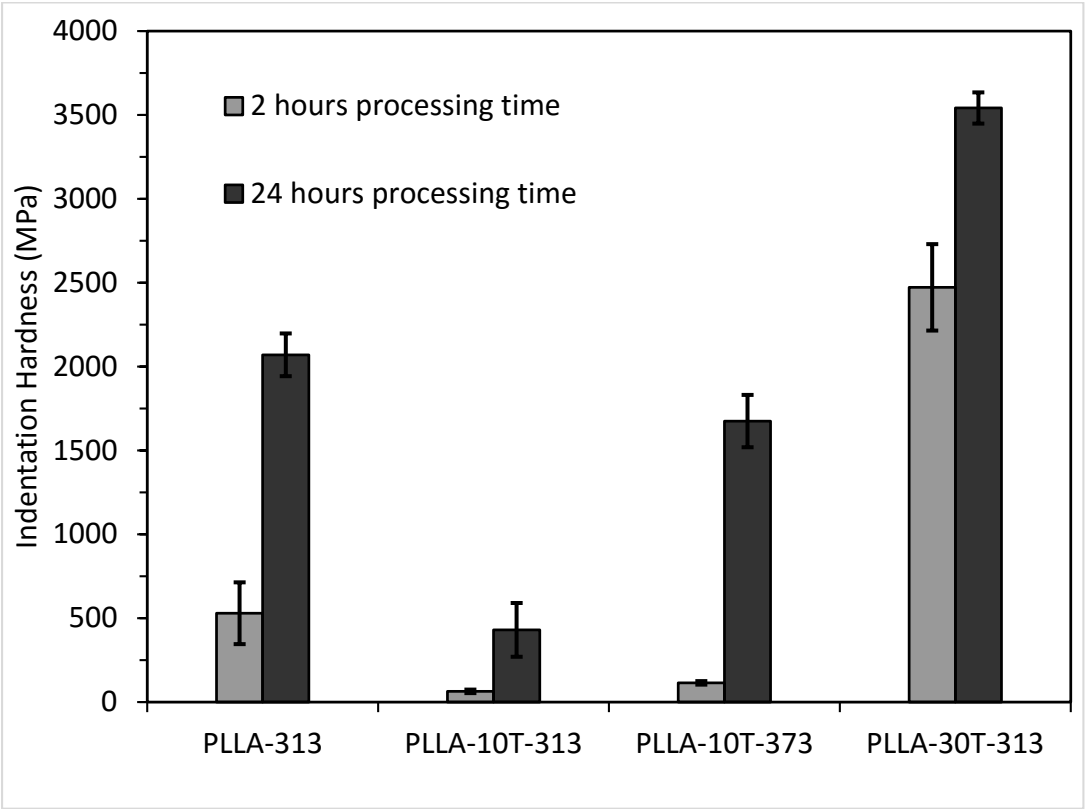

Figure 3.17 Indentation hardness of the samples

Finally by comparing the sample with and without the addition of TFPOSS, it can be seen that at the same processing temperature addition of 10% TFPOSS decreases the hardness. This can be because of the porosity achieved with the addition of TFPOSS, before which there were no pores. The hardness of the sample was expected to decrease because of the presence of the pores. However when the TFPOSS concentration was increased furthermore to 30%, significant increase in indentation

hardness was observed. This result is unexpected because after the processing the structure obtained was more porous than the film with addition of 10% TFPOSS, thus lower hardness was expected. Moreover in PLLA-30T film, similar to PLLA-10T film, after the processing there were no TFPOSS left in the structure because of the complete extraction. Therefore the observed increase in hardness, cannot be attributed to the reinforcement effect of TFPOSS. On the contrary, this increase in hardness observed in PLLA-30T film could be due to the extraction of the TFPOSS during the $scCO_2$ processing. With the extraction of the CO_2-philic additive, the polymer, which would have already been plasticized with CO_2, could be more flexible due to the increase in the free volume of the polymer chains, giving them more space to move. This would allow the polymer chains to reorganize themselves more effectively, and enhance their interactions with each other leading to an increase in the polymer hardness.

3.1.5 Differential Scanning Calorimetry (DSC) Results

The thermal properties of the films were obtained by the means of DSC analysis. Complete result of the DSC analysis is given in Table 3.4 and the thermogram of all samples are given in APPENDIX D. All of the data is taken from the first heating result. Additionally, crystallinity values of the samples were also calculated by using the DSC analysis result with the following equation:

$$\%Crystallinity = \frac{\Delta H_m - \Delta H_c}{\Delta H_m^0} \cdot 100\%$$

Where ΔH_m is the specific enthalpy of melting of the films is, ΔH_c is the specific enthalpy of crystallization of the films, and ΔH_m^0 is the specific enthalpy of melting of 100% crystalline PLLA obtained from literature ($\Delta H_m^0 = 93.1\ J.g^{-1}$) [61]. For all samples cold crystallization was not observed during the first heating.

The resulting crystallinity data is plotted in Figure 3.18, Figure 3.19, and Figure 3.20 for PLLA, PLLA-10T and PLLA-30T samples respectively. In the plot and table, the first number after the sample name refers to the processing temperature and the

second number refers to the processing time. C after the sample name refers to unprocessed (control) sample. From the graphs it can be seen that crystallinity of the

Table 3.4 DSC results of the samples

Sample Name	**T_g (K)**	**T_m (K)**	**ΔH_m $(J.g^{-1})$**	**Crystallinity (%)**
PLLA-C	324.2	444.9	42.5	45.7
PLLA-313-2	337.6	447.8	48.5	52.1
PLLA-313-24	333.3	446.9	53.7	57.7
PLLA-373-2	334.8	445.2	51.9	55.8
PLLA-373-24	334.7	446.4	69.4	74.6
PLLA-393-2	330.4	443.8	56.0	60.2
PLLA-393-24	332.0	445.9	59.4	63.8
PLLA-10T-C	322.1	442.7	45.7	49.1
PLLA-10T-313-2	328.1	447.5	48.0	51.6
PLLA-10T-313-24	337.3	446.7	55.4	59.5
PLLA-10T-373-2	333.8	448.4	68.3	73.4
PLLA-10T-373-24	334.8	445.7	62.1	66.7
PLLA-10T-393-2	335.3	444.4	52.5	56.3
PLLA-10T-393-24	331.4	440.5	51.6	55.4
PLLA-30T-C	321.0	443.2	34.1	36.6
PLLA-30T-313-2	333.7	447.1	47.5	51.0
PLLA-30T-313-24	335.0	448.1	44.1	47.4

samples always increased after the $scCO_2$ processing. This shows that CO_2 had a plasticizing effect on the solid polymer, so that polymer chains gain some mobility and reorganize themselves due to $scCO_2$ processing which is leading to higher crystallinity. The most dominant increase in crystallinity was observed at 373 K for both P_LLA and P_LLA-10T films. For P_LLA samples, the crystallinity of the films

always increased as the processing time increased. This is because as time increases, the polymer chains will have more time to reorganize themselves and the polymer exhibits higher crystallinity. After the addition of TFPOSS, both P_LLA-10T and P_LLA-30T samples, consistent effect of processing time was not observed anymore. This can be due to the addition of POSS causing irregularity in the polymer structure, which in turn change the resulting crystallinity value also. However no consistent effect of processing temperature to the resulting crystallinity of the samples was observed from the DSC result.

Similar to crystallinity, the glass transition temperature (T_g) of the films were observed to always increase also after the scCO_2 processing, which can be still attributed to the plasticization effect of the CO_2 on the polymer chains. The effect of processing parameters on the T_g was observed to be not significant.

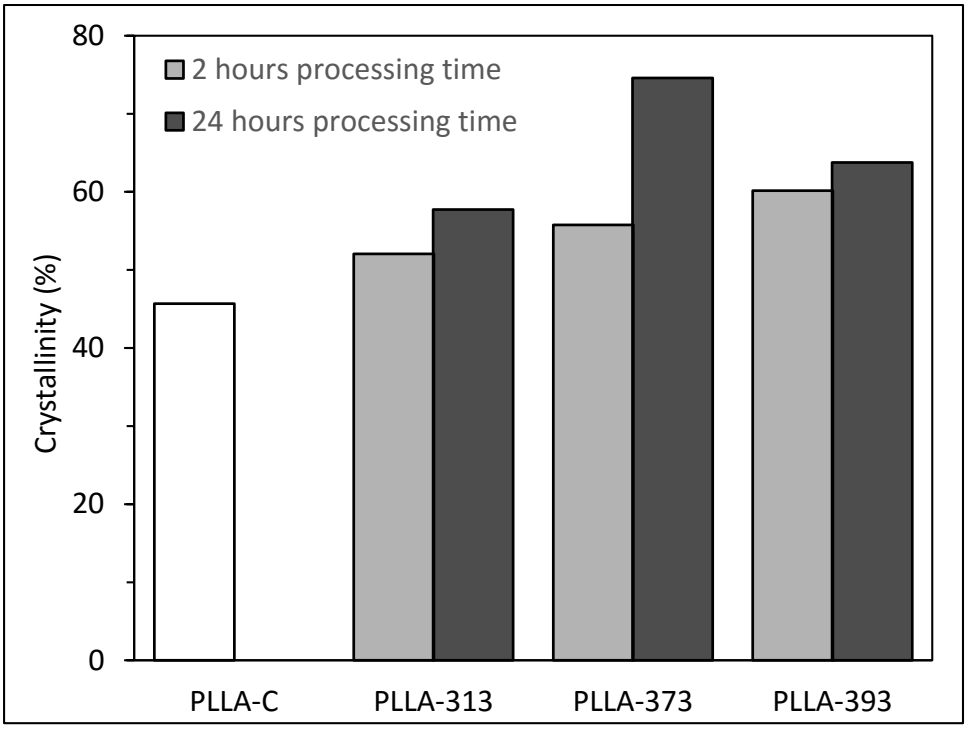

Figure 3.18 Crystallinity of P_LLA samples before and after scCO_2 processing

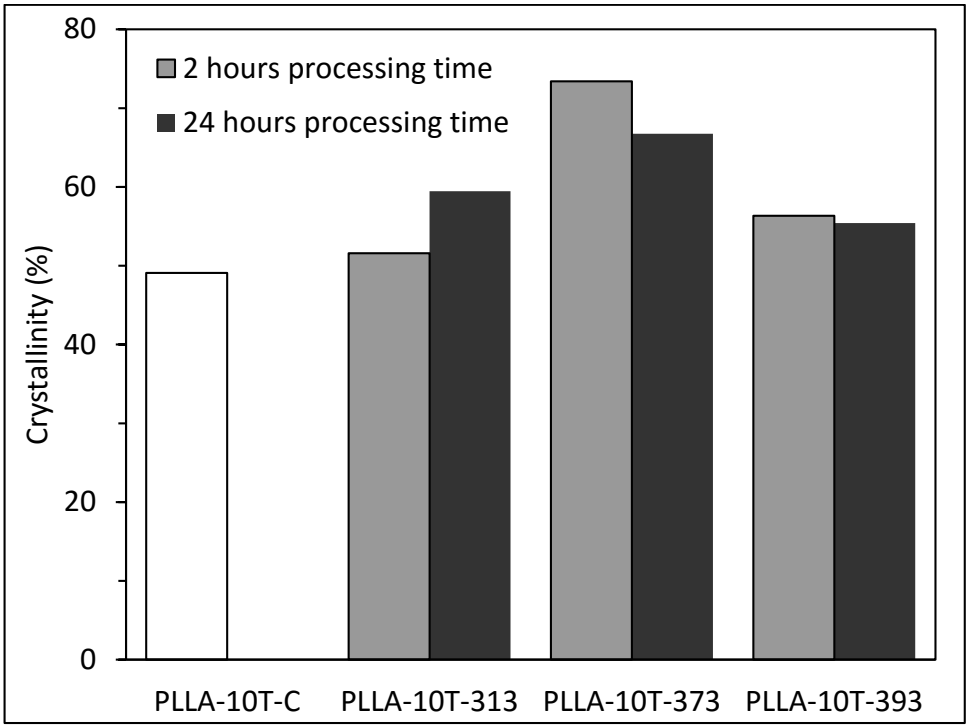

Figure 3.19 Crystallinity of P_LLA-10T samples before and after $scCO_2$ processing

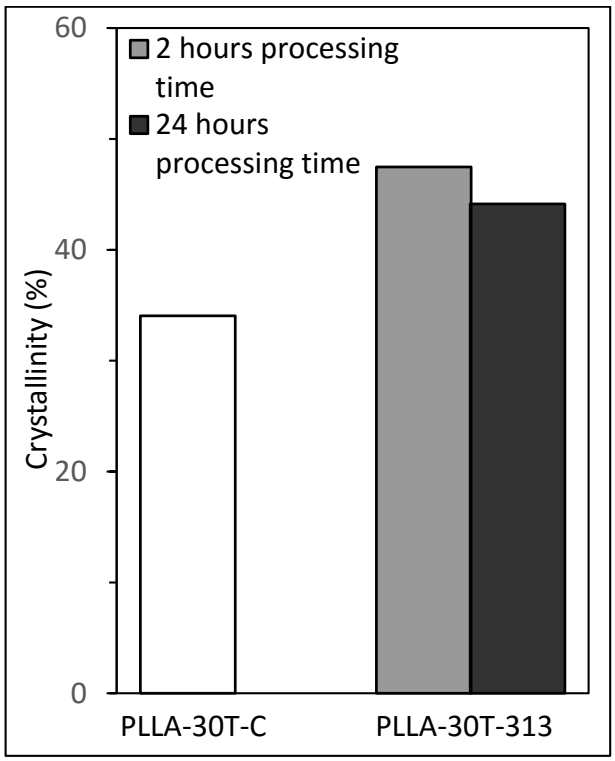

Figure 3.20 Crystallinity of P_LLA-30T samples before and after $scCO_2$ processing

3.1.2 Drug Releases Studies

3.1.2.1 Drug Loading

The drug loading process was carried out by using the vacuum-pressure cycle. The films used in this part of the study had an average size of approximately 0.7 cm x 0.7 cm. In this cycle a drop of drug solution is introduced to the surface of the film. The drug is forced to enter the pores of the film by the help of applied vacuum and pressure cycle.

During the loading it was observed that the surface of the film is hydrophobic, such that the solution cannot easily distribute itself on the surface of the film. Because of this it is possible that the loading process might not be optimum because the drug solution did not cover the entire surface of the film. To improve this, it was tried to apply plasma to the film, 50W for 5min, to increase the hydrophilicity of the surface and also to etch the outer most layer of the surface that might be covering the pores.

From Figure 3.17.1 it can be seen that before the application of plasma the surface of the sample was not homogeneously porous. There existed a skin layer that cover some of pores which can be observed in $scCO_2$ processing of polymers. After the application of plasma Figure 3.17.2 it can be seen that almost all the skin layer was removed and the pores were exposed. The formation of skin layer has been observed also in previous works [24,35]. Because of this it was expected that it would be possible to load the film with plasma application better than the one without plasma.

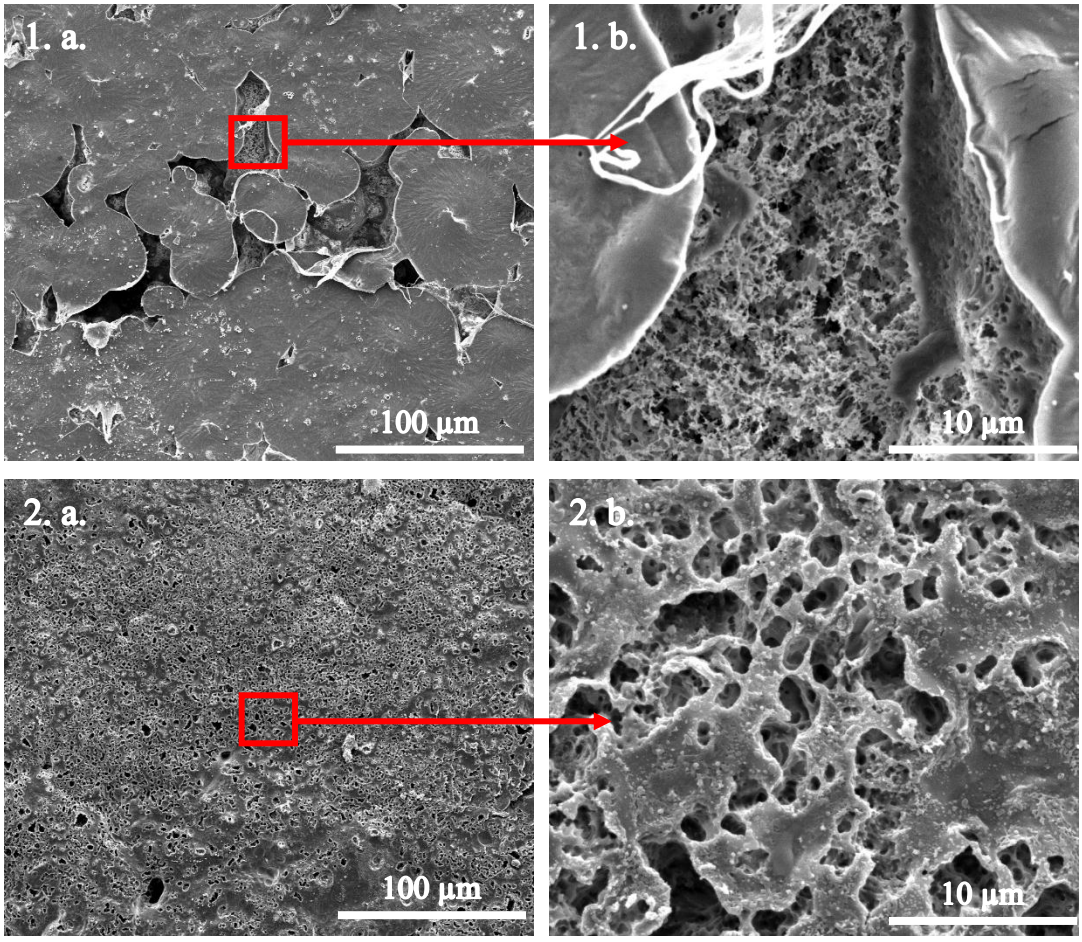

Figure 3.17 SEM micrographs of the surface of the processed thin P_LLA-30T film samples processed at *SP* = 20.7 MPa, *ST* = 313 K, *VR* = 10.3 MPa.min^{-1} and *Stime* = 2 h; (1) before plasma application (2) after plasma application (a) 1000x magnification (b) 10000x magnification

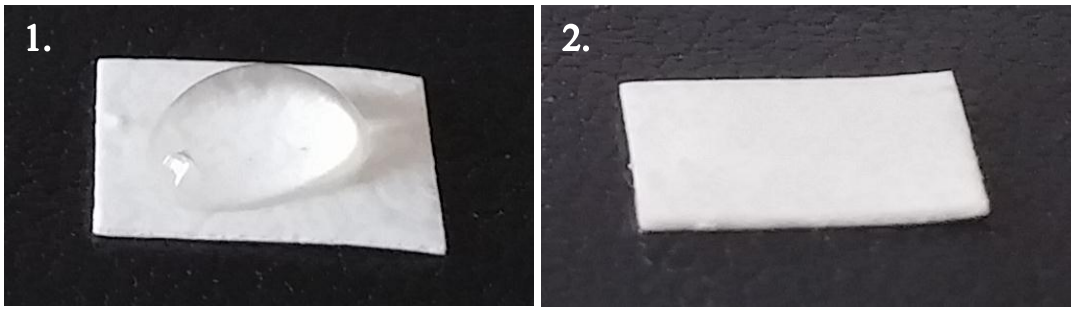

Figure 3.18 Picture of drop of drug solution on top of the P_LLA-30T films (1) before plasma application, (2) after plasma application

In fact during loading, it was observed that the hydrophilicity of the film after plasma application increased. The hydrophilicity increased due to formation of polar groups on the surface during plasma treatment[71]. After dropping the drug solution it was observed that the drug solution easily dispersed itself on the surface of the film (Figure 3.22). Thus it was expected that the film with plasma application would be able to be loaded with more amount of drugs than the one without plasma.

3.1.6.2 Release Studies

The drug release experiment was conducted to see the effect of pores on the resulting rate of drug release. The release was performed by immersing the films in PBS solutions. For each film that was investigated, three replicates were used in the drug release analysis to ensure reproducibility of the results. The results are given in Figure 3.23. From the figure, by considering the standard deviation, it can be seen that all films had similar release rate, and burst release was observed in all films, where about 90% of the drugs were released in the first 30 minutes. After this burst release, the release of the drug continued slowly within one week. This release behavior would be suitable for antibiotic applications because burst release would be needed to kill all the bacteria at first. Then slow continuous release would be needed to keep the bacteria from infecting the treated site again.

From previous analysis conducted on the obtained films, it was clearly seen that some of the films were obtained with various porosity levels after $scCO_2$ processing. Also surfaces of some of the films were also improved by using plasma treatment, enhancing the hydrophilicity and removing the skin layer to eliminate blocking of the porous structure. However from the release test it was observed that there were no differences between the rates of the non-porous film, porous film, and porous film with skin layer removed. This might be due to insufficient interconnectivity of the pore structure of the film deeper in the matrix. Because of this, during the loading, the drug might not have been able to penetrate deeply to the film and most of them

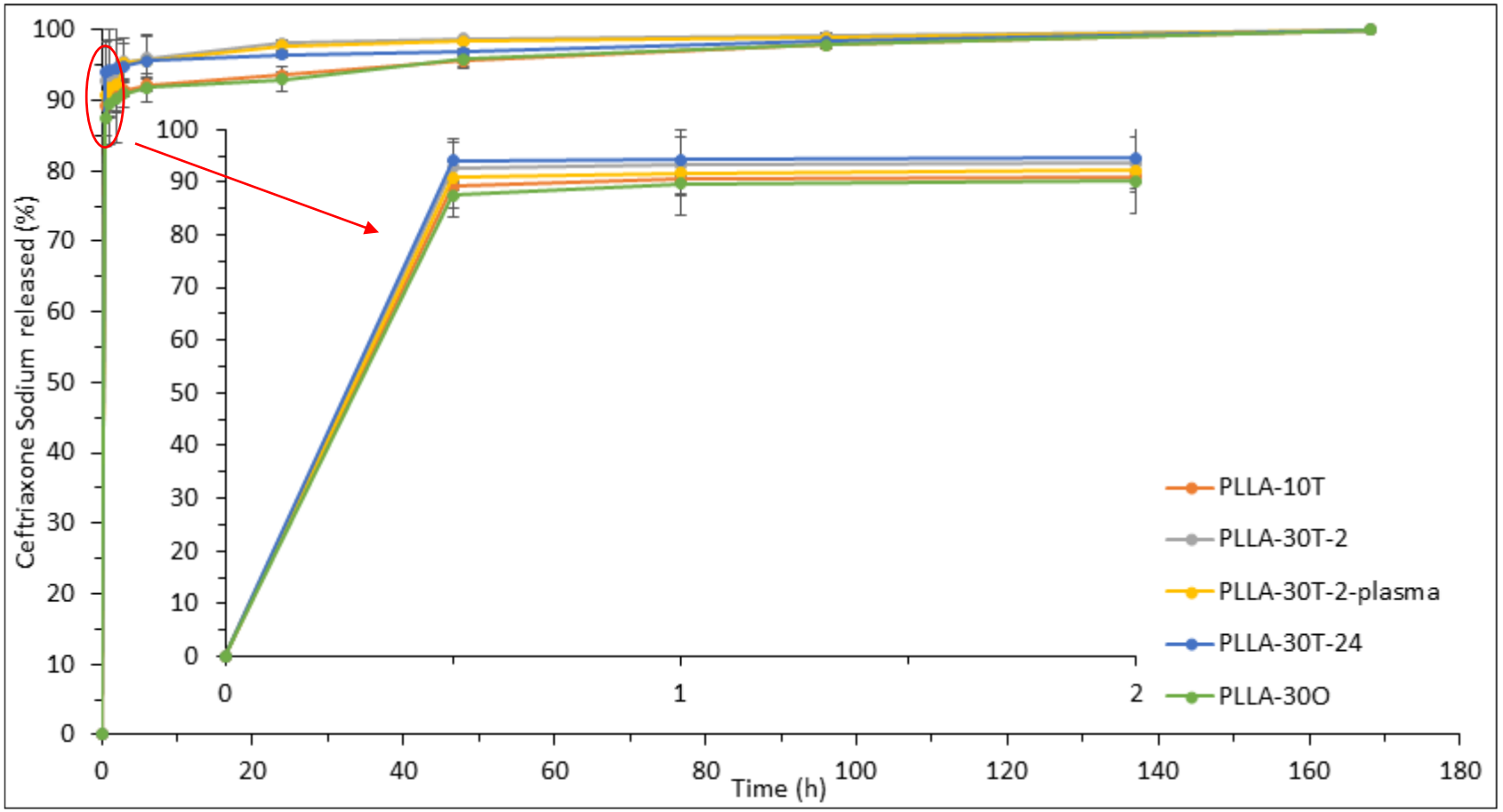

Figure 3.23 Drug release result of Ceftriaxone Sodium with using different processed films.

stayed in the pores near to the surface of the film. This causes most of the drug (about 90%) to be immediately in contact with the PBS solution during the first minutes of release experiments and immediately released. Only about 10% of the drugs were left in the porous structure, which were released slowly over the span of 1 week.

3.2 Solubility Modelling Result

The experimental solubility data of TFPOSS in scCO2 were available at 308 and 323 K [60]. Data set of both temperatures for TFPOSS was fitted by each model to obtain the model parameters giving the best predictions for both of the temperatures. All of the experimental and predicted solubility data are given in Table 3.5 and plotted in Figure 3.24 and Figure 3.25 for 308 K and 323 K respectively. The parameters obtained with each model to correlate the solubility data of the TFPOSS in $scCO_2$ and their respective *AARD* are given in Table 3.6

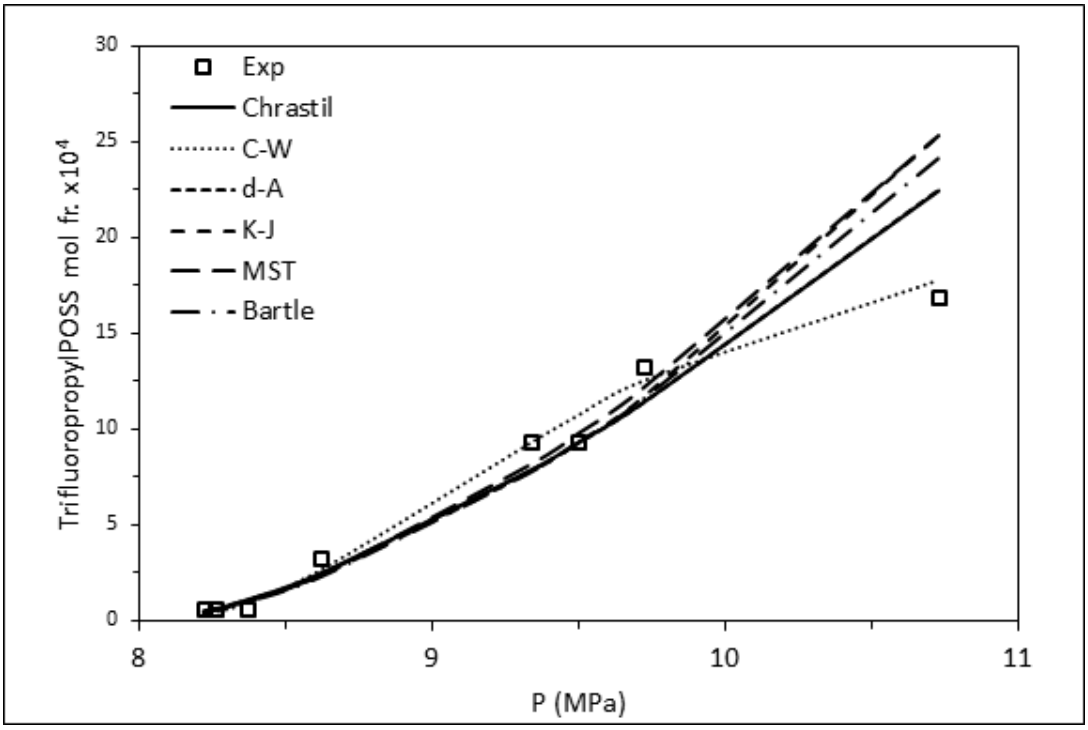

Figure 3.24 Experimental solubility data for trifluoropropylPOSS and the correlations with semi-empirical models at 308 K.

Table 3.5 Solubility data for TrifluoropropylPOSS at 308 K and 323 K

T (K)	**P (MPa)**	**ρ (kg/m^3)**	**Exp**	**Chrastil**	**C-W**	**d-A**	**K-J**	**MST**	**Bartle**
308	8.22	561.1	0.00006	0.00004	0.00003	0.00004	0.00005	0.00005	0.00004
	8.26	572.6	0.00006	0.00006	0.00004	0.00006	0.00006	0.00006	0.00006
	8.37	596.9	0.00006	0.00011	0.00009	0.00011	0.00010	0.00011	0.00010
	8.62	632.4	0.00033	0.00025	0.00026	0.00025	0.00023	0.00024	0.00023
	9.34	685.9	0.00093	0.00079	0.00093	0.00079	0.00078	0.00082	0.00078
	9.50	694.0	0.00093	0.00093	0.00107	0.00093	0.00093	0.00098	0.00093
	9.72	703.8	0.00133	0.00114	0.00125	0.00114	0.00116	0.00121	0.00115
	10.73	738.3	0.00169	0.00225	0.00178	0.00224	0.00253	0.00253	0.00241
323	11.58	557.9	0.00006	0.00007	0.00006	0.00007	0.00007	0.00007	0.00007
	12.00	587.1	0.00014	0.00013	0.00014	0.00014	0.00014	0.00014	0.00014
	13.04	639.6	0.00047	0.00046	0.00047	0.00047	0.00046	0.00043	0.00045
	13.07	640.9	0.00047	0.00047	0.00048	0.00048	0.00047	0.00044	0.00047
	14.24	680.9	0.00096	0.00111	0.00096	0.00114	0.00116	0.00103	0.00113
	14.81	696.4	0.00164	0.00153	0.00118	0.00157	0.00164	0.00141	0.00158

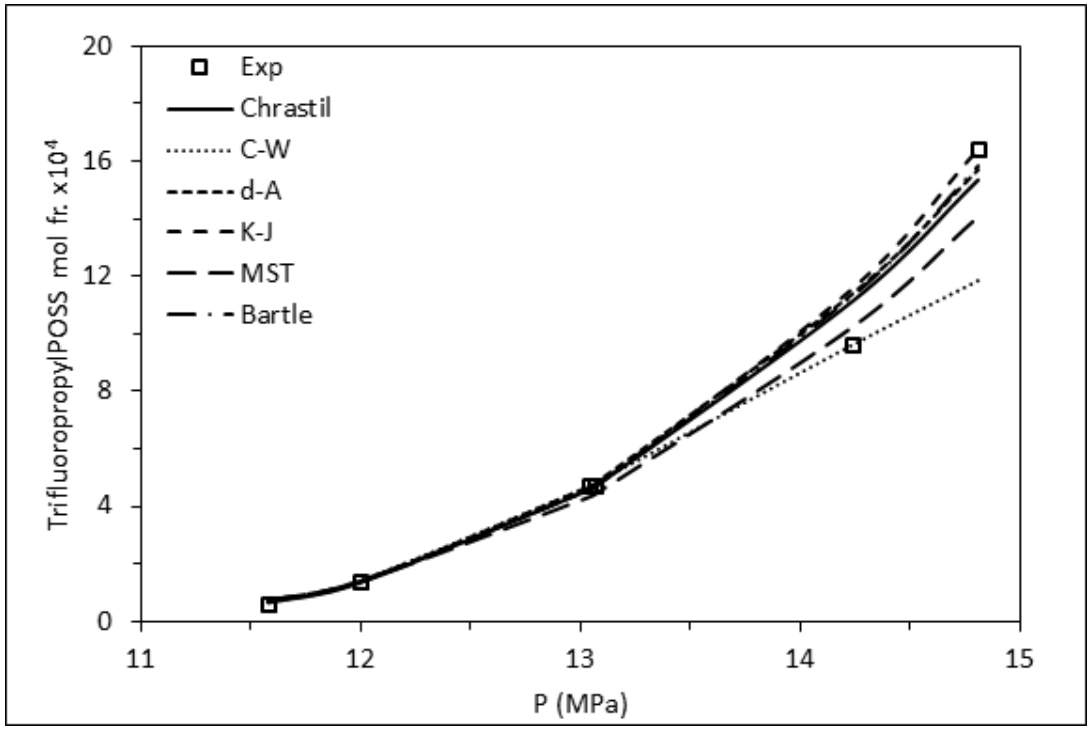

Figure 3.25 Experimental solubility data for trifluoropropylPOSS and the correlations with semi-empirical models at 323 K.

Table 3.6 *AARD* and parameters of all the models for trifluoropropylPOSS

Model	***AARD* (%)**	**a**	**b**	**c**	**d**
Chrastil	16.5	1.5E+01	-3.0E+03	-8.7E+01	
C-W	15.9	1.1E+02	-2.9E+04	4.0E-02	-9.9E+00
d-A	16.6	1.5E+01	-3.1E+03	-8.7E+01	-5.4E+03
K-J	17.8	-1.2E+01	-3.4E+03	2.0E-02	
MST	18.7	-1.0E+04	7.4E+00	1.2E+01	
Bartle	17.7	1.7E+01	-6.1E+03	2.0E-02	
Average *AARD* = 17.21%					

In Table 3.6 it can be seen that the *AARD* for all model for TFPOSS ranged from 16 to 19%, with the average *AARD* of 17.21%. The lowest *AARD* was obtained with Chrastil modified by Wang model, a model with 4 parameters, with *AARD* of 15.93%. From Figure 3.24 and Figure 3.25 it can be also seen that compared to the other models, the C-W model can predict the solubility data more accurately, with one exception for the data at the highest pressure (14.81 MPa) at 323 K. The correlated solubility data of TFPOSS with C-W model in linear plot is given in Figure 3.26. The plot for other models are given in APPENDIX E.

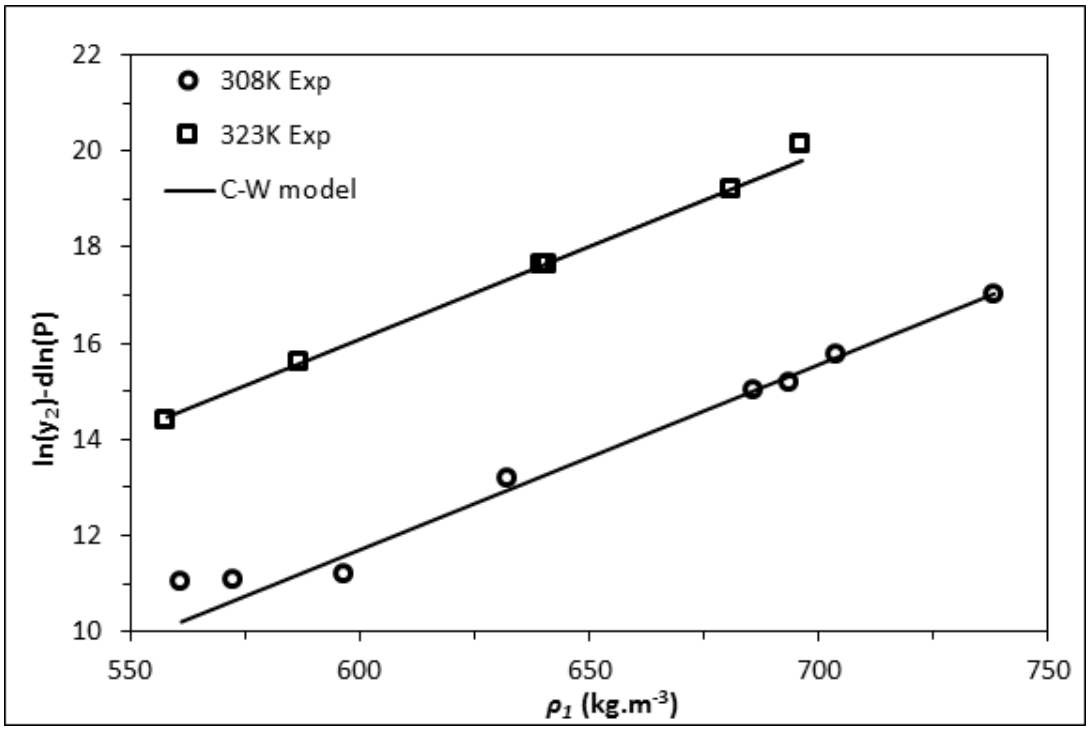

Figure 3.26 Linear plot of the experimental solubility data of TFPOSS and the C-W model

To further improve the prediction of the solubility of trifluoropropylPOSS in $scCO_2$, the C-W model, which gave the lowest *AARD*, was fitted to the experimental data separately for each temperature. The resulting *AARD* and parameters are given in

Table 3.7 and the resulting linear plot is given in Figure 3.27. By comparing Figure 3.27 and Figure 3.26, it can be seen that fitting the model separately to each temperature gave better predictions, especially at lower CO_2 density at 308 K and at higher CO_2 density at 323 K. Furthermore, fitting the model separately for each temperature also decreased the *AARD*, especially at the higher temperature compared to at the lower temperature. At 323 K, a significant decrease in *AARD* can be seen, from 15.93% to 5.11%, while at 308 K the decrease was less, from 15.93% to 11.37%, improving the prediction with approximately 4% decrease in *AARD*. Even though the new set of the parameters obtained at each temperature gave more accurate predictions, they can only be used to predict the isotherm solubility.

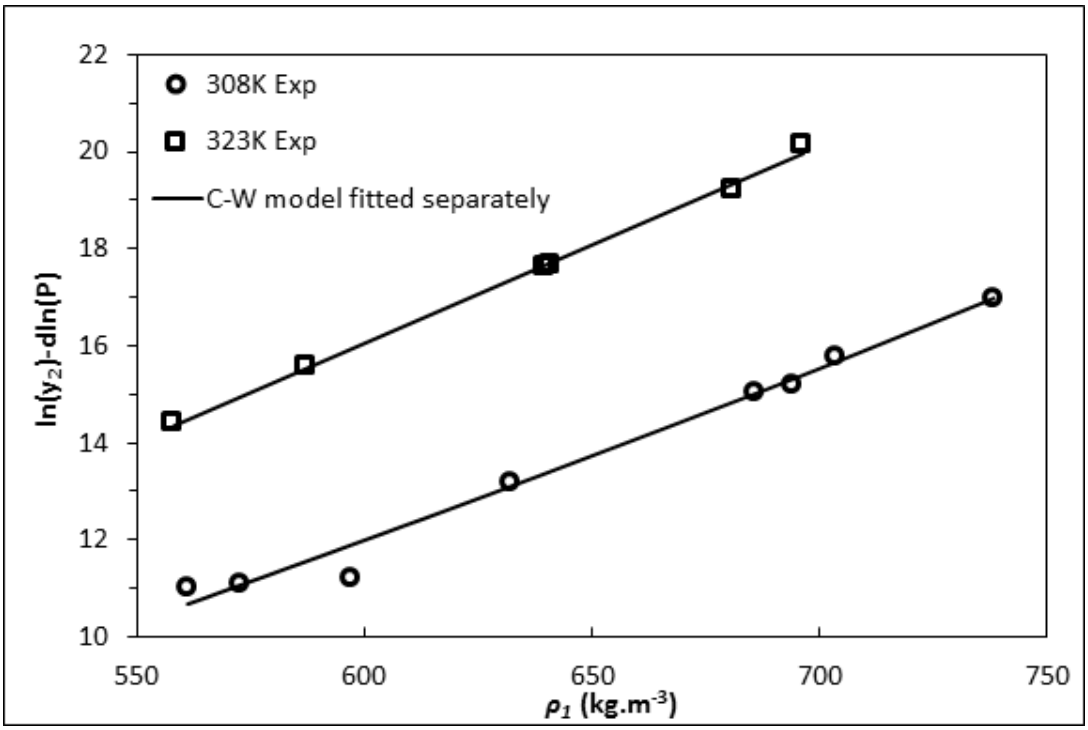

Figure 3.27 Linear plot of the experimental solubility data of TFPOSS and the C-W model fitted separately for each temperature

Table 3.7 *AARD* and parameters for C-W model fitted separately for each temperature for trifluoropropylPOSS

Temperature (K)	*AARD* (%)	a	b	c	d
308	11.4	-1.7E+00	2.8E+03	3.0E-02	-8.2E+00
323	5.1	4.0E-02	-2.8E+04	-1.0E-02	1.7E+01

Additionally, self-consistency test was performed by using the C-W model, which fit the experimental data the best with the least *AARD*. Based on the C-W model, the plot of experimental data at all temperature in the form of:

$$\ln(y_2) - a - \frac{b}{T} - dln(P)$$

against the density of the $scCO_2$ should be a linear plot. The parameters used in this self-consistency test were the ones fitted to both temperature at the same time, not separately because this fit should represent the solubility data at all temperatures. The plot is given in Figure 3.28. The plot for other models are given in APPENDIX F.

Figure 3.28 shows that from the self-consistency test, the TFPOSS experimental solubility data exhibit linear behavior when fitted by the C-W model. There exist some small deviations at some of the data points, but overall the data follow the linear trend. The linearity of the plot confirms that the experimental data are self-consistent and thus the model can be used to predict the solubility data of the TFPOSS at different temperatures and pressures close to the vicinity of the experimental conditions of the used data set.

The model was then used to predict the solubility of TFPOSS in $scCO_2$ at the processing condition of polymer film that was in the vicinity of the experimental data. The only temperature satisfying this condition is 313 K and also this is the temperature at which all the POSS was extracted from the polymeric film with $scCO_2$. The detail of the calculation is given in APPENDIX G.

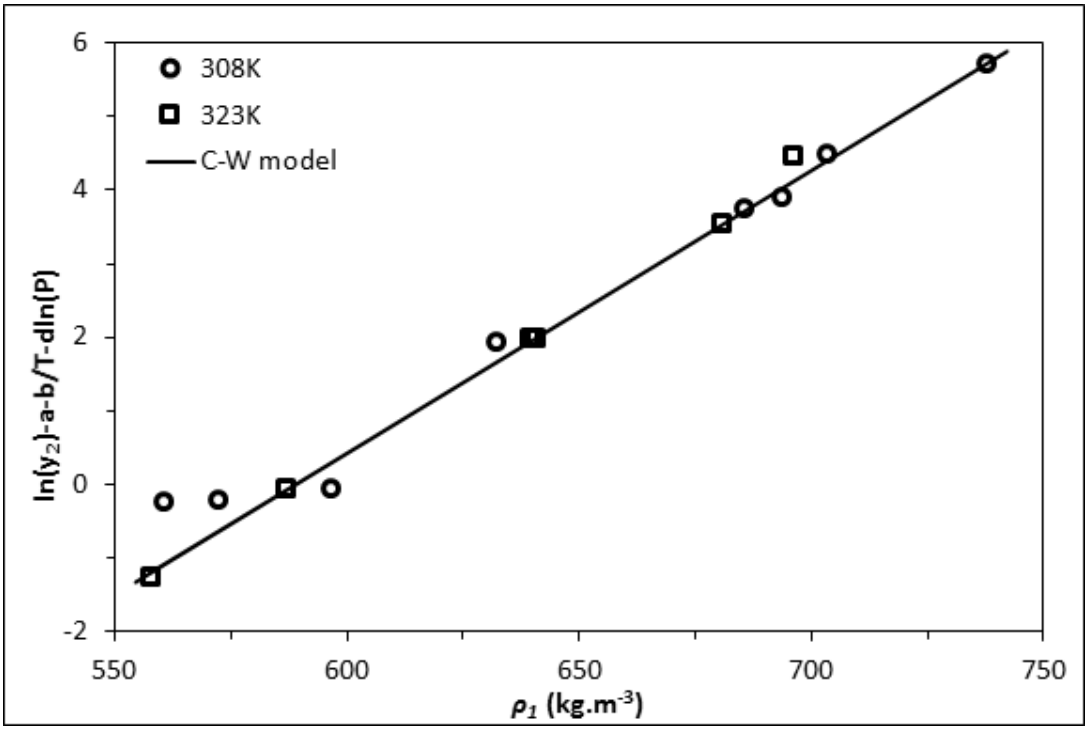

Figure 3.28 Self-consistency plot of trifluoropropylPOSS, by using the C-W model.

It was obtained that the solubility of TFPOSS in $scCO_2$ at 313 K and 20.7 MPa is 0.00081, and the highest mol fraction of the TFPOSS during processing was calculated as 0.00002 for P_LLA-30T films in the supercritical solution during the processing in case of complete extraction of the TFPOSS from the film. This result showed that the amount of TFPOSS used during the processing at 313 K and 20.7 MPa was way below the solubility limit, and thus the $scCO_2$ would be able to dissolve all of the TFPOSS. Additionally this result also showed that it would be possible to extract all of the TFPOSS from the film by using scCO2 giving enough time without mass transfer restrictions. In fact this was confirmed the EDX analysis result, where it was obtained that all of the TFPOSS was extracted after processing with $scCO_2$ at 313 K and 20.7 MPa.

CHAPTER 4

CONCLUSIONS

In this study the effect of addition of a CO_2-philic additive (trifluoropropyl polyhedral oligomeric silsesquioxane, TFPOSS) and a non-CO_2-philic additive (octamethyl polyhedral oligomeric silsesquioxane, OMPOSS) on the foamability and pore structure of poly(l-lactic acid) (P_LLA) thin films prepared by supercritical carbon dioxide ($scCO_2$) processing were studied for the first time at different processing conditions. The obtained films were studied for the biomedical application of drug delivery. The studied processing parameters were saturation temperature (*ST*), saturation pressure (*SP)*, venting rate (*VR*), saturation time (*Stime*) and additive concentration in the ranges of 313-393 K, 10.3-20.7 MPa, 0.2-10.3 $MPa.min^{-1}$, 2-24 h, 10-30 wt% respectively.

After processing with $scCO_2$ the resulting films were analysed with Scanning Electron Microscopy (SEM) and micro Computed Tomography (µ-CT) for the pores morphology, Energy-Dispersive X-ray Spectroscopy (EDX) for the quantification and to obtain the distribution of the additive in the cross-section, mechanical test (nanoindentation) to obtain the indentation hardness, Differential Scanning Calorimetry (DSC) to obtain the thermal properties and crystallinity, and drug release test to see the viability of the films for the biomedical application. The following conclusions were obtained:

1. It was observed that the addition of TFPOSS significantly improved the foamability of P_LLA, making it possible to produce pores on the film by processing at *ST*, *SP*, and *Stime* as low as 313 K, 10.3 MPa and 2 h,

respectively. It was not possible to obtain a porous structure with neat PLLA film at these conditions.

2. Addition of TFPOSS decreased the pore size, compared to the pores formed in the neat PLLA films.
3. Both PLLA and PLLA-10T films processed at *ST* = 373 K and 393 K showed deformation and color change on the film. Deformation caused the films to lose their shapes, while color change indicated degradation of the film. Thus these conditions were not preferable for film processing.
4. As temperature increased less but larger pores were obtained in the PLLA-10T films. Increase in pressure resulted in increased nucleation density and smaller pores. Additionally, slower venting rate causing a lower supersaturation degree, resulted in formation of smaller pores.
5. Increase in saturation time allowed more $scCO_2$ to diffuse to the PLLA film which allows pore formation to some extent after processing for 24 h at 313 K without any additives. At higher temperature, 373 K, the crystallinity increase effect was more dominant, and no pore formation observed, which could be attributed to the high crystallinity up to 74.58%, induced with the processing. Increasing the time does not have significant change in the distribution and pore structure of PLLA film with addition of 10 wt% TFPOSS (PLLA-10T) and PLLA film with addition of 30 wt% TFPOSS (PLLA-30T).
6. Different type of additive and different concentration resulted in different porous structure. TFPOSS, which is a CO_2-philic additive, improved the foamability of the films while OMPOSS, which is non CO_2-philic additive, did not improve the foamability of the film. This shows that the affinity of the additive to CO_2 plays an important role in the foaming process. Addition of only 10 wt% TFPOSS allowed pore formation by processing at 313 K, 10.3 MPa and 2 h, while neat PLLA film without the addition of additive exhibited no pore formation at these processing conditions. Further increase in TFPOSS concentration allowed more homogeneous distribution of pores with higher porosity. According to the μ-CT results, the porosity of PLLA-10T film was

obtained to be 27.3% after processing with $scCO_2$ at *ST*, *SP,* and *Stime* as low as 313 K, 20.7 MPa and 2 h. μ-CT analysis also showed that further increase of TFPOSS weight fraction to 30 wt% improved the porosity up to 40.2% at the same processing conditions.

7. Processing with $scCO_2$ allowed extraction of the additive if they were soluble in $scCO_2$. The extraction process was highly dependent on the processing parameters. At low temperature, 313 K, it was possible to extract all of the TFPOSS from the films that contain 30 wt% POSS in only 2 h processing time. However, at higher temperature, 373 K, where the solubility of TFPOSS is lower, it was not possible to extract all of the TFPOSS from the film that contained only 10 wt% TFPOSS even after processing for 24 h which was attributed to the solubility decrease of TFPOSS in $scCO_2$ with isobaric increase in temperature. The extraction phenomena during supercritical foaming can be important in targeted applications that require high purity, such as biomedical applications.
8. Nanoindentation test shows that the hardness of the film increased as the processing time and/or processing temperature increased. Also the reinforcement effect of TFPOSS could only be seen when the concentration was high enough. In this case addition of 10 wt% of TFPOSS did not show increase in hardness while increasing the TFPOSS concentration to 30 wt% significantly increased the hardness.
9. From the DSC results it was also observed that the crystallinity of the samples always increased after processing. This shows that CO_2 had a plasticizing effect on the solid polymer, so that polymer chains gain some mobility and reorganize themselves due to $scCO_2$ processing which is leading to higher crystallinity.
10. Drug release test shows that different structure of the pores did not give significant difference in drug release rate. This can be attributed: to the lack of connectivity between the formed porous regions in the film, which

restricted the deeper penetration of the drug into the polymeric matrix, and thus its effective loading.

11. From the modelling study, it was obtained that Chrastil modified by Wang model gave the lowest absolute average relative deviation (*AARD*). Additionally, self-consistency test also showed that the data gave sufficiently linear behaviour when it was compared with the model. Thus the model can be used to predict solubility of TFPOSS in the vicinity of the conditions where the data were obtained.
12. The solubility of TFPOSS at processing conditions of 313 K, and 20.7 MPa was predicted with the Chrastil modified by Wang model. The value was obtained to be 0.00081. This value was much higher than the highest concentration of TFPOSS that could be obtained in the vessel during processing upon the complete extraction of the TFPOSS from the P_LLA-30T film, which is 0.00002. This shows that complete extraction of TFPOSS by $scCO_2$ could be achieved, which was shown previously in the EDX analysis.
13. Among all of the conditions, 313 K saturation temperature, 20.7 MPa saturation pressure, 10.3 $MPa.min^{-1}$ venting rate and 2 h processing time was determined to be the preferable conditions for P_LLA-10T and P_LLA-30T film processing because of the formation of the most homogeneous pores, low processing temperature, short processing time and absence of deformation and color change.

REFERENCES

[1] X. Liao, H. Zhang, T. He, Preparation of porous biodegradable polymer and its nanocomposites by supercritical CO 2 foaming for tissue engineering, Journal of Nanomaterials. 2012 (2012). doi:10.1155/2012/836394.

[2] A.R.C. Duarte, V.E. Santo, A. Alves, S.S. Silva, J. Moreira-Silva, T.H. Silva, et al., Unleashing the potential of supercritical fluids for polymer processing in tissue engineering and regenerative medicine, The Journal of Supercritical Fluids. 79 (2013) 177–185. doi:10.1016/j.supflu.2013.01.004.

[3] a R.C. Duarte, J.F. Mano, R.L. Reis, Supercritical fluids in biomedical and tissue engineering applications: a review, International Materials Reviews. 54 (2009) 214–222. doi:10.1179/174328009X411181.

[4] X. Zhang, S. Heinonen, E. Levänen, Applications of supercritical carbon dioxide in materials processing and synthesis, RSC Adv. 4 (2014) 61137–61152. doi:10.1039/C4RA10662H.

[5] Ž. Knez, E. Markočič, M. Leitgeb, M. Primožič, M. Knez Hrnčič, M. Škerget, Industrial applications of supercritical fluids: A review, Energy. 77 (2013) 235–243. doi:10.1016/j.energy.2014.07.044.

[6] B. Gupta, N. Revagade, J. Hilborn, Poly(lactic acid) fiber: An overview, Progress in Polymer Science. 32 (2007) 455–482. doi:10.1016/j.progpolymsci.2007.01.005.

[7] C.R. Álvarez-Chávez, S. Edwards, R. Moure-Eraso, K. Geiser, Sustainability of bio-based plastics: general comparative analysis and recommendations for improvement, Journal of Cleaner Production. 23 (2012) 47–56. doi:10.1016/j.jclepro.2011.10.003.

[8] R. Auras, B. Harte, S. Selke, An overview of polylactides as packaging materials., Macromolecular Bioscience. 4 (2004) 835–64. doi:10.1002/mabi.200400043.

[9] S. Bourbigot, G. Fontaine, Flame retardancy of polylactide: an overview, Polymer Chemistry. 1 (2010) 1413. doi:10.1039/c0py00106f.

[10] M. Nofar, C.B. Park, Poly (lactic acid) foaming, Progress in Polymer Science. 39 (2014) 1721–1741. doi:10.1016/j.progpolymsci.2014.04.001.

[11] C. Reti, M. Casetta, Flammability properties of intumescent PLA including starch and lignin, Polymers for Advanced Technologies. 19 (2008) 628–635.

[12] G. Bang, S.W. Kim, Biodegradable poly(lactic acid)-based hybrid coating materials for food packaging films with gas barrier properties, Journal of Industrial and Engineering Chemistry. 18 (2012) 1063–1068. doi:10.1016/j.jiec.2011.12.004.

[13] J.R. Eisenbrey, O.M. Burstein, R. Kambhampati, F. Forsberg, J.-B. Liu, M. a Wheatley, Development and optimization of a doxorubicin loaded poly(lactic acid) contrast agent for ultrasound directed drug delivery., Journal of Controlled Release : Official Journal of the Controlled Release Society. 143 (2010) 38–44. doi:10.1016/j.jconrel.2009.12.021.

[14] C.S. Proikakis, P. a. Tarantili, a. G. Andreopoulos, The role of polymer/drug interactions on the sustained release from poly(dl-lactic acid) tablets, European Polymer Journal. 42 (2006) 3269–3276. doi:10.1016/j.eurpolymj.2006.08.023.

[15] S. Molladavoodi, M. Gorbet, J. Medley, H.J. Kwon, Investigation of microstructure, mechanical properties and cellular viability of poly(L-lactic acid) tissue engineering scaffolds prepared by different thermally induced phase separation protocols., Journal of the Mechanical Behavior of Biomedical Materials. 17 (2013) 186–97. doi:10.1016/j.jmbbm.2012.08.021.

[16] M. Okamoto, B. John, Synthetic biopolymer nanocomposites for tissue engineering scaffolds, Progress in Polymer Science. 38 (2013) 1487–1503. doi:10.1016/j.progpolymsci.2013.06.001.

[17] N.M.S. Bettahalli, H. Steg, M. Wessling, D. Stamatialis, Development of poly(l-lactic acid) hollow fiber membranes for artificial vasculature in tissue engineering scaffolds, Journal of Membrane Science. 371 (2011) 117–126. doi:10.1016/j.memsci.2011.01.026.

[18] T.-R. Kuang, H.-Y. Mi, D.-J. Fu, X. Jing, B. Chen, W.-J. Mou, et al., Fabrication of Poly(lactic acid)/Graphene Oxide Foams with Highly Oriented and Elongated Cell Structure via Unidirectional Foaming Using Supercritical Carbon Dioxide, Industrial & Engineering Chemistry Research. 54 (2015) 758–768. doi:10.1021/ie503434q.

[19] N. Uzun, T.D. Martins, G.M. Teixeira, N.L. Cunha, R.B. Oliveira, E.J. Nassar, et al., Poly(l-lactic acid) membranes: Absence of genotoxic hazard and

potential for drug delivery, Toxicology Letters. 232 (2015) 513–518. doi:10.1016/j.toxlet.2014.11.032.

[20] A.P.S. Immich, M.L. Arias, N. Carreras, R.L. Boemo, J.A. Tornero, Drug delivery systems using sandwich configurations of electrospun poly(lactic acid) nanofiber membranes and ibuprofen, Materials Science and Engineering C. 33 (2013) 4002–4008. doi:10.1016/j.msec.2013.05.034.

[21] a. I. Cooper, Porous Materials and Supercritical Fluids, Advanced Materials. 15 (2003) 1049–1059. doi:10.1002/adma.200300380.

[22] M.L. Mather, M. Brion, L.J. White, K.M. Shakesheff, S.M. Howdle, S.P. Morgan, et al., Time-lapsed imaging for in-process evaluation of supercritical fluid processing of tissue engineering scaffolds, in: Biotechnol. Prog., 2009: pp. 1176–1183. doi:10.1002/btpr.191.

[23] C. Gualandi, L.J. White, L. Chen, R. a Gross, K.M. Shakesheff, S.M. Howdle, et al., Scaffold for tissue engineering fabricated by non-isothermal supercritical carbon dioxide foaming of a highly crystalline polyester., Acta Biomaterialia. 6 (2010) 130–6. doi:10.1016/j.actbio.2009.07.020.

[24] L.J. White, V. Hutter, H. Tai, S.M. Howdle, K.M. Shakesheff, The effect of processing variables on morphological and mechanical properties of supercritical CO2 foamed scaffolds for tissue engineering, Acta Biomaterialia. 8 (2012) 61–71. doi:10.1016/j.actbio.2011.07.032.

[25] L.-T. Lim, R. Auras, M. Rubino, Processing technologies for poly(lactic acid), Progress in Polymer Science. 33 (2008) 820–852. doi:10.1016/j.progpolymsci.2008.05.004.

[26] C. a. García-González, A. Concheiro, C. Alvarez-Lorenzo, Processing of Materials for Regenerative Medicine Using Supercritical Fluid Technology, Bioconjugate Chemistry. (2015). doi:10.1021/bc5005922.

[27] C.M. Stafford, T.P. Russell, T.J. McCarthy, Expansion of Polystyrene Using Supercritical Carbon Dioxide: Effects of Molecular Weight, Polydispersity, and Low Molecular Weight Components, Macromolecules. 32 (1999) 7610–7616. doi:10.1021/ma9902100.

[28] O.R. Davies, A.L. Lewis, M.J. Whitaker, H. Tai, K.M. Shakesheff, S.M. Howdle, Applications of supercritical CO2 in the fabrication of polymer systems for drug delivery and tissue engineering., Advanced Drug Delivery Reviews. 60 (2008) 373–87. doi:10.1016/j.addr.2006.12.001.

[29] E. Kiran, Foaming strategies for bioabsorbable polymers in supercritical fluid mixtures. Part I. Miscibility and foaming of poly(l-lactic acid) in carbon dioxide+acetone binary fluid mixtures, The Journal of Supercritical Fluids. 54 (2010) 296–307. doi:10.1016/j.supflu.2010.05.005.

[30] W. Groot, J. van Krieken, O. Sliekersl, S. de Vos, Production and Purification of Lactic Acid and Lactide, in: Poly(Lactic Acid), John Wiley & Sons, Inc., 2010: pp. 1–18. doi:10.1002/9780470649848.ch1.

[31] S.P. Nalawade, F. Picchioni, J.H. Marsman, L.P.B.M. Janssen, The FT-IR studies of the interactions of CO2 and polymers having different chain groups, Journal of Supercritical Fluids. 36 (2006) 236–244. doi:10.1016/j.supflu.2005.06.005.

[32] N. Oliveira, J. Dorgan, Gas solubility of carbon dioxide in poly (lactic acid) at high pressures: Thermal treatment effect, Journal of Polymer Science: Part B: Polymer Physics. (2007) 616–625. doi:10.1002/polb.

[33] R. Pini, G. Storti, M. Mazzotti, H. Tai, K.M. Shakesheff, S.M. Howdle, Sorption and Swelling of Poly (DL -lactic acid) and Poly (lactic- co -glycolic acid) in Supercritical CO 2 : An Experimental and Modeling Study, Journal of Polymer Science: Part B: Polymer Physics. 46 (2007) 483–496. doi:10.1002/polb.

[34] E. Aionicesei, M. Škerget, Ž. Knez, Measurement of CO2 solubility and diffusivity in poly(l-lactide) and poly(d,l-lactide-co-glycolide) by magnetic suspension balance, The Journal of Supercritical Fluids. 47 (2008) 296–301. doi:10.1016/j.supflu.2008.07.011.

[35] H. Tai, M. Mather, D. Howard, W. Wang, Control of pore size and structure of tissue engineering scaffolds produced by supercritical fluid processing, European Cells and Materials. 14 (2007) 64–77. http://www.ecmjournal.org/journal/papers/vol014/pdf/v014a07.pdf (accessed February 15, 2015).

[36] D. Rouholamin, P.J. Smith, E. Ghassemieh, Control of morphological properties of porous biodegradable scaffolds processed by supercritical CO2 foaming, Journal of Materials Science. 48 (2013) 3254–3263. doi:10.1007/s10853-012-7109-4.

[37] J. Yu, C. Tang, Y. Guan, S. Yao, Z. Zhu, Sorption and Diffusion Behavior of Carbon Dioxide into Poly(l-lactic acid) Films at Elevated Pressures, Chinese Journal of Chemical Engineering. 21 (2013) 1296–1302. doi:10.1016/S1004-9541(13)60623-0.

[38] A.M. López-Periago, A. Vega, P. Subra, A. Argemí, J. Saurina, C. a. García-González, et al., Supercritical CO2 processing of polymers for the production of materials with applications in tissue engineering and drug delivery, Journal of Materials Science. 43 (2008) 1939–1947. doi:10.1007/s10853-008-2461-0.

[39] L.M. Mathieu, M.-O. Montjovent, P.-E. Bourban, D.P. Pioletti, J.-A.E. Månson, Bioresorbable composites prepared by supercritical fluid foaming., Journal of Biomedical Materials Research. Part A. 75 (2005) 89–97. doi:10.1002/jbm.a.30385.

[40] C. Delabarde, C.J.G. Plummer, P.-E. Bourban, J.-A.E. Månson, Biodegradable polylactide/hydroxyapatite nanocomposite foam scaffolds for bone tissue engineering applications., Journal of Materials Science. Materials in Medicine. 23 (2012) 1371–85. doi:10.1007/s10856-012-4619-1.

[41] L. Nasri, S. Bensaad, Z. Bensetiti, Modeling the Solubility of Dihydroxybenzoic Acid and Methylbenzoic Acid Isomers in Supercritical Carbon Dioxide, International Journal of Thermodynamics. 17 (2014) 81–85. doi:10.5541/ijot.513.

[42] H. Sim Yeoh, G. Hean Chong, N. Mohd Azahan, R. Abdul Rahman, T.S. Yaw Choong, Solubility measurement method and mathematical modeling in supercritical fluids, Engineering Journal. 17 (2013) 67–78. doi:10.4186/ej.2013.17.3.67.

[43] X. Yang, L. Chen, T. He, H. Wang, X. Wang, Equilibrium Solubilities of Iso-eicosane in Supercritical Carbon Dioxide, Journal of Chemical & Engineering Data. 60 (2015) 621–626. doi:10.1021/je5007554.

[44] M. Škerget, Ž. Knez, M. Knez-Hrnčič, Solubility of Solids in Sub- and Supercritical Fluids: a Review, Journal of Chemical & Engineering Data. 56 (2011) 694–719. doi:10.1021/je1011373.

[45] M. Sauceau, J.J. Letourneau, D. Richon, J. Fages, Enhanced density-based models for solid compound solubilities in supercritical carbon dioxide with cosolvents, Fluid Phase Equilibria. 208 (2003) 99–113. doi:10.1016/S0378-3812(03)00005-0.

[46] S.J. Macnaughton, I. Kikic, N.R. Foster, P. Alessi, A. Cortesi, I. Chimica, et al., Solubility of Anti-Inflammatory Drugs in Supercritical Carbon Dioxide, 41 (1996) 1083–1086. doi:10.1021/je960103q.

[47] M.. Mirzajanzadeh, F.. Zabihi, M. Ardjmand, Measurement and Correlation of Ibuprofen in Supercritical Carbon Dioxide Using Stryjek and Vera EOS,

Iranian Journal of Chemical Engineering. 7 (2010) 42–49. doi:10.1007/s11814-010-0265-9.

[48] Z. Tang, J. Jin, Z. Zhang, H. Liu, New Experimental Data and Modeling of the Solubility of Compounds in Supercritical Carbon Dioxide, Industrial & Engineering Chemistry Research. 51 (2012) 5515–5526. doi:10.1021/ie2016224.

[49] B. Hadi, H.-A. Ali, L. Nader, Thermodynamic modeling of solid solubility in supercritical carbon dioxide: Comparison between mixing rules, Chemical Industry and Chemical Engineering Quarterly. 19 (2012) 74–74. doi:10.2298/CICEQ120203074B.

[50] C.B. Kautz, G.M. Schneider, J.-J. Shim, B. Wagner, D. Tuma, Solubilities of a 1,4-Bis(alkylamino)-9,10-anthraquinone Series in Compressed Carbon Dioxide, Journal of Chemical & Engineering Data. 53 (2008) 2356–2371. doi:10.1021/je800252z.

[51] J. Chrastil, Solubility of solids and liquids in supercritical gases, Journal of Physical Chemistry. 86 (1982) 3016–3021. doi:10.1021/j100212a041.

[52] A. Tabernero, E.M.M. del Valle, M.Á. Galán, A comparison between semiempirical equations to predict the solubility of pharmaceutical compounds in supercritical carbon dioxide, Journal of Supercritical Fluids. 52 (2010) 161–174. doi:10.1016/j.supflu.2010.01.009.

[53] J.M. del Valle, J.M. Aguilera, An improved equation for predicting the solubility of vegetable oils in supercritical CO2, Industrial & Engineering Chemistry Research. 27 (1988) 1551–1553. doi:10.1021/ie00080a036.

[54] S.K. Kumar, K.P. Johnston, Modelling the solubility of solids in supercritical fluids with density as the independent variable, The Journal of Supercritical Fluids. 1 (1988) 15–22. doi:10.1016/0896-8446(88)90005-8.

[55] J. Méndez-Santiago, A.S. Teja, The solubility of solids in supercritical fluids, Fluid Phase Equilibria. 158-160 (1999) 501–510. doi:10.1016/S0378-3812(99)00154-5.

[56] K.D. Bartle, A.A. Clifford, S.A. Jafar, G.F. Shilstone, Solubilities of Solids and Liquids of Low Volatility in Supercritical Carbon Dioxide, Journal of Physical and Chemical Reference Data. 20 (1991) 713–757. doi:10.1063/1.555893.

[57] S.A. Shojaee, A.Z. Hezave, S. Aftab, M. Lashkarbolooki, F. Esmaeilzadeh, Solubility of gabapentin in supercritical carbon dioxide, Journal of Supercritical Fluids. 78 (2013) 1–6. doi:10.1016/j.supflu.2013.02.003.

[58] C. Wang, S.N. Leung, M. Bussmann, W.T. Zhai, C.B. Park, Numerical Investigation of Nucleating-Agent-Enhanced Heterogeneous Nucleation, Industrial & Engineering Chemistry Research. 49 (2010) 12783–12792. doi:10.1021/ie1017207.

[59] S. Costeux, L. Zhu, Low density thermoplastic nanofoams nucleated by nanoparticles, Polymer. 54 (2013) 2785–2795. doi:10.1016/j.polymer.2013.03.052.

[60] C. Dilek, Supercritical carbon dioxide-soluble polyhedral oligomeric silsesquioxane (POSS) nanocages and polymer surface modification, The Journal of Supercritical Fluids. 73 (2013) 171–177. doi:10.1016/j.supflu.2012.10.012.

[61] E.W. Fischer, H. Sterzel, G. Wegner, Investigation of the structure of solution grown crystals of lactide copolymers by means of chemical reactions, Kolloid-Zeitschrift Und Zeitschrift Für Polymere. 251 (1973) 980–990. doi:10.1007/BF01498927.

[62] X. Liao, A. V. Nawaby, The sorption behaviors in PLLA-CO2 system and its effect on foam morphology, Journal of Polymer Research. 19 (2012) 9827. doi:10.1007/s10965-012-9827-3.

[63] G. Li, H. Li, L.S. Turng, S. Gong, C. Zhang, Measurement of gas solubility and diffusivity in polylactide, Fluid Phase Equilibria. 246 (2006) 158–166. doi:10.1016/j.fluid.2006.05.030.

[64] H. Tai, M.L. Mather, D. Howard, W. Wang, L.J. White, J. a. Crowe, et al., Control of pore size and structure of tissue engineering scaffolds produced by supercritical fluid processing, European Cells and Materials. 14 (2007) 64–76. doi:vol014a07 [pii].

[65] M. Mihai, M. a. Huneault, B.D. Favis, Crystallinity development in cellular poly(lactic acid) in the presence of supercritical carbon dioxide, Journal of Applied Polymer Science. 113 (2009) 2920–2932. doi:10.1002/app.30338.

[66] X.L. Jiang, T. Liu, Z.M. Xu, L. Zhao, G.H. Hu, W.K. Yuan, Effects of crystal structure on the foaming of isotactic polypropylene using supercritical carbon dioxide as a foaming agent, Journal of Supercritical Fluids. 48 (2009) 167–175. doi:10.1016/j.supflu.2008.10.006.

[67] A.M. López-Periago, A. Vega, P. Subra, A. Argemí, J. Saurina, C. a. García-González, et al., Supercritical CO2 processing of polymers for the production of materials with applications in tissue engineering and drug delivery, Journal of Materials Science. 43 (2008) 1939–1947. doi:10.1007/s10853-008-2461-0.

[68] D.M. Fox, J. Lee, C.J. Citro, M. Novy, Flame retarded poly(lactic acid) using POSS-modified cellulose. 1. Thermal and combustion properties of intumescing composites, Polymer Degradation and Stability. 98 (2013) 590–596. doi:10.1016/j.polymdegradstab.2012.11.016.

[69] R. Bouza, L. Barral, F.J. Díez, J. López, B. Montero, M. Rico, et al., Study of thermal and morphological properties of a hybrid system, iPP/POSS. Effect of flame retardance, Composites Part B: Engineering. 58 (2014) 566–572. doi:10.1016/j.compositesb.2013.11.010.

[70] M.E. Mngomezulu, M.J. John, V. Jacobs, A.S. Luyt, Review on flammability of biofibres and biocomposites, Carbohydrate Polymers. 111 (2014) 149–182. doi:10.1016/j.carbpol.2014.03.071.

[71] B.M.P. Ferreira, L.M.P. Pinheiro, P. a P. Nascente, M.J. Ferreira, E. a R. Duek, Plasma surface treatments of poly(l-lactic acid) (PLLA) and poly(hydroxybutyrate-co-hydroxyvalerate) (PHBV), Materials Science and Engineering C. 29 (2009) 806–813. doi:10.1016/j.msec.2008.07.026.

APPENDIX A

PARTICLE SIZE DISTRIBUTION OF THE ADDITIVES

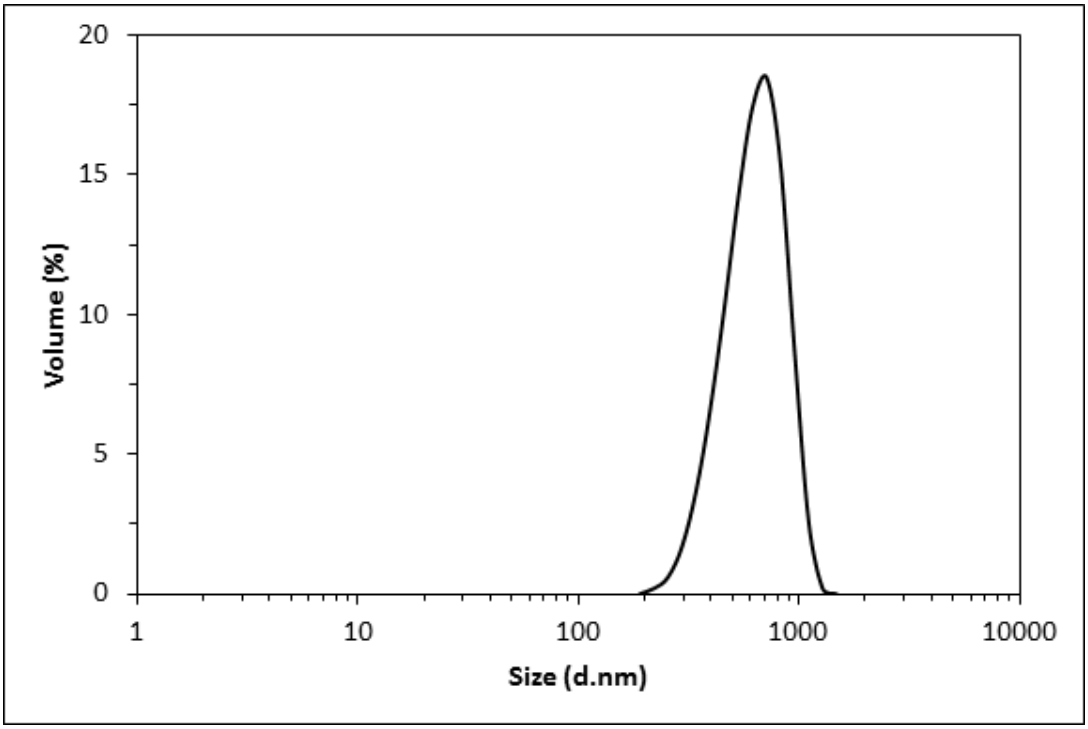

Figure A.1 Particle size distribution of TFPOSS with average size of 648.5nm

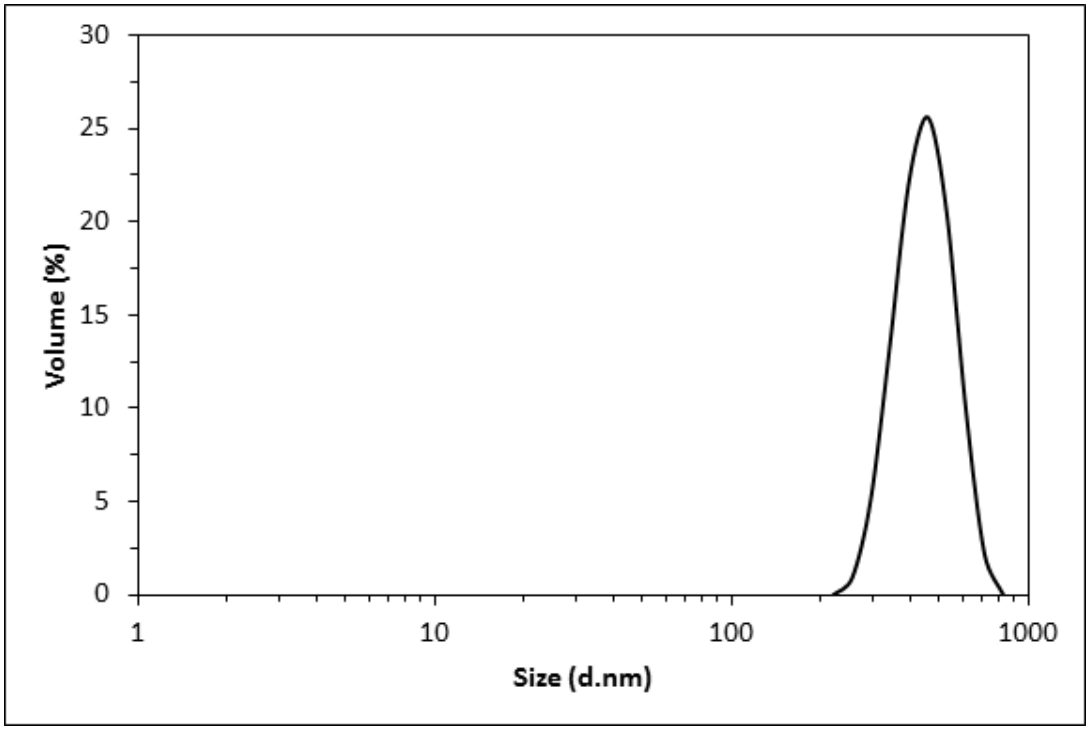

Figure A.2 Particle size distribution of OMPOSS with average size of 455.1nm

APPENDIX B

CALIBRATION CURVE

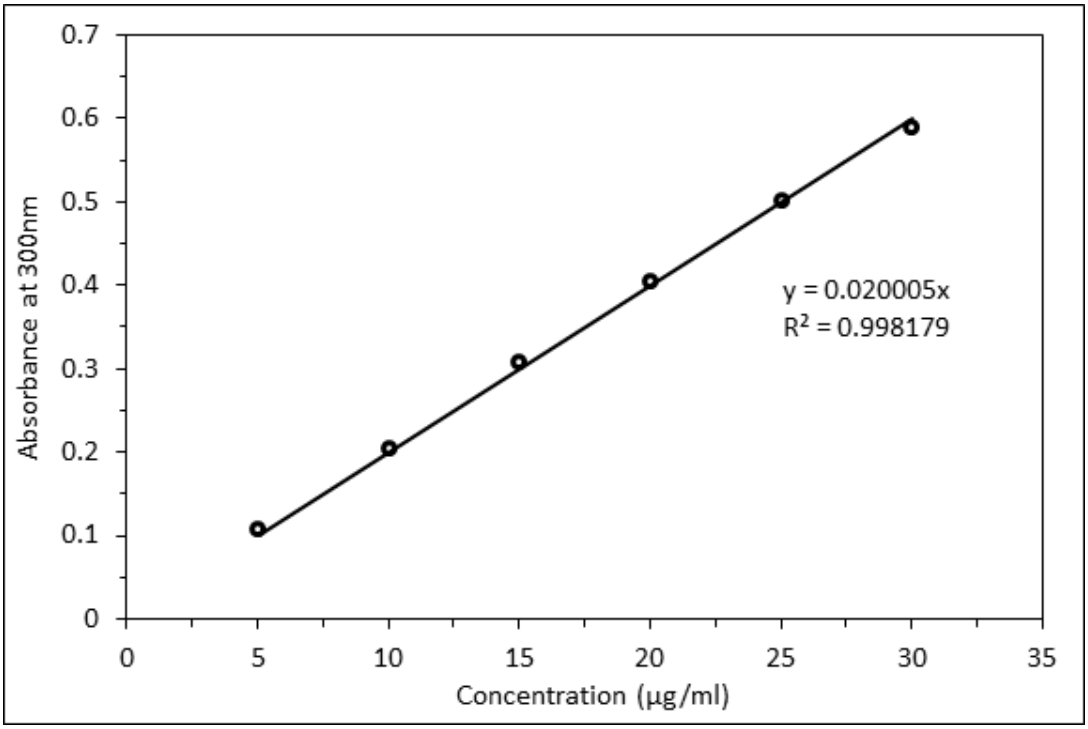

Figure B.1 Calibration curve of ceftriaxone sodium

APPENDIX C

EDX MAPPING RESULT

This mapping data compliment the local EDX analysis result for PLLA-10T given in the text.

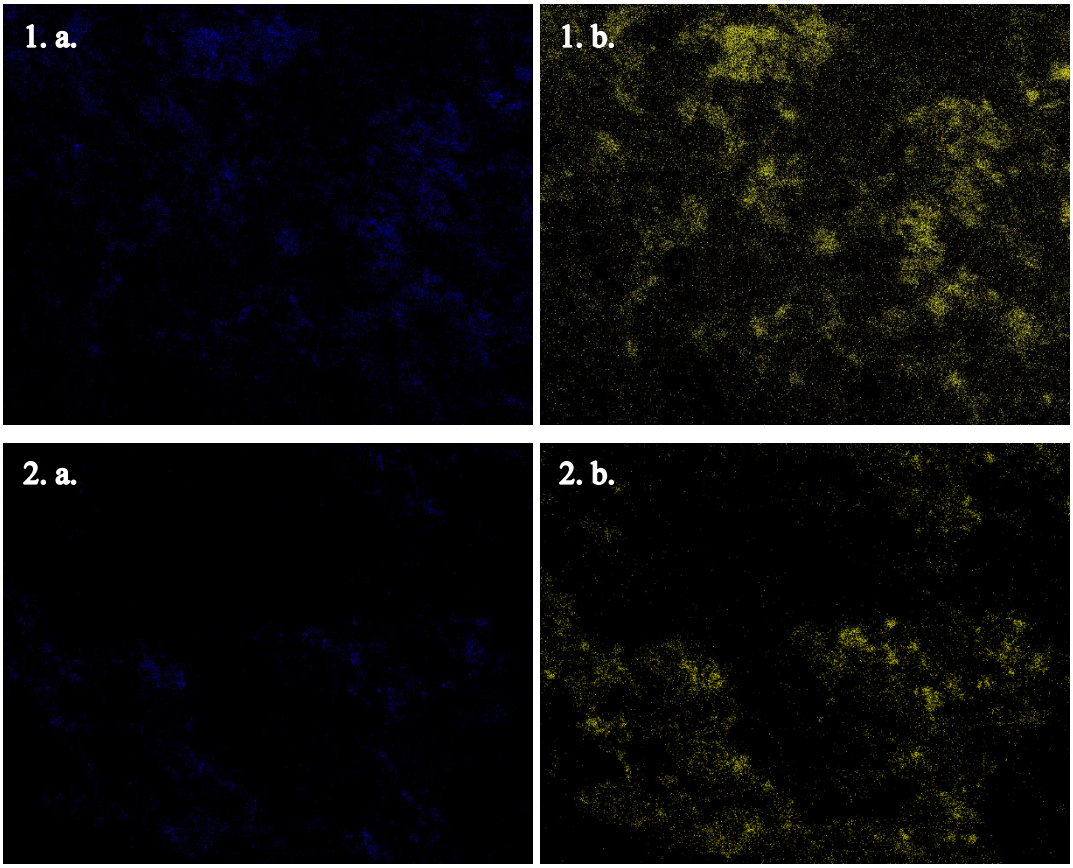

Figure C.1 EDX mapping results of PLLA-10T film samples processed at *ST* = 313 K, *SP* = 20.7 MPa, *VR* = 10.3 MPa.min^{-1} and *Stime* = (1) 2 h, (2) 24 h; (a) Fluorine map, (b) Silicon map

APPENDIX D

DSC THERMOGRAM

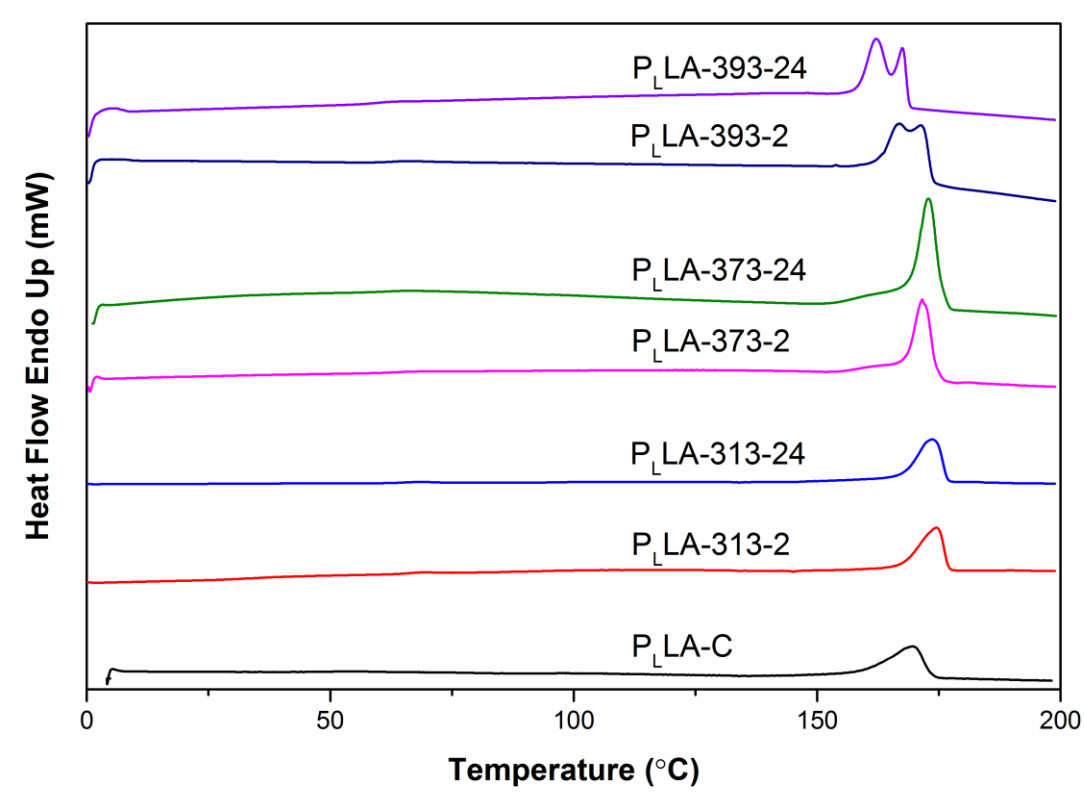

Figure D.1 First heating DSC thermogram of the neat PLLA films processed at different conditions.

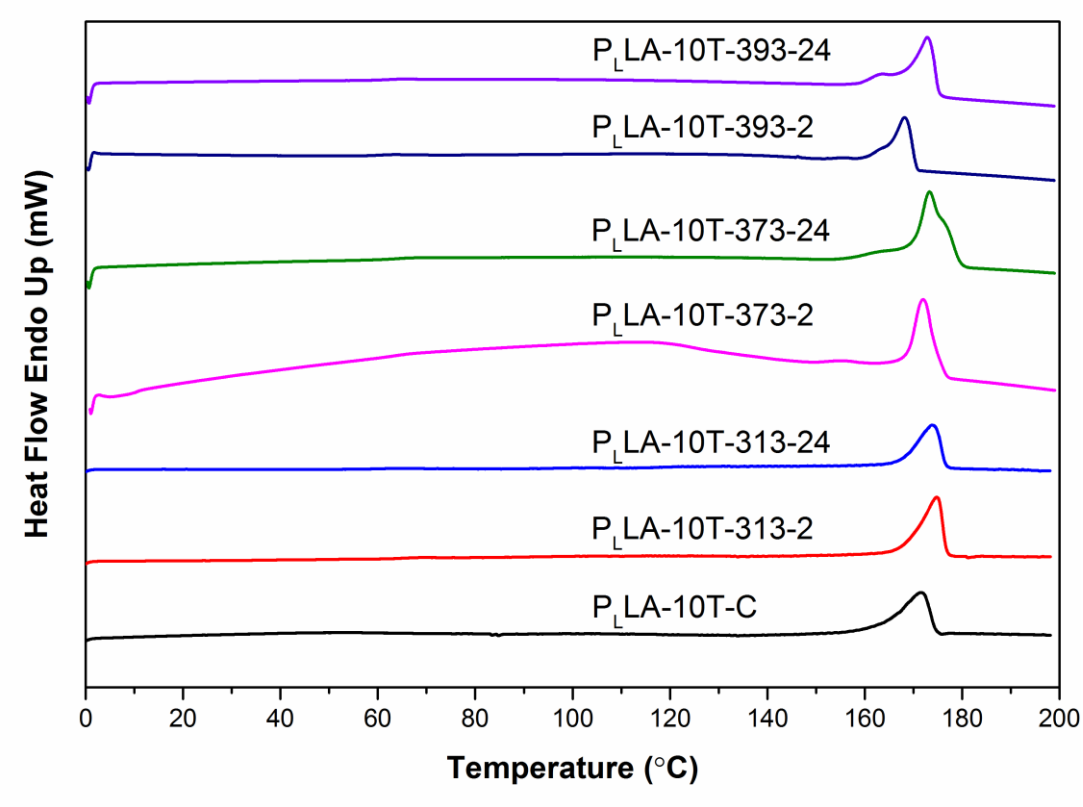

Figure D.2 First heating DSC thermogram of the PLLA-10T films processed at different conditions.

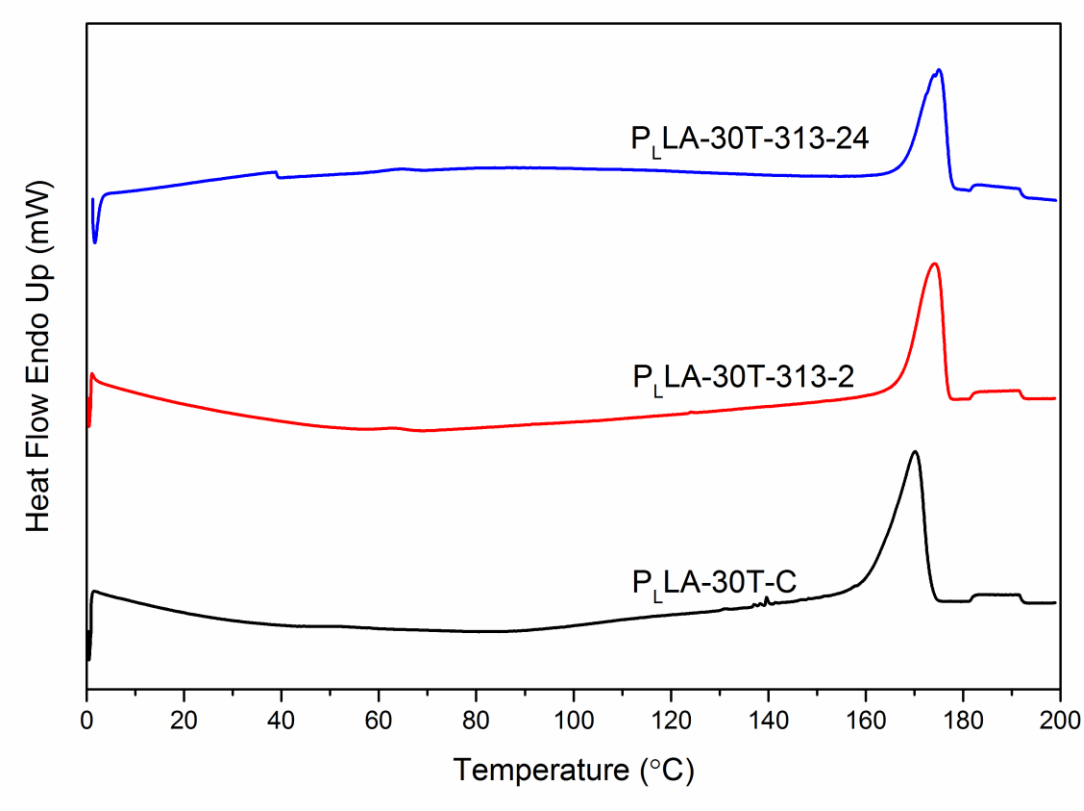

Figure D.3 First heating DSC thermogram of the P_LLA-30T films processed at different conditions.

APPENDIX E

CORRELATED TFPOSS SOLUBILITY WITH DIFFERENT MODELS

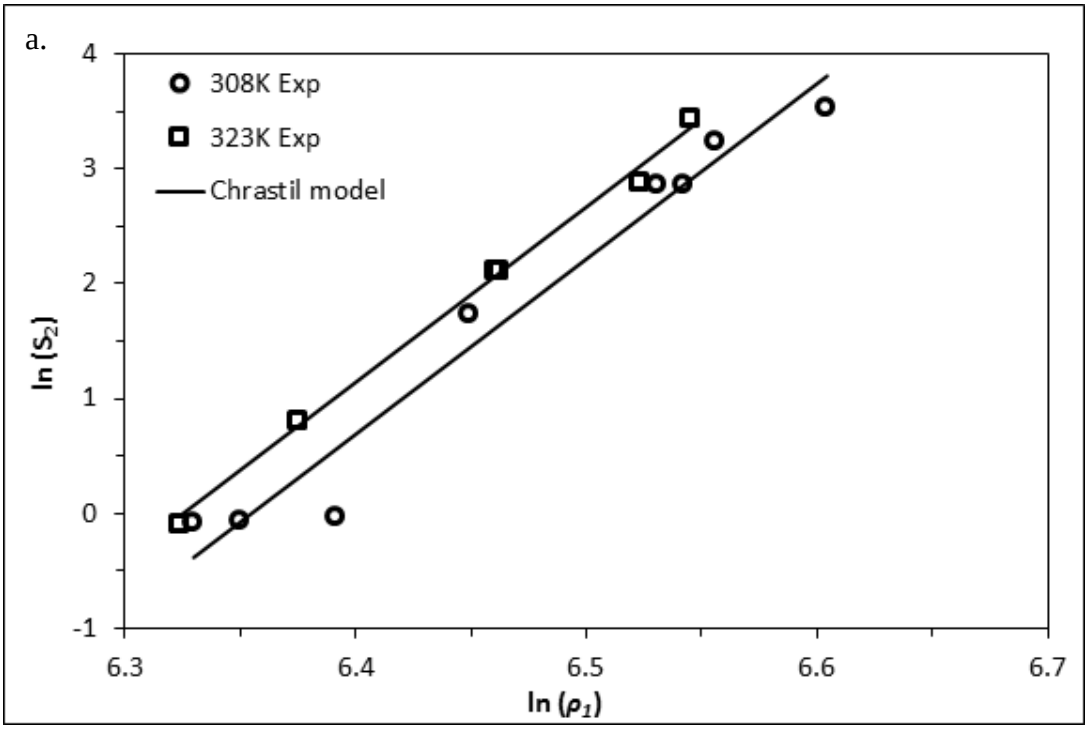

Figure E.1 The correlated solubility data of trifluoropropylPOSS with different models, (a) Chrastil, (b) d-A, (c) K-J, (d) MST, (e) Bartle models

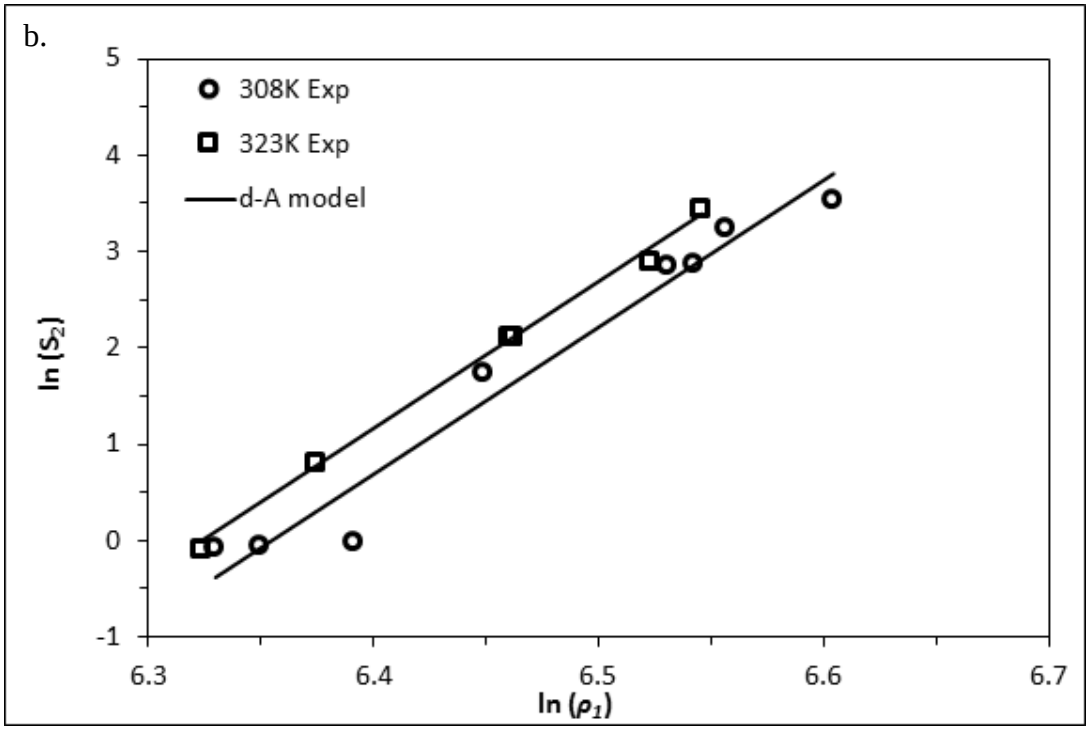

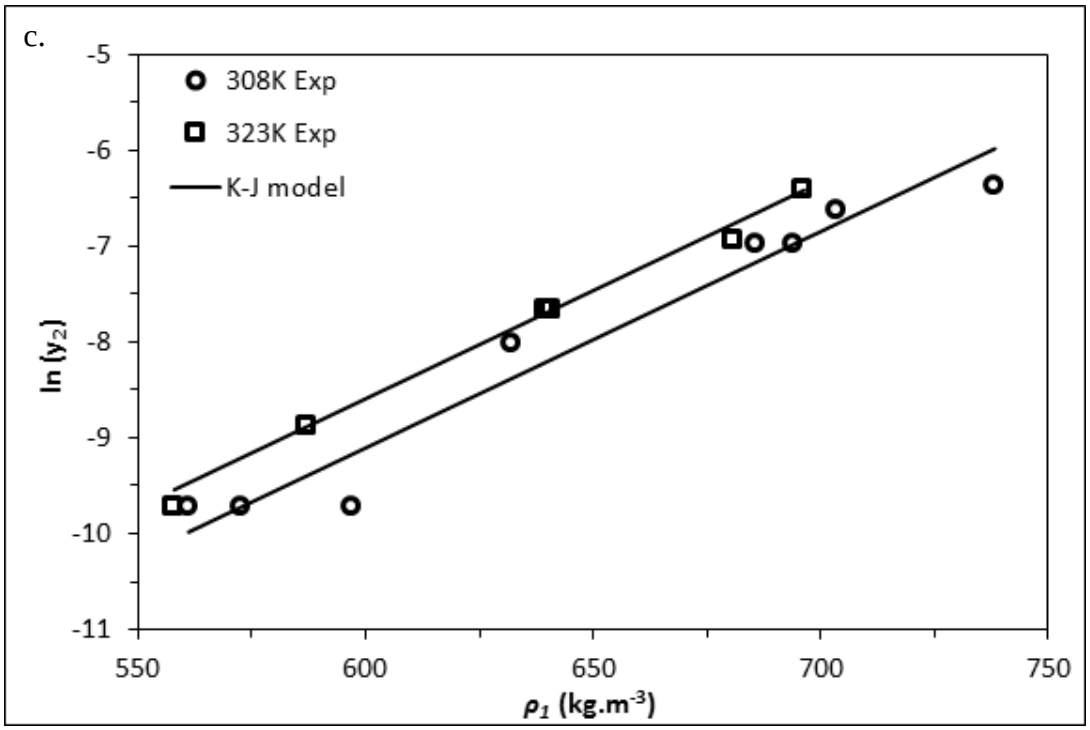

Figure E.1 (continued)

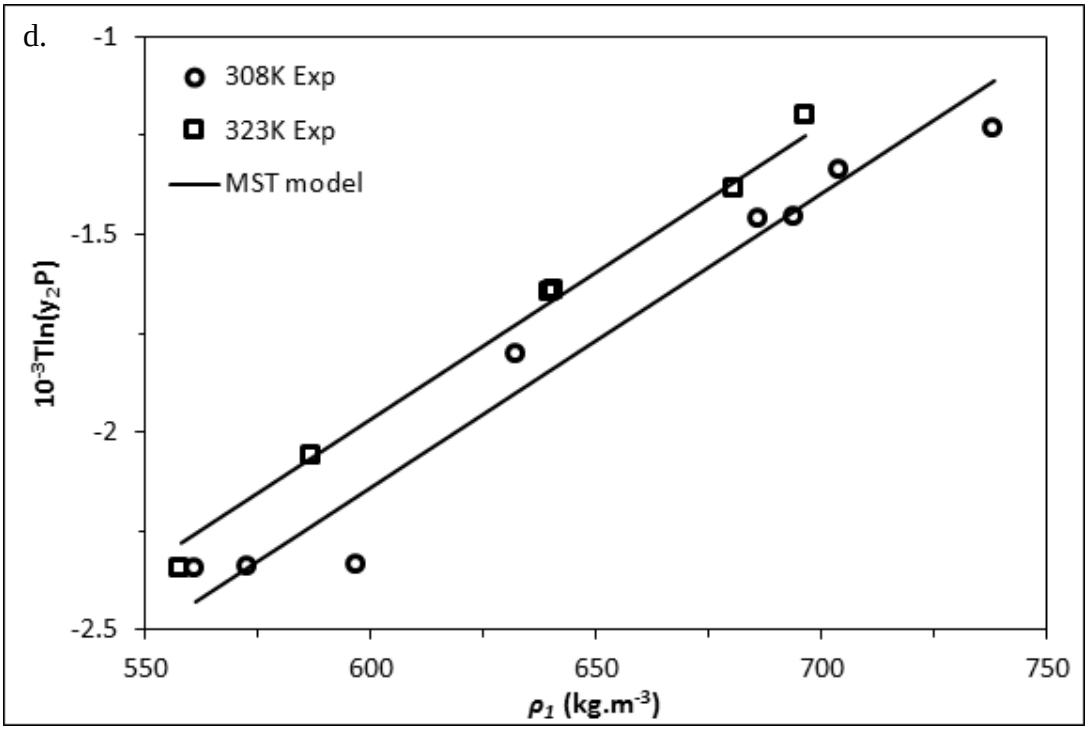

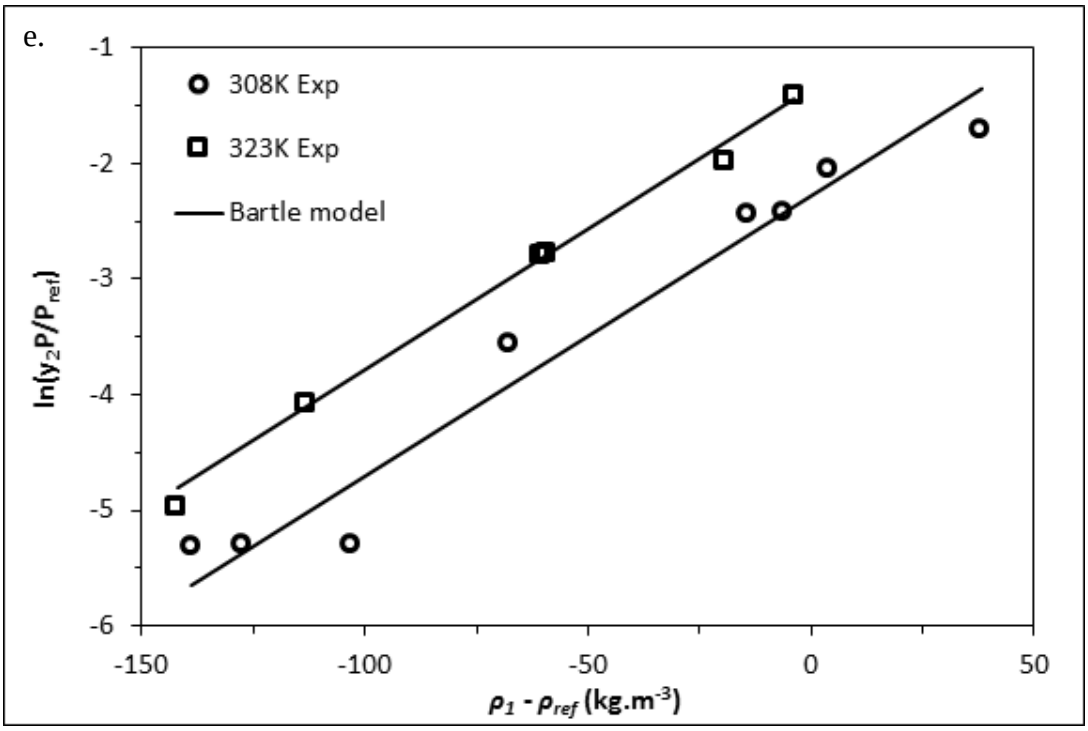

Figure E.1 (continued)

APPENDIX F

SELF-CONSISTENCY TESTS OF TRIFLUOROPROPYLPOSS WITH DIFFERENT MODELS

F.1 Chrastil Model

For Chrastil model, the plot of experimental data at all temperature in the form of:

$$\ln(S_j) - \frac{b}{T} - c$$

against the density of the $scCO_2$ should be a linear plot.

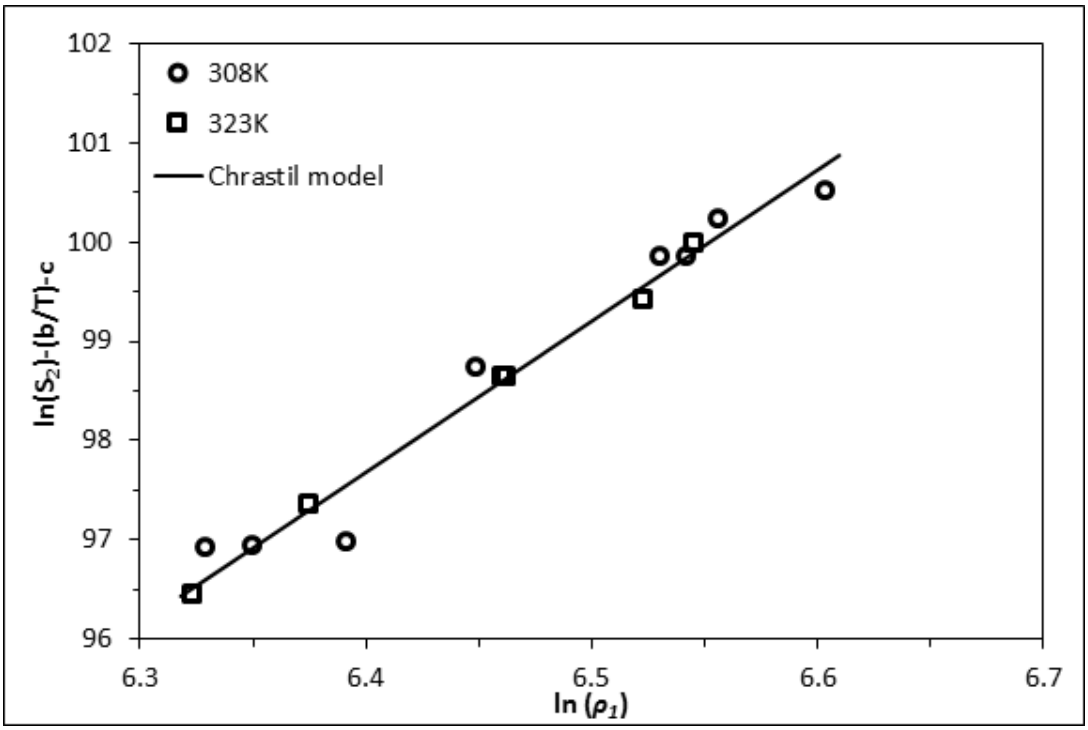

Figure F.1 Self-consistency tests of trifluoropropylPOSS with Chrastil model

F.2 Del Valle and Aguilera Model

For del Valle and Aguilera model, the plot of experimental data at all temperature in the form of:

$$\ln(S_j) - \frac{b}{T} - \frac{c}{T^2} - d$$

against the density of the $scCO_2$ should be a linear plot.

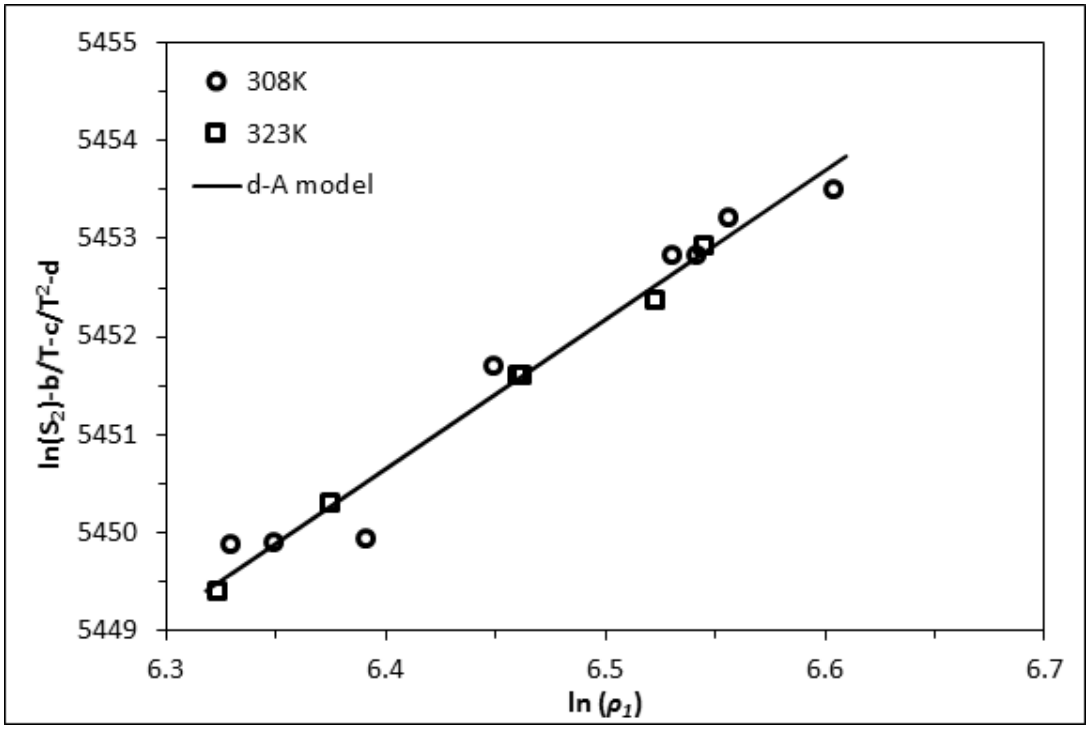

Figure F.2 Self-consistency tests of trifluoropropylPOSS with del Valle and Aguilera model

F.3 Kumar and Johnston Model

For Kumar and Johnston model, the plot of experimental data at all temperature in the form of:

$$\ln(y_j) - \frac{b}{T}$$

against the density of the $scCO_2$ should be a linear plot.

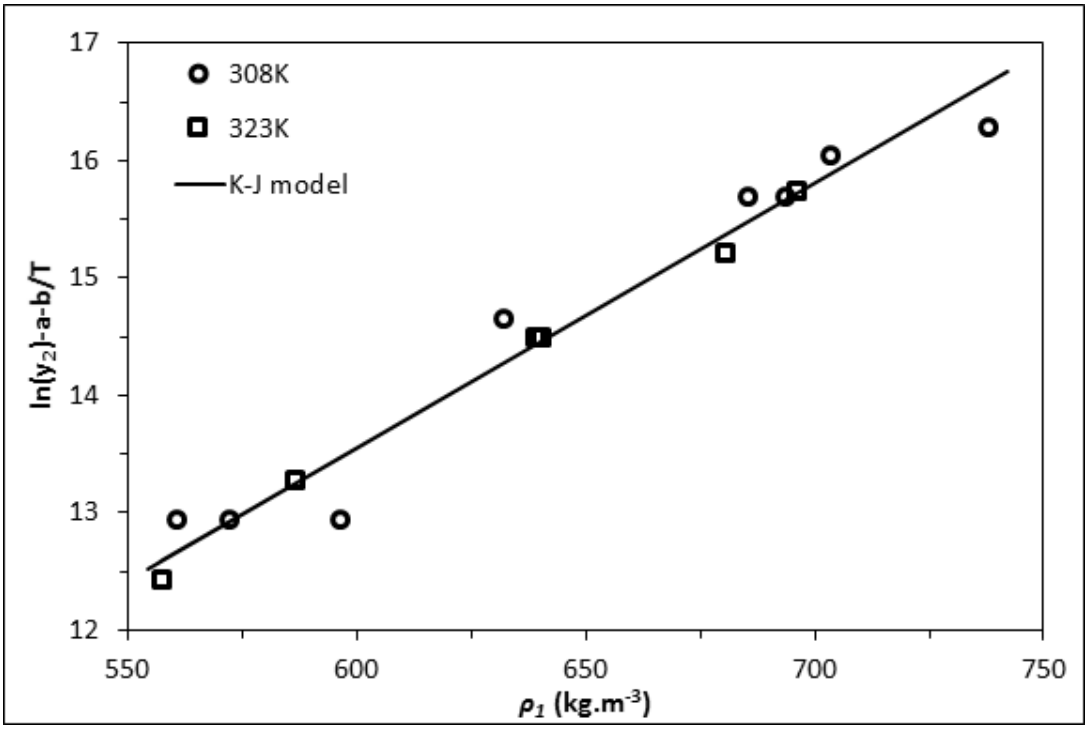

Figure F.3 Self-consistency tests of trifluoropropylPOSS with Kumar and Johnston model

F.4 Mendez-Santiago and Teja Model

For Mendez-Santiago and Teja model, the plot of experimental data at all temperature in the form of:

$$T\ln(y_j P) - a - cT$$

against the density of the $scCO_2$ should be a linear plot.

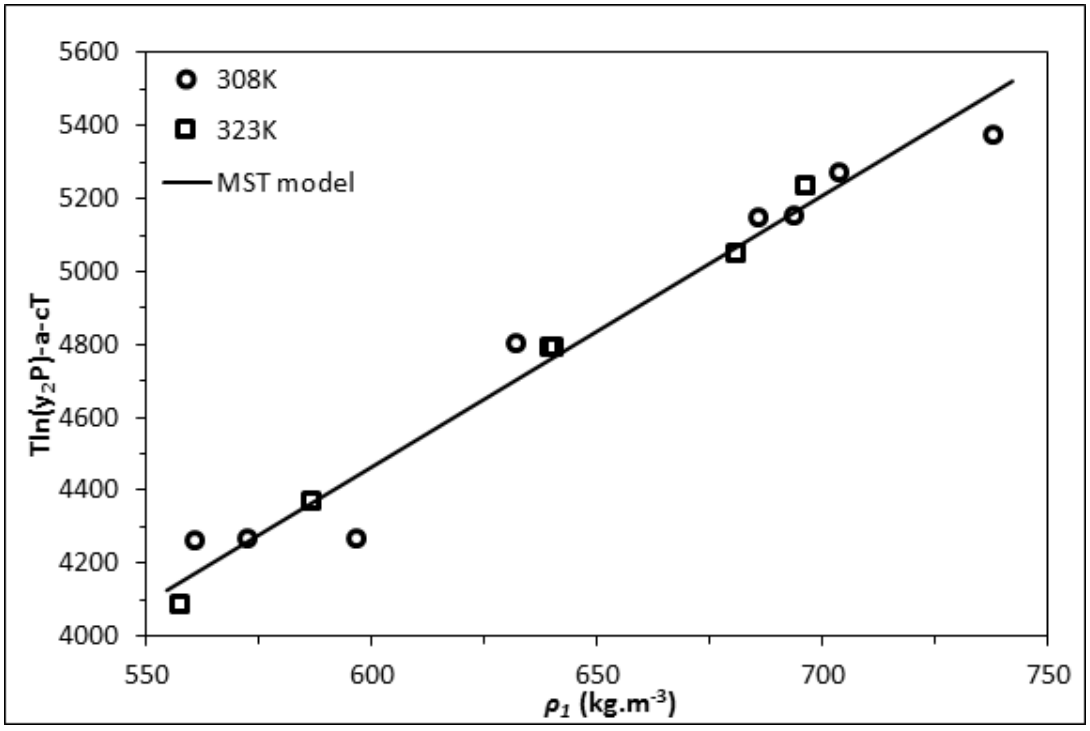

Figure F.4 Self-consistency tests of trifluoropropylPOSS with Mendez-Santiago and Teja model

F.5 Bartle Model

For Bartle model, the plot of experimental data at all temperature in the form of:

$$\ln\left(\frac{y_j P}{P_{ref}}\right) - a - \frac{b}{T} + c(\rho_1 - \rho_{ref})$$

against the difference between the density of $scCO_2$ and the reference density $(\rho_1 - \rho_{ref})$ should be a linear plot.

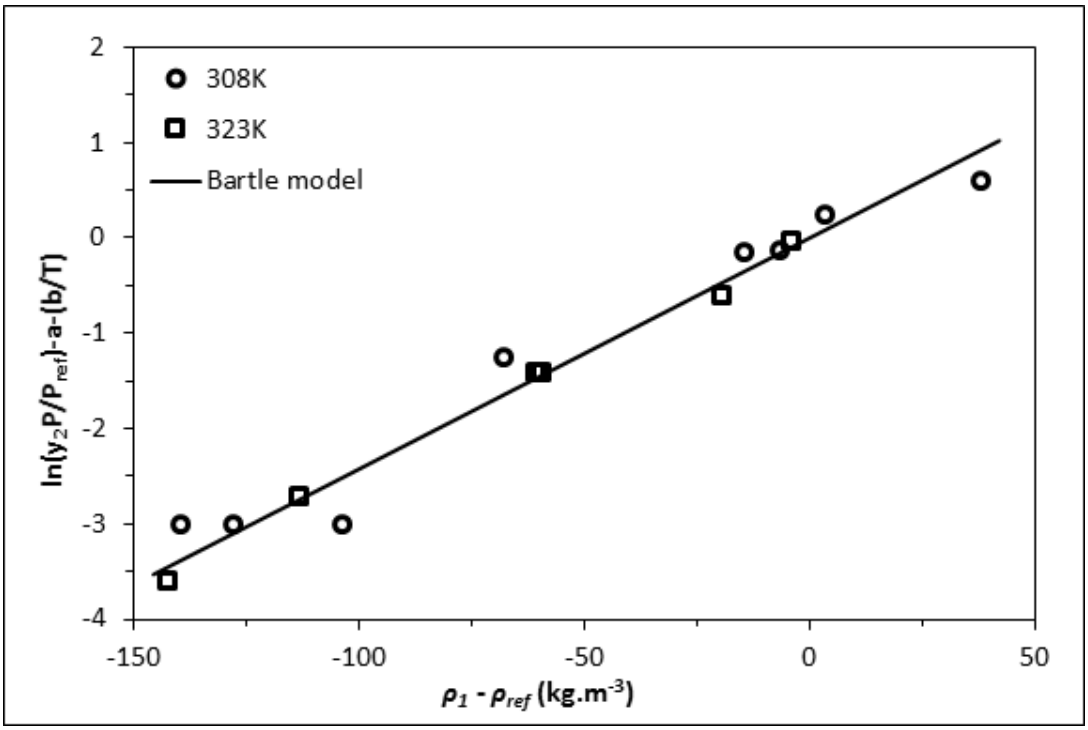

Figure F.5 Self-consistency tests of trifluoropropylPOSS with Bartle model

APPENDIX G

CALCULATION OF TFPOSS SOLUBILITY

The solubility data of TFPOSS is calculated for one of the processing condition of the polymer, which is at 313 K and 20.7 MPa. Chrastil modified by Wang model is given by:

$$\ln(y_2) = a + \frac{b}{T} + c\,\rho_1 + d\,\ln(P)$$

The parameters for the model obtained are:

Table G.1 Parameters for C-W model

Model	a	b	c	d
C-W	1.1E+02	-2.9E+04	4.0E-02	-9.9E+00

Density of CO_2 at 313 K and 20.7 MPa is 846.81 kg.m^{-3}. Substituting the numbers to the equation, the solubility of TFPOSS at 313 K and 20.7 MPa in scCO_2 is obtained to be 0.00081.

The mol fraction of TFPOSS during processing at 313 K and 20.7 MPa is calculated by using the following parameters.

Table G.2 Parameters for TFPOSS mol fraction calculation

Parameters	**Symbol**	**Value**
Vessel volume	V	50 ml
CO_2 density	ρ_1	846.81 $kg.m^{-3}$
TFPOSS molecular weight	MW_2	1193.15 $g.mol^{-1}$
CO_2 molecular weight	MW_1	44.01 $g.mol^{-1}$
Mass of polymer film	m	44 mg
TFPOSS weight percent in film	wt	10-30 %

Additionally, in the calculation the volume of the films are assumed to be negligible. Thus all of the vessel volume is assumed to be occupied by the CO_2 completely.

Mol fraction of TFPOSS inside the vessel during processing is given by:

$$y = \frac{\frac{wt \cdot m}{MW_2}}{\frac{wt \cdot m}{MW_2} + \frac{V \cdot \rho_1}{MW_1}}$$

The mol fraction is calculated to be 0.000004 when the TFPOSS weight fraction in the film is 10% and 0.00002 when the TFPOSS weight fraction in the film is 30%.